NASA CR-135338
ERIM

NASA

Final Report

ATMOSPHERIC TRANSFORMATION OF MULTISPECTRAL REMOTE SENSOR DATA

ROBERT E. TURNER
Infrared and Optics Division

NOVEMBER 1977

Prepared for
NATIONAL AERONAUTICS AND SPACE ADMINISTRATION

Lewis Research Center
Cleveland, Ohio 44135
Contract No. NAS3-20483
Technical Monitor: Thom Coney

ENVIRONMENTAL
RESEARCH INSTITUTE OF MICHIGAN
FORMERLY WILLOW RUN LABORATORIES THE UNIVERSITY OF MICHIGAN
BOX 8618 • ANN ARBOR • MICHIGAN 48107

TECHNICAL REPORT STANDARD TITLE PAGE

1 Report No	2 Government Accession No	3 Recipient's Catalog No
126100-3-F		

4 Title and Subtitle	5 Report Date
Atmospheric Transformation of Multispectral Remote Sensor Data	November 1977
	6 Performing Organization Code

7 Author(s)	8 Performing Organization Report No
Robert E. Turner	126100-3-F

9 Performing Organization Name and Address	10 Work Unit No
Environmental Research Institute of Michigan Infrared & Optics Division P.O. Box 8618 Ann Arbor, Michigan 48107	11 Contract or Grant No NASA NAS3-20483, NASA CR-135338
	13 Type of Report and Period Covered Final Report 2 Nov 76 - 1 Oct 77
12 Sponsoring Agency Name and Address NASA Lewis Research Center Contracts Sect. D (500-312) 21000 Brookpark Rd. Cleveland, Ohio 44135	14 Sponsoring Agency Code

15 Supplementary Notes

Mr. Thom Coney was the Technical Monitor

16 Abstract

The purpose of this report is to develop a mathematical algorithm for the transformation of multispectral remote sensor data in order to determine the intrinsic properties of Earth's surface

The aerosol component of the atmosphere which accounts for hazes and fogs scatters and absorbs radiation reflected by Earth's surface The result of the scattering and absorption is that the radiation received by a remote sensor depends not only upon the reflectance properties of the surface but also upon the intervening atmosphere at the time of observation In this investigation the effects of Earth's atmosphere were accounted for and a simple mathematical algorithm, based upon a radiative-transfer model, was developed to determine the radiance at Earth's surface free of atmospheric effects

Actual multispectral remote sensor data for Lake Erie and associated optical thickness data were used to demonstrate the effectiveness of the atmospheric transformation algorithm. The basic transformation algorithm is general in nature and can be applied to the large-scale processing of multispectral aircraft or satellite remote sensor data

17 Key Words		18 Distribution Statement
Aerosol	Scattering	Initial Distribution is listed at the end of this document
Algorithm	Radiative Transfer	
Atmospheric Model	Reflectance	
Particulates	Transformation	

19 Security Classif (of this report)	20 Security Classif (of this page)	21 No of Pages	22 Price
Unclassified	Unclassified	xiv + 93	

PRECEDING PAGE BLANK NOT FILMED

PREFACE

This report describes part of a research program in the remote sensing of the Great Lakes. The research has been conducted for NASA's Lewis Research Center, Cleveland, Ohio, by the Environmental Research Institute of Michigan (ERIM), formerly the Willow Run Laboratories, Institute of Science and Technology, The University of Michigan. The main objective of this program is to use remote sensing as a practical technique for the analysis of water in the Great Lakes.

Remote sensing of the environment involves the transfer of radiation from a target on the Earth's surface through the atmosphere to a sensor located at a point either within or outside of the atmosphere As a result of scattering and absorption the atmosphere alters the radiation reflected from the surface. In this report we develop the mathematical algorithms based upon a practical radiative transfer model which are then used to determine the reflectance of the surface. In effect, the algorithm "inverts" the radiative transfer problem to eliminate the atmosphere from the remotely sensed data

The research described in this report was performed under Contract NAS3-20483 and covers the period from 2 November 1976 through 1 October 1977. Mr. Thom Coney served as Technical Monitor The program was directed by R. R Legault, Vice President of ERIM, Q A Holmes, Head of ERIM's Information Systems and Analysis Department, and R F Nalepka, Head of ERIM's Multispectral Analysis Section The ERIM number of this report is 126100-3-F.

The author wishes to acknowledge the direction provided by R. R. Legault and Q A. Holmes. The author also wishes to thank S. Westin for his computer programming assistance and D Dickerson for her secretarial assistance in the preparation of this report.

CONTENTS

CONTENTS (Cont'd)

FIGURES

FIGURES (Cont'd)

TABLES

SYMBOLS

a_ℓ	dimensionless parameter from Ricatti-Bessel function
$A(\lambda)$	ozone absorption coefficient
b_ℓ	dimensionless parameter from Ricatti-Bessel function
C	count value
D_z	ozone equivalent thickness
e	base of the natural logarithms
$E(\lambda)$	irradiance of wavelength λ
$E_o(\lambda)$	extraterrestrial solar irradiance
E_s	diffuse sky irradiance
f	ratio of diffuse sky irradiance to the total irradiance
f_s	the ratio of the scattering part of aerosol optical thickness to the total aerosol optical thickness
F	multiplicative operator to remove atmospheric effects
G	additive operator to remove atmospheric effects
H	helicity vector
H(v)	aerosol scale height
I	column density for the permanent gases in the atmosphere
$I_A(z)$	particulate column density
$I_G(z)$	integrated column density for ozone at altitude z
$J(\lambda)$	wavelength-dependent part of the aerosol extinction coefficient
k	Boltzmann's constant
$L(\tau,\mu,\phi)$	spectral radiance
L_B	beam radiance

L_D	diffuse radiance (due to the sky)
L_P	path radiance
L_I	intrinsic radiance
L_S	sky radiance
m	complex valued index of refraction
$m(\lambda)$	index of refraction
$m_1(\lambda)$	real part of the index of refraction
$m_2(\lambda)$	imaginary part of the index of refraction
M_3	molecular weight of ozone
n_s	refractive index of air
N_o	Avogadro's number
$N(r)$	number density of particles of radius r
N_s	number density of air
$p(z)$	atmospheric pressure at altitude z
p_s	standard atmospheric pressure (mb)
$p(\mu,\phi)$	scattering phase function in the direction μ,ϕ
$p(\tau;\ \mu,\phi,\mu',\phi')$	single-scattering phase function at an optical depth τ
Q	efficiency factor
$R(\lambda)$	wavelength-dependent scaling function
T	absolute temperature
V_o	volume of 1 Kmol of ideal gas at STP
V	visual range (km)
z	altitude (meters)

(GREEK SYMBOLS)

$\alpha(\lambda,z)$	volume absorption coefficient
$\beta(\lambda,z)$	volume scattering coefficient
γ	dimensionless parameter in a transcendental equation
$\delta(x)$	Dirac delta function
ρ	hemispherical albedo
ρ_n	depolarization parameter
ρ_s	bidirectional reflectance for a specular surface
$\rho(\mu,\phi)$	directional-hemispherical reflectance
$\rho(\mu,\phi,\mu',\phi')$	bidirectional reflectance function
ρ_3	ozone density (gm/m^3)
η	forward scattering fraction
θ	zenith coordinate in the standard spherical coordinate system
$\kappa_A(\lambda,z)$	aerosol scattering coefficient (cm^{-1})
$\kappa_G(\lambda,z)$	ozone extinction coefficient (cm^{-1})
$\kappa_R(\lambda,z)$	Rayleigh scattering coefficient (cm^{-1})
$\kappa(\lambda,z)$	volume extinction coefficient
$\kappa(\lambda,V,z)$	volume extinction coefficient with explicit dependence of aerosol extinction on the visual range
λ	wavelength of electromagnetic radiation
μ	$\cos(\theta)$ (a useful argument for integrating over the unit sphere)
μ_o	cosine of the solar zenith angle
$\sigma_a(r)$	absorption cross section due to an aerosol particle of radius r

$\sigma_R(\lambda)$	Rayleigh scattering cross section (cm^2)
$\sigma_s(r)$	scattering cross section due to an aerosol particle of radius
$\sigma_t(r)$	total cross section due to an aerosol particle of radius
$\overline{\sigma}(\lambda)$	mean extinction cross section
$\tau(\lambda,z)$	optical depth at altitude z
$\tau_A(\lambda,z)$	aerosol optical depth at altitude z
$\tau_G(\lambda,z)$	ozone optical depth at altitude z
$\tau_{o,A}(\lambda)$	aerosol optical thickness of the entire atmosphere
$\tau_{o,G}(\lambda)$	ozone optical thickness of the entire atmosphere
$\tau_{o,R}(\lambda)$	Rayleigh optical thickness of the entire atmosphere
$\tau_R(\lambda,z)$	Rayleigh optical depth at the altitude z
$\tau_U(\lambda,z)$	Elterman's "Universal" optical depth which is independent of visual range
ϕ	azimuthal coordinate in the standard spherical coordinate system
χ	angle of refraction
χ_o	root of a transcendental equation
$\psi(v)$	particulate size distribution function
$\omega_o(\tau)$	single scattering albedo

1

SUMMARY

In the remote sensing of surface features using multispectral sensors aboard aircraft or spacecraft the Earth's atmosphere can have adverse effects on the classification of various objects of interest. It is therefore desirable to remove the effects of the atmosphere from the multispectral data prior to the implementation of classification processing algorithms Previous attempts to account for atmospheric effects in remote sensing problems have been based upon the use of statistical analyses of multispectral data or purely theoretical analyses of probable atmospheric conditions. In this investigation we make use of an atmospheric-radiative-transfer model and experimental values of critical atmospheric optical parameters to remove the atmospheric effects from multispectral image data.

Of particular interest in this investigation is the reflectance of the water in Lake Erie. Multispectral scanner data were collected by NASA/Lewis Research Center in various high-altitude aircraft flights over Lake Erie under different atmospheric conditions Simultaneous with these flights ancillary multispectral data were also obtained at the surface in order to determine the important parameters to be used in the atmospheric removal algorithm. These parameters, along with the multispectral image data, were then input to a computer program embodying this algorithm Typical output of this program is a multispectral image in which each of the original observations has been replaced by the corresponding value of "intrinsic" radiance or the effective reflectance of the surface.

INTRODUCTION

In the analysis of multispectral remote sensor data obtained by aircraft or spacecraft one finds variable effects which oftentimes preclude the simple determination of basic features of interest. For this study the quantity of interest is the spectral reflectance of the water in the Great Lakes There are certainly many effects which should be considered in the detailed analysis of water reflectance; the wind is often present and this tends to affect the reflectance properties, the sun angle is important; the degree of cloudiness, and the amount of haze in the sky. These are extrinsic quantities which affect the radiation from the surface to the sensor Intrinsic parameters such as the degree of particulate sedimentation in the water, temperature, and currents are also of interest in water quality studies In the present investigation, however, we shall be concerned with the analysis of actual multispectral imagery to eliminate an important extrinsic quantity from the data, namely the effect of atmospheric haze

Radiation from the sun enters the Earth's atmosphere and is absorbed and scattered by the gases and particulates which compose the atmosphere. The radiation reflected from the surface is then attenuated as it propagates from the target to the sensor. In addition, the scattered radiation contributes to the attenuated radiation a quantity called the path radiance which must be taken into account in the preprocessing algorithm. The path radiance is calculated by means of radiative-transfer theory applied to a plane-parallel, horizontally spatially homogeneous, isotropic atmospheric medium which is defined in terms of standard optical parameters Once the path radiance, irradiance, and transmittance are calculated in terms of the measured and estimated optical parameters the radiance at the surface, the intrinsic radiance, and the effective surface reflectance can then

be computed for each picture element (pixel) of multispectral image data. Within the limitations of the model and the errors inherent in the measurement of the model parameters the computer algorithm created during this study will remove the effects of atmospheric haze from the data. The current model is applicable to any degree of haze from near fog conditions to the clearest possible atmosphere and can be used on imagery collected at any latitude. This model includes the effects of multiple scattering by gases and particulates in the atmosphere and of absorption by ozone in the near ultraviolet and visible parts of the spectrum. At the present time the model does not include absorption by other gaseous constituents which are of greater importance in the infrared part of the spectrum. With these limitations the model is applicable in the wavelength region from 0.4 μm to 2.20 μm.

3
ATMOSPHERIC RADIATION MODEL

In this section we will describe the physics of the transfer of radiant energy through the Earth's atmosphere under conditions encountered in realistic situations.

3.1 COMPOSITION OF THE ATMOSPHERE

Earth's atmosphere consists of the permanent gases oxygen (O_2), nitrogen (N_2), and argon (A) which have little effect on the absorption of radiation in the visible and infrared part of the spectrum. The more variable gaseous components such as water vapor (H_2O), carbon dioxide (CO_2), and ozone (O_3) do, however, absorb significant amounts of radiant energy especially in the ultraviolet and infrared part of the spectrum. In the remote sensing of Earth's surface the wavelength bands of an optical sensor are usually chosen so as to avoid the strong gaseous absorption regions For this reason we will consider an atmospheric radiation model which takes into consideration only the multiply scattered radiation and the absorption by the gas ozone and the particulates in the atmosphere. Thus, the model will be applicable to the spectral region from 0 40 μm to ∿2 2 μm with the exception of the strong absorption regions in the near infrared.

Besides the gases the atmosphere contains a semi-permanent suspension of particulates called an aerosol. The particulates arise from a variety of sources, some of which are natural as volcanic eruptions, forest fires, dust storms, and ocean spray, whereas other sources are anthropogenic in nature such as efflux from smokestacks, vehicle tire wear, and large-scale cultivation of the soil All of these sources contribute to the total worldwide particulate load which exists in the stratosphere and which has a resident time measured in years. The troposphere has a much more variable aerosol component which is highly dependent upon load or regional sources.

The particulates can have a variety of compositions and shapes. Pure water aerosols or those with a large portion of water have a spherical or nearly spherical shape whereas the dry particulates can have any complex shape. The composition is generally that of sulfates and phosphates and the composite aerosol usually is characterized by a refractive index which in the visible part of the spectrum is given by

$$m(\lambda) = m_1(\lambda) - im_2(\lambda) \tag{1}$$

where $m_1(\lambda)$ is the real part and $m_2(\lambda)$ is the imaginary part for a wavelength λ For most "general" aerosols found over large regions of the world the index is given by

$$m(\lambda) = 1.5 - 0.1i \tag{2}$$

which indicates that the aerosol is not pure water and that because of the non-zero imaginary term it absorbs radiation. The details of particulates and how they affect remote sensing will be dealt with in a later section

3.2 ATTENUATION OF RADIATION

3.2.1 CROSS SECTIONS

Of all the scattering and absorption processes occurring in the atmosphere the scattering of radiation by the permanent gases is the easiest to account for. The scattering cross section is given by the following equation [1]:

$$\sigma_R(\lambda) = \frac{8\pi^3(n_s^2 - 1)^2}{3\lambda^4 N_s^2}\left(\frac{6 + 3\rho_n}{6 - 7\rho_n}\right) \tag{3}$$

where this so-called Rayleigh cross section is given in cm^2 and n_s is the refractive index of air at 15^oC and 1013 250 mb pressure. The

quantity N_s is the molecular number density of air under standard conditions; ρ_n is the depolarization parameter, and λ is the wavelength of the radiation. According to Edlén [2] the refractive index is given by

$$(n_s - 1) \times 10^8 = 8342.13 + \frac{2406030}{130 - 1/\lambda^2} + \frac{15997}{38.9 - 1/\lambda^2} \tag{4}$$

where λ is the wavelength in μm The number density of standard air is

$$N_s = \frac{\bar{\mu}_H \, p_s \, N_o}{k \, T_s} \tag{5}$$

where $\bar{\mu}_H$ is the atomic mass unit, p_s is the standard atmospheric pressure of 1013.250 mb, N_o is Avogadro's constant, k is Boltzmann's constant, and T_s is the temperature 288.15°K. Using the latest values of these physical constants we get for the standard number density of air

$$N_s = 2\ 5468926 \times 10^{19} \text{ molecules/cm}^3 \tag{6}$$

Thus, with a depolarization parameter ρ_n of 0 0350 [1] we obtain for the Rayleigh scattering cross section

$$\sigma_{Ray} = 1\ 3521891 \times 10^{-21} \frac{(n_s^2 - 1)^2}{\lambda^4} \tag{7}$$

A plot of the cross section σ_{Ray} as a function of wavelength λ is given in Figure 1

Another atmospheric constituent which we will consider is ozone. It is the primary absorber in the ultraviolet region and has some strong absorption bands in the infrared. In the visible region there

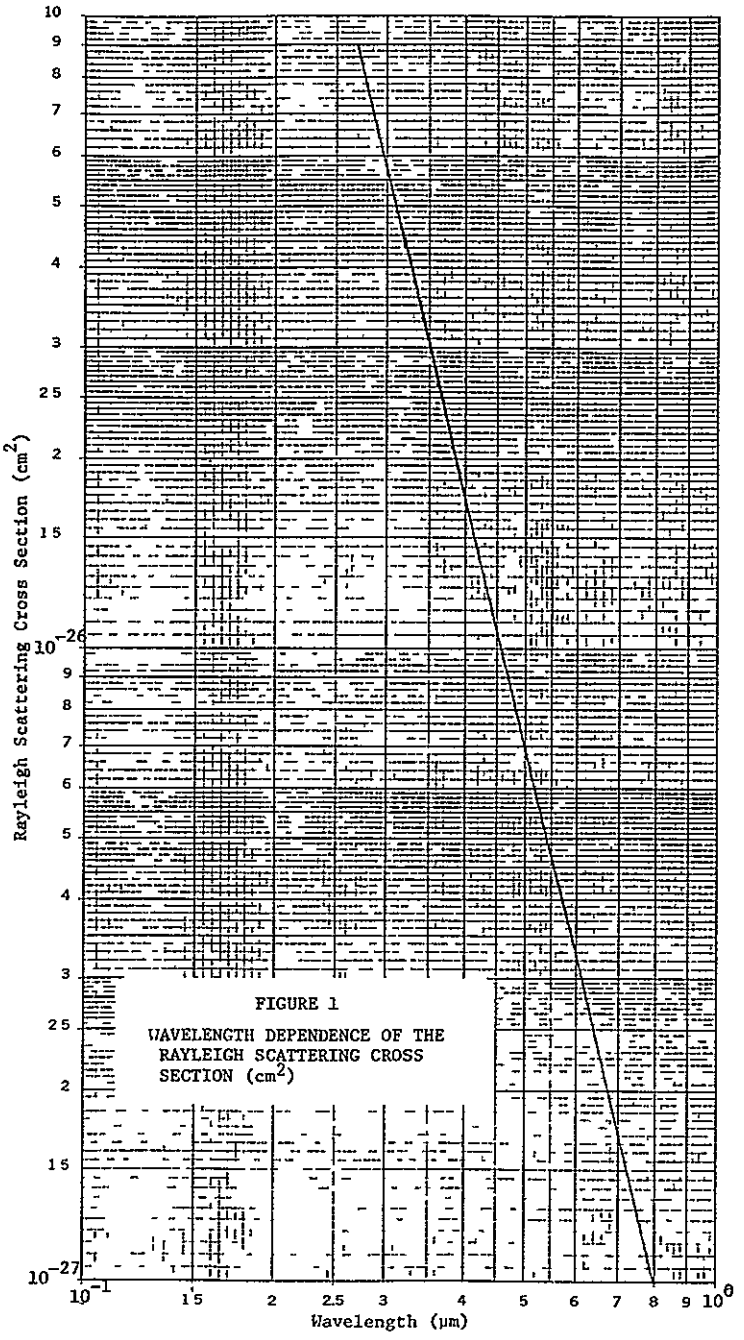

FIGURE 1

WAVELENGTH DEPENDENCE OF THE RAYLEIGH SCATTERING CROSS SECTION (cm^2)

is some absorption due to the weak Chappuis bands near 0.6 μm and we will consider the absorption due to these bands only. The ozone absorption is dependent upon wavelength and temperature but for the visible region the temperature dependence is weak and we will neglect it. The ozone absorption coefficient A is given in cm^{-1} and is depicted in Figure 2 according to Vigroux [3].

The next atmospheric component which we will consider is the aerosol. Lacking information on the shape of the particulates we will assume that they are uniform spheres. Even if the particles have very irregular shapes the interaction of radiation with a large concentration of irregularly shaped particles oriented in random directions probably produces a scattered radiation field not too different from that for spherical particles. The theory of the scattering of electromagnetic plane waves from dielectric spheres was developed by Mie [4] in 1908 More modern treatments of the theory along with further developments are given by van de Hulst [5], and Kerker [6]. The scattering, total, and absorption cross sections are given in terms of the dimensionless parameter $x(= 2\pi r/\lambda)$ where r is the radius of the particle and λ is the wavelength of the radiation They are the following:

$$\sigma_s(r) = \frac{2\pi r^2}{x^2} \sum_{\ell=1}^{\infty} (2\ell+1) \left[|a_\ell|^2 + |b_\ell|^2\right] \tag{8}$$

$$\sigma_t(r) = \frac{2\pi r^2}{x^2} \sum_{\ell=1}^{\infty} (2\ell+1) \, \mathrm{Re}[a_\ell + b_\ell] \tag{9}$$

$$\sigma_a(r) = \sigma_t(r) - \sigma_s(r) \tag{10}$$

where the parameters a_ℓ and b_ℓ are given in terms of the Ricatti-Bessel functions It is sometimes more convenient to use the dimensionless

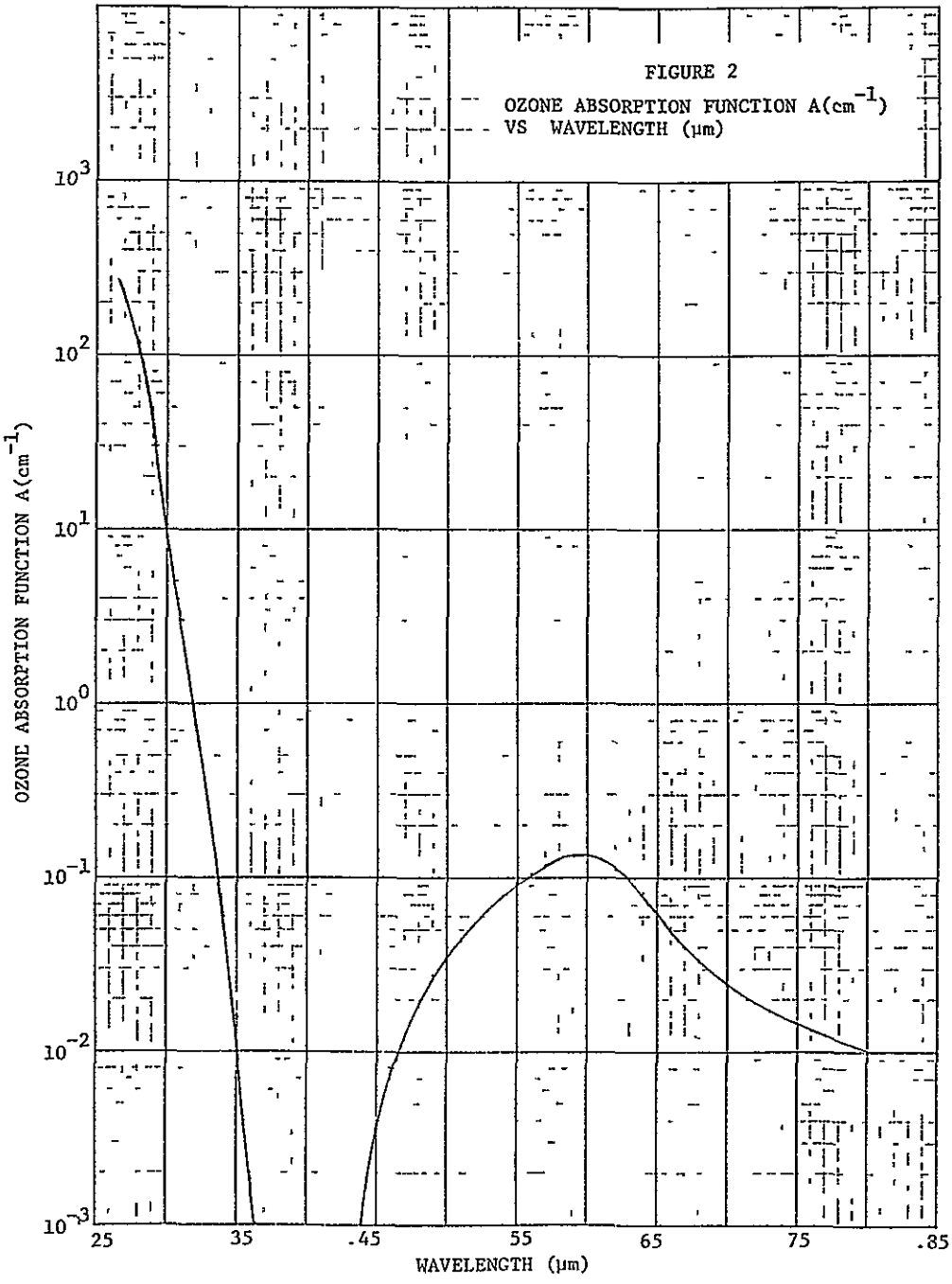

efficiency factors defined as

$$Q = \frac{\sigma}{\pi r^2} \tag{11}$$

For large particles, i.e , for large values of x many terms in the series must be taken into account and this is why computers must be used in a detailed analysis of Mie scattering. The efficiency factors for particles of various refractive indices have been calculated by many investigators and examples by Turner [7] are presented in Figures 3, 4, and 5.

3.2 2 ATTENUATION COEFFICIENTS

Having defined the basic interaction cross sections we must now determine the attenuation coefficients which are dependent upon the concentration of particles in the medium.

For the Rayleigh scattering coefficient we have

$$\kappa_R(\lambda,z) = N(z)\sigma_R(\lambda) \tag{12}$$

where N(z) is the number of molecules of air per unit volume and $\sigma_R(\lambda)$ is the scattering cross section as given by Equation 7. The coefficient $\kappa_R(\lambda,z)$ is then expressed in reciprocal length, usually km^{-1}. Thus, if one has the molecular number density as a function of altitude the scattering coefficient can be determined. For our purposes we will use the number density profile as given by the 1976 U.S Standard Atmosphere [8] It will be found that variations as the result of seasonal and latitude changes alter the profile very little, at least as compared to changes in the aerosol density.

The ozone extinction coefficient $\kappa_G(\lambda,z)$ is given by

$$\kappa_G(\lambda,z) = A(\lambda)D(z) \tag{13}$$

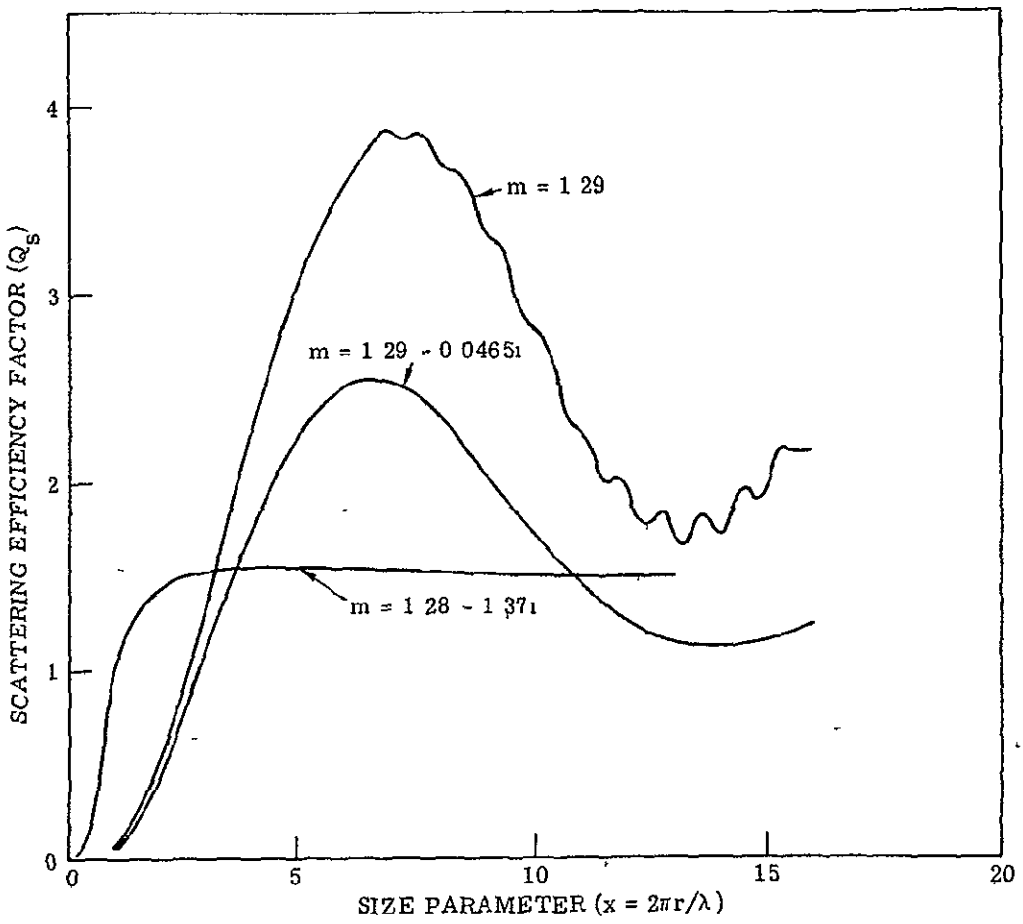

FIGURE 3. SCATTERING EFFICIENCY FACTOR FOR HOMOGENEOUS SPHERES OF COMPLEX REFRACTIVE INDEX m

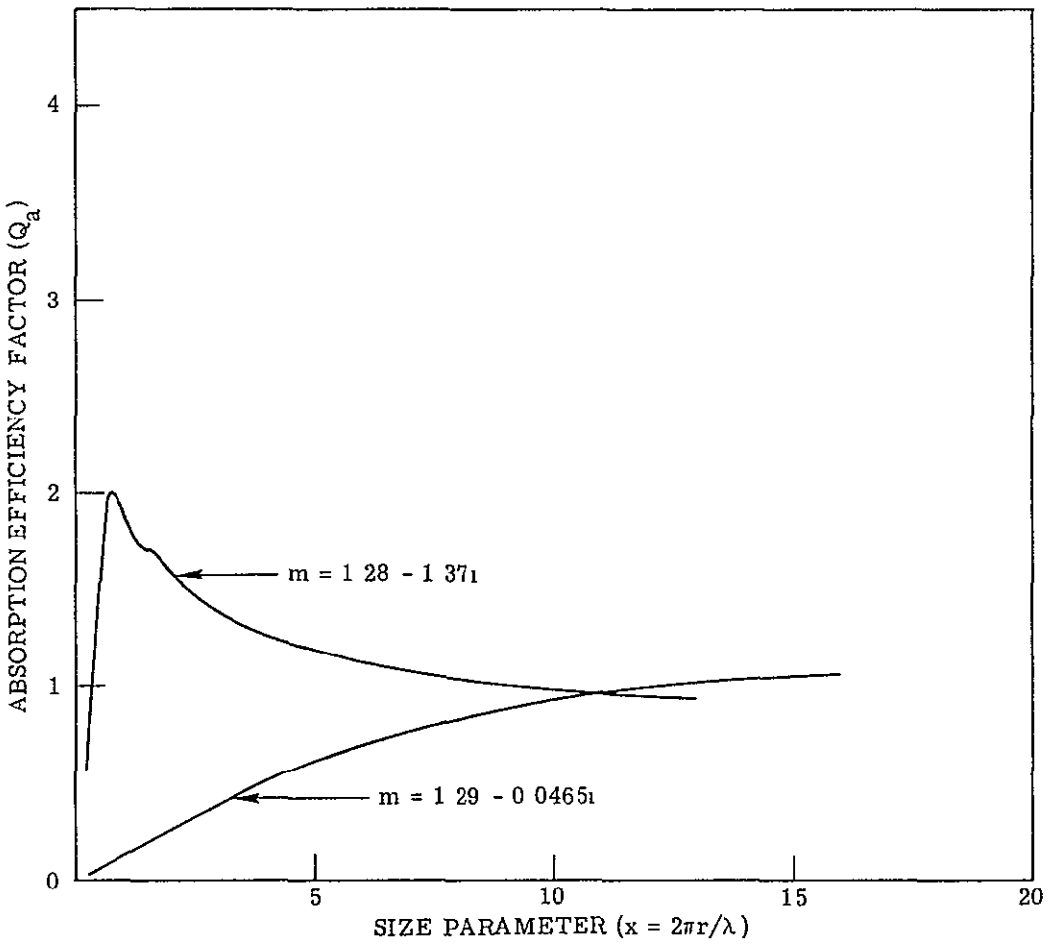

FIGURE 4. ABSORPTION EFFICIENCY FACTOR FOR HOMOGENEOUS SPHERES OF COMPLEX REFRACTIVE INDEX m

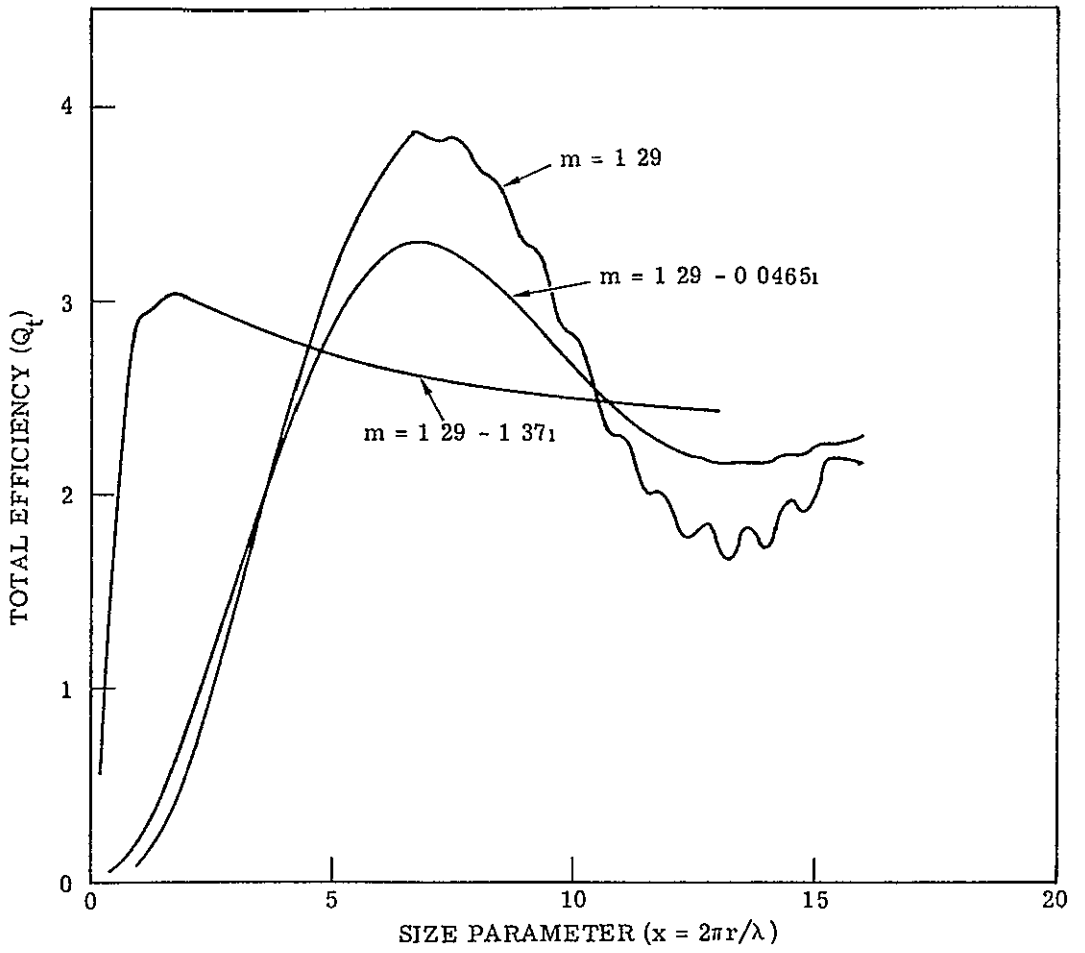

FIGURE 5. TOTAL EFFICIENCY FACTOR FOR HOMOGENEOUS SPHERES OF COMPLEX REFRACTIVE INDEX m

where D(z) is the ozone equivalent thickness (cm/km) and A(λ) is the ozone absorption coefficient The determination of ozone variability at a function of season, latitude, longitude, altitude, and time of day has been the subject of much investigation over many years. Most of these details are not of much importance to the present investigation because they deal with the ultraviolet part of the spectrum. We will make use of ozone number densities as provided by McClatchey et al [9] and Krueger and Minzner [10] Additional information on ozone variability is given by Vassy [11], Green [12], and Valley [13].

The ozone equivalent thickness D(z) is given by

$$D(z) = \frac{V_o}{M_3} 10^2 \rho_3(z) = 4.66968 \times 10^1 \rho_3(z) \qquad (14)$$

where V_o is the volume of an ideal gas at STP, i.e , 22.4136 m^3/kmol, M_3 is the ozone molecular weight of 47 9982 kg/kmol, and $\rho_3(z)$ is the ozone density in gms/m^3.

For the aerosol the calculations are more involved because we must consider a spectrum of particle sizes The smallest particles are called Aitken nuclei and have little effect on optical phenomena Their sizes range from 10^{-3} μm to 10^{-1} μm The condensation nuclei or large particles range in size from 10^{-1} μm to 1 μm and are important for optics Giant particles are those greater than 1 μm in radius Deirmendjian [14] has parameterized the particle size distribution with the following equation.

$$N(r) = ar^{\delta}\exp(-br^{\gamma}) \qquad (15)$$

where the constants determined the type of haze The volume absorption, scattering, and extinction coefficients are then given by the following

$$\alpha(\lambda,z) = \int_0^{\infty} \sigma_a(r)N(z,r)dr \qquad (16)$$

$$\beta(\lambda,z) = \int_0^\infty \sigma_s(r)N(z,r)dr \tag{17}$$

$$\kappa(\lambda,z) = \int_0^\infty \sigma_t(r)N(z,r)dr \tag{18}$$

where $N(z,r)$ is the number of particulates per unit volume in size range Δr, and the cross sections are functions of the wavelength dependent complex refractive index $m(\lambda)$

3 2.3 OPTICAL DEPTH

One of the most important parameters in radiative-transfer analysis is the optical depth. It is a dimensionless parameter and is basically the distance which a photon travels in a medium measured in mean free paths. If the total optical thickness τ_o of a medium is much less than one then the radiation is probably scattered only once, whereas if the optical thickness is much greater than one there are many scatterings and the photon "diffuse" through the medium. In either case these are approximations which can be used to determine the radiation field Unfortunately, in the visible region of the Earth's atmosphere the optical thickness is nearly one which means that the complete radiative-transfer theory for multiple scattering must be considered.

For a Rayleigh atmosphere the optical depth $\tau_R(\lambda,z)$ at altitude z is given by

$$\tau_R(\lambda,z) = \sigma_R(\lambda) \int_z^\infty N(z')dz' \tag{19}$$

For the entire atmosphere the optical thickness $\tau_{o,R}(\lambda)$ is

$$\tau_{o,R}(\lambda) = \sigma_R(\lambda)\ I \tag{20}$$

where I is the column density for the permanent gases in the atmosphere. Using the 1976 U.S. Standard Atmosphere we have integrated the molecular number density (Figure 6) over altitude to determine I_s, i e , I for a standard atmosphere It is 2.16374 x 10^{25} cm^{-2}.

If the Rayleigh optical thickness $\tau_{o,R}(\lambda)$ is known at a particular site then the optical depth is given by the following:

$$\tau_R(\lambda,z) = \frac{p(z)}{p_o} \tau_{o,R}(\lambda) \tag{21}$$

where p(z) is the pressure at altitude z and p_o is the pressure at the site. It should be noted that optical depth is defined to be zero at the top of the atmosphere. Typical values of the Rayleigh optical thickness are 0 450 at λ = 0.38 μm and 0.021 at λ = 0.80 μm.

The ozone optical depth $\tau_g(\lambda,z)$ at altitude z is given by

$$\tau_G(\lambda,z) = C\ A(\lambda) \int_z^\infty \rho_3(z')dz' \tag{22}$$

where

$$C = 46.6968 \tag{23}$$

and

$$I_G(z) = \int_o^z \rho_3(z')dz' \tag{24}$$

is the integrated column density for ozone. Hence,

$$\tau_G(\lambda,z) = \tau_G(\lambda) - CA(\lambda)\ I_G(z) \tag{25}$$

where $\tau_G(\lambda)$ is the ozone optical thickness at wavelength λ. Typical values are 0 012 at λ = 0.50 μm and 0 045 at the peak of the Chappuis band at λ = 0.60 μm.

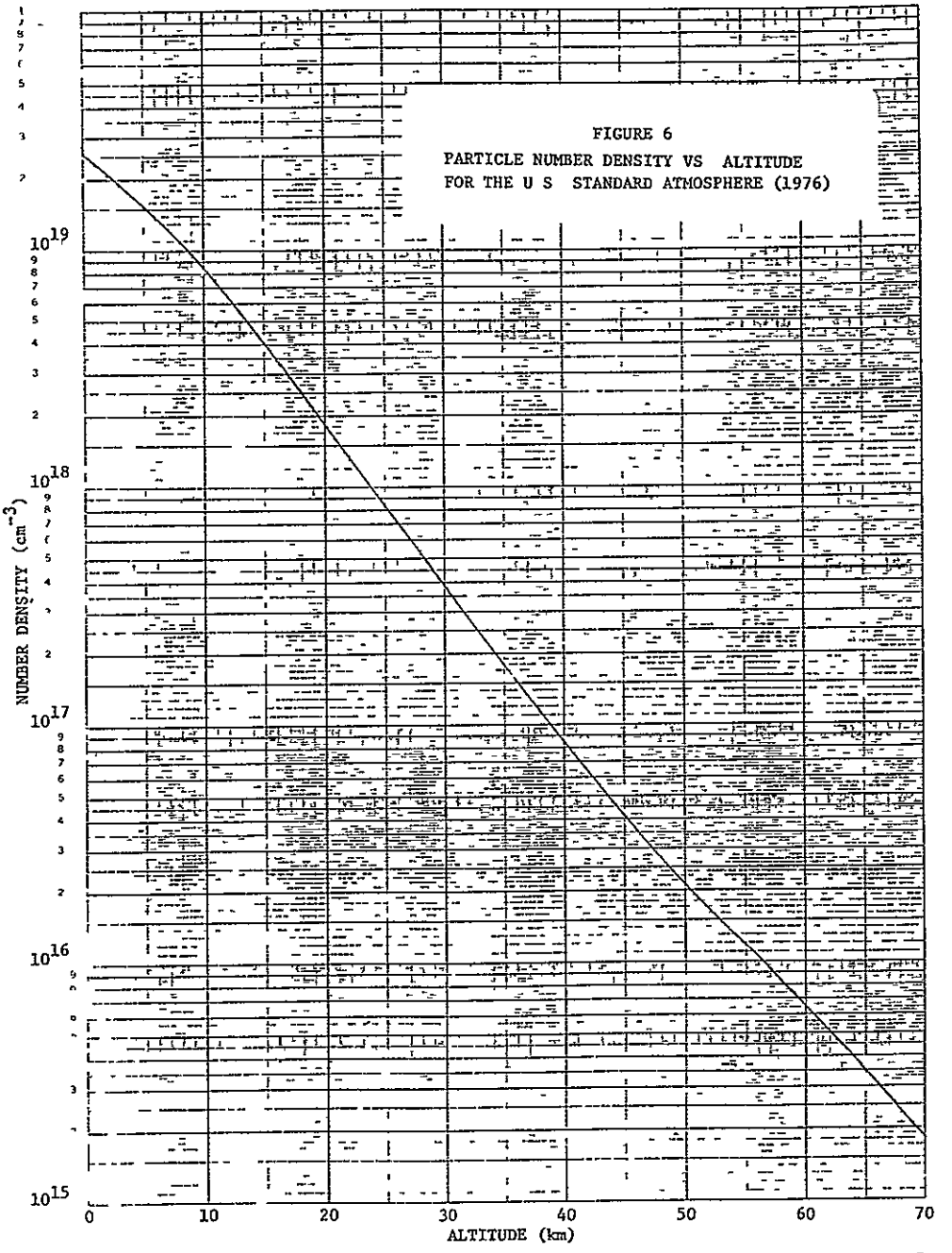

FIGURE 6
PARTICLE NUMBER DENSITY VS ALTITUDE
FOR THE U S STANDARD ATMOSPHERE (1976)

The aerosol optical depth is given by

$$\tau_A(\lambda,z) = \int_z^\infty \kappa(\lambda,z')\, dz' \tag{26}$$

Now, experiments have shown that the size distribution is approximately independent of altitude which means that we can use the following:

$$N(z,r) \tilde{=} N(z)\ \psi(r) \tag{27}$$

where $N(z)$ is the particulate number density and $\psi(r)$ is the size spectrum. Using Equations 18 and 27 we get

$$\tau_A(\lambda,z) = \overline{\sigma}(\lambda)\ I_A(z) \tag{28}$$

where $\overline{\sigma}(\lambda)$ is the mean extinction cross section integrated over the size spectrum and $I_A(z)$ is the particulate column density, i e ,

$$\overline{\sigma}(\lambda) = \int_o^\infty \sigma_t(r)\ \psi(r)dr \tag{29}$$

and

$$I_A(z) = \int_z^\infty N(z')dz' \tag{30}$$

Typical values of the aerosol optical thickness at a wavelength of 0 55 μm are 1.7 at a visual range of 2 km and 0.25 at a visual range of 23 km

Of all the optical depths the aerosol optical depth is by far the most variable one. In general, we have then

$$\tau(\lambda,z) = \tau_R(\lambda,z) + \tau_G(\lambda,z) + \tau_A(\lambda,z) \tag{31}$$

for the total optical depth of Earth's atmosphere and

$$\tau_o(\lambda) = \tau_{o,R}(\lambda) + \tau_{o,G}(\lambda) + \tau_{o,A}(\lambda) \tag{32}$$

for the total optical thickness of Earth's atmosphere

3.2.4 PHASE FUNCTIONS

In multiple scattering one must consider the angular distribution of the radiation. Mie theory allows one to calculate the differential scattering cross section or the single-scattering phase function for any size particle. Likewise, the Rayleigh phase function can be calculated or derived from the Mie formulas as $\lambda >> r$. The phase function $p(\mu,\phi)$ which is wavelength dependent is defined such that

$$\frac{1}{4\pi} \int_0^{2\pi} \int_{-1}^{1} p(\mu,\phi)\, d\mu d\phi = 1 \tag{33}$$

where $\theta (= \cos^{-1}\mu)$ and ϕ are the usual spherical coordinates. For a Rayleigh atmosphere with no molecular anisotropy the radiation field scattered by a single particle is of the dipole form

$$p(\mu) = \frac{3}{4}(1 + \mu^2) \tag{34}$$

If molecular anisotropy is taken into account the formula becomes [15]

$$p(\mu) = R_1 + R_2\mu^2 \tag{35}$$

where

$$R_1 = \frac{3}{2}\left(\frac{1 + \rho_n}{2 + \rho_n}\right) \tag{36}$$

$$R_2 = \frac{3}{2}\left(\frac{1 - \rho_n}{2 + \rho_n}\right) \tag{37}$$

and ρ_n is the depolarization parameter ~ 0.035.

The calculation of the particulate phase function is much more complicated. An example of these calculations is illustrated in Figure 7 for a so-called continental haze distribution for particles with various amounts of absorption. As illustrated the phase function is highly anisotropic, the amount of radiation scattered in the forward direction being about 300 times the amount scattered at 120^{o} An indication of the relative amount of scattering in a Rayleigh atmosphere as opposed to a hazy atmosphere is depicted in Figure 8 For the situations which we will consider in the model presented in this work the phase functions for various wavelengths and angles have already been computed and stored in data arrays It is then only necessary to interpolate to find the phase function for any desired wavelength and angle.

3.3 THE MODEL ATMOSPHERE

The "Rayleigh" part of the atmosphere, i e., that part characterized by the permanent gases is well known and is essentially only dependent upon the atmosphere. Likewise, the "ozone" part is known in the sense that the ozone number density can be found for various latitudes and times of year. The "aerosol" part of the atmosphere is subject to many variations and we must rely on semi-empirical methods to characterize the optical state of the atmosphere

There is evidence [15,16] that the particulate distribution is exponential with altitude, i e , it can be designated by an exponential decrease in number density with a scale height which is dependent upon the visual range. In our analysis here we will use the Elterman model [15] in which the aerosol extinction coefficients below 5 km altitude are dependent upon the visual range. Thus,

$$\kappa(\lambda,V,z) = \kappa_A(\lambda,V,z) + \kappa_G(\lambda,z) + \kappa_R(\lambda,z) \qquad (38)$$

where V is a parameter to denote the visual range. It should be stated that we use V as an atmospheric parameter only to characterize the

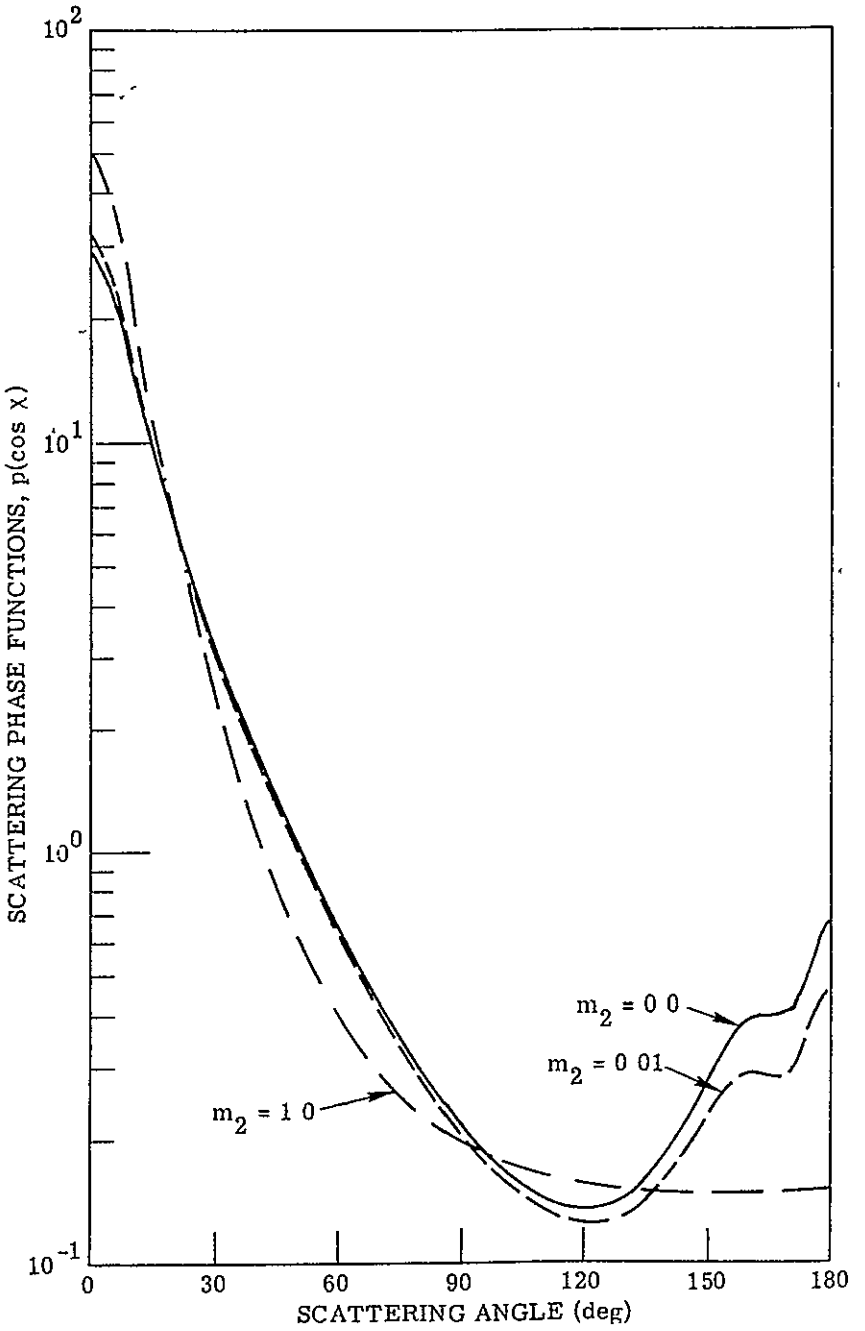

FIGURE 7. SCATTERING PHASE FUNCTIONS AS CALCULATED FROM MIE THEORY FOR HAZE L—COMPLEX REFRACTIVE INDEX m = 1.5 - im_2 Wavelength = 0 55μm

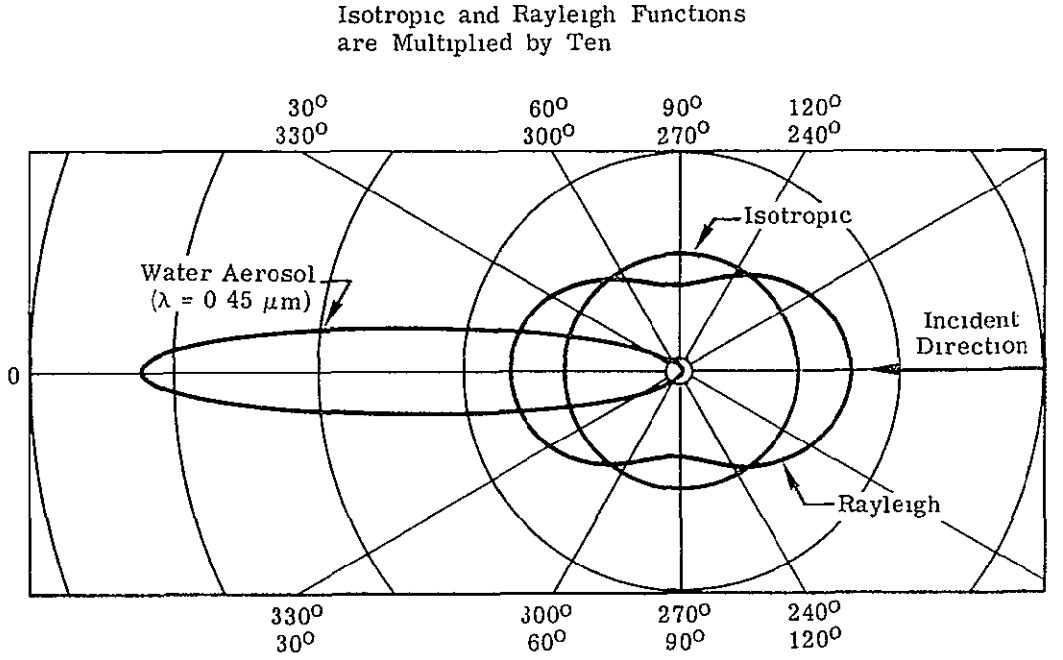

FIGURE 8. ANGULAR DEPENDENCE OF SINGLE-SCATTERING PHASE FUNCTIONS IN ANY AZIMUTHAL PLANE

degree of turbidity of the atmosphere; neither the model itself nor the results depend upon a measurement of visual range. Now, the aerosol extinction coefficient is

$$\kappa_A(\lambda,V,z) = \kappa_A(\lambda,V,o)\ e^{-z/H(V)} \tag{39}$$

for $z \leq 5$ km. Thus, the aerosol scale height H(V) is

$$H(V) = \frac{z}{\ell n\left[\frac{\kappa_A(\lambda,V,o)}{\kappa_A(\lambda,V,z)}\right]} . \tag{40}$$

According to Eltermann [16] experiments indicate that at z = 5 km

$$\kappa_A(\lambda_o,V,5) = 5.0 \times 10^{-3}\ km^{-1} \tag{41}$$

where $\lambda_o = 0.55$ μm Now, since $\kappa_A(\lambda,V,z)$ can be written as the product of number density and some function of wavelength

$$\kappa_A(\lambda,V,z) = N(z)J(\lambda) \tag{42}$$

where $J(\lambda)$ is the wavelength-dependent part of the aerosol extinction coefficient, we have

$$\frac{\kappa_A(\lambda,V',z)}{\kappa_A(\lambda,V,z)} = \frac{N'(z)}{N(z)} \tag{43}$$

a quantity which is independent of the wavelength λ. According to Koschmieder's formula [17] the horizontal visual range is defined by

$$\kappa(\lambda_o,V,o) = \frac{\ell n\ 50}{V} . \tag{44}$$

Hence, knowing that $\kappa_R(\lambda_o,o) = 1\ 162 \times 10^{-2}\ km^{-1}$ and $\kappa_G(\lambda_o,o) = 2.57766 \times 10^{-4}\ km^{-1}$ from McClatchey et al. [9] and using Equations 40

and 41 for an altitude of 5 km we can determine the scale height, i.e ,

$$H(V) = \frac{5}{\ell n \left[\frac{782\ 4046}{V} - 2.3755532 \right]} \tag{45}$$

where V is in km. Now, by using a scaling relation we can determine the aerosol coefficient at the surface in terms of its value at the measured visual range of 4 km Thus,

$$\kappa_A(\lambda,V,o) = \kappa_A(\lambda,4,o) \left[\frac{\frac{\ell n\ 50}{V} - \kappa_R(\lambda_o,o) - \kappa_G(\lambda_o,o)}{\frac{\ell n\ 50}{4} - \kappa_R(\lambda_o,o) - \kappa_G(\lambda,o)} \right] \tag{46}$$

or

$$\kappa_A(\lambda,V,o) = \kappa_A(\lambda,4,o) \left[\frac{4.0491768}{V} - 0.0122942 \right] \tag{47}$$

where the coefficient $\kappa_A(\lambda,4,o)$ is illustrated in Figure 9.

Having determined the scale height H(V) and the aerosol coefficient $\kappa_A(\lambda,V,o)$ at the surface we now have a complete model of the particulate distribution below 5 km. In Elterman's model the assumption is that above 5 km there exists a "universal" distribution independent of visual range With these formulas and the definition of optical depth we can then write

$$\tau_A(\lambda,V,z) = \kappa_A(\lambda,V,o)H(V) \left[e^{-z/H(V)} - e^{-5/H(V)} \right] + \int_5^\infty \kappa_A(\lambda,z')dz' \tag{48}$$

for $z \leq 5$ km and

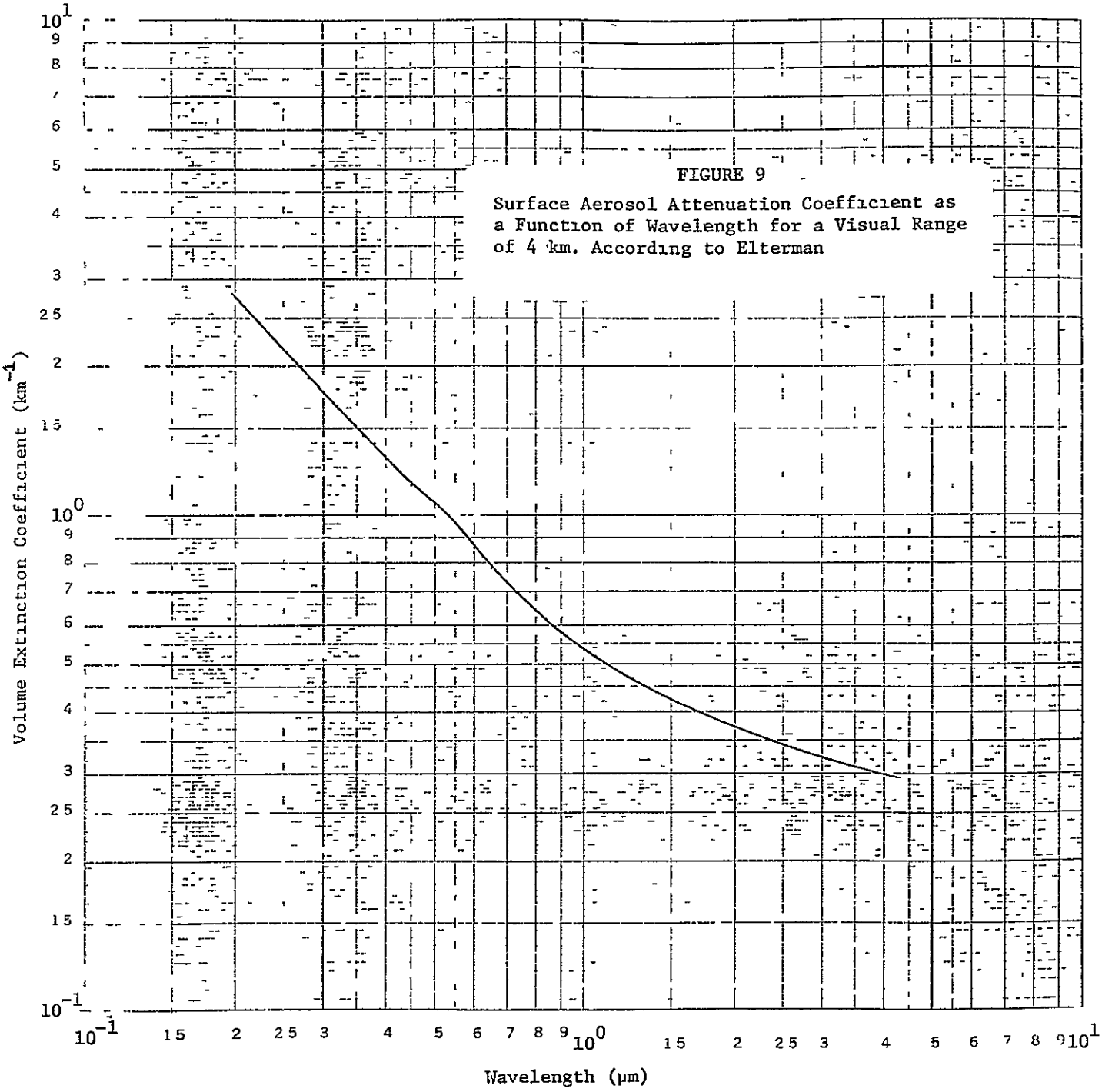

FIGURE 9

Surface Aerosol Attenuation Coefficient as a Function of Wavelength for a Visual Range of 4 km. According to Elterman

$$\tau_A(\lambda,V,z) = \int_z^\infty \kappa_A(\lambda,z')dz' \tag{49}$$

for $z > 5$ km. The aerosol optical thickness $\tau_{o,A}(\lambda,V)$ is

$$\tau_{o,A}(\lambda,V) = \kappa_A(\lambda,V,o)H(V)\left[1 - e^{-5/H(V)}\right] + \int_5^\infty \kappa_A(\lambda,z')dz' \tag{50}$$

Based upon this model we will now see how a single measurement of the total optical thickness $\tau_o(\lambda,V)$ at the Earth's surface allows us to determine the optical depth $\tau(\lambda,z)$ for any altitude z. A spectroradiometer at the Earth's surface pointing in the direction of the Sun will measure the irradiance $E(\lambda)$, i.e.,

$$E(\lambda) = E_o(\lambda)e^{-\tau_o(\lambda,V)/\mu_o} \tag{51}$$

where $E_o(\lambda)$ is the known extraterrestrial solar irradiance and μ_o is the cosine of the solar zenith angle θ_o. Now,

$$\tau_o(\lambda,V) = \tau_{o,R}(\lambda) + \tau_{o,G}(\lambda) + \tau_{o,A}(\lambda,V) \tag{52}$$

and

$$\tau(\lambda,V,z) = \tau_R(\lambda,z) + \tau_G(\lambda,z) + \tau_A(\lambda,V,z) \tag{53}$$

where $\tau_o(\lambda,V)$ is measured according to Equation 51 and $\tau_{o,R}(\lambda)$, $\tau_{o,G}(\lambda)$, $\tau_R(\lambda,z)$, and $\tau_G(\lambda,z)$ are assumed to be known. We want to determine $\tau(\lambda,V,z)$. From a measurement of $\tau_o(\lambda,V)$ we can determine $\tau_{o,A}(\lambda,V)$ from Equation 52. Therefore, we have

$$\tau_A(\lambda,V,z) = \tau_{o,A}(\lambda,V) - \kappa_A(\lambda,V,o)H(V)\left[1 - e^{-z/H(V)}\right] \tag{54}$$

for $z \leq 5$ km and

$$\tau_A(\lambda,V,z) = \int_z^\infty \kappa_A(\lambda,z')dz' = \tau_U(\lambda,z) \tag{55}$$

for $z > 5$ km. $\tau_U(\lambda,z)$ is the "universal" optical depth which is independent of visual range. By a simple scaling relation we have

$$\tau_U(\lambda,z) = R(\lambda) \int_z^\infty \kappa_A(\lambda_o,z')dz' \tag{56}$$

where $R(\lambda)$ is given by

$$R(\lambda) = \frac{\kappa_A(\lambda,o)}{\kappa_A(\lambda_o,o)} \tag{57}$$

and is illustrated in Figure 10. Likewise,

$$\tau_{o,U}(\lambda) = R(\lambda) \int_5^\infty \kappa_A(\lambda_o,z')dz' \tag{58}$$

Now,

$$\tau_{o,A}(\lambda,V) - \tau_{o,U}(\lambda) = \kappa_A(\lambda,V,o)H(V)\left[1 - e^{-5/H(V)}\right] \tag{59}$$

Since the left-hand side of this equation is known we can solve Equation 59 for V. After performing an analysis similar to what was done in deriving the model we have the following transcendental equation to solve:

$$e^x - \gamma x - 1 = 0 \tag{60}$$

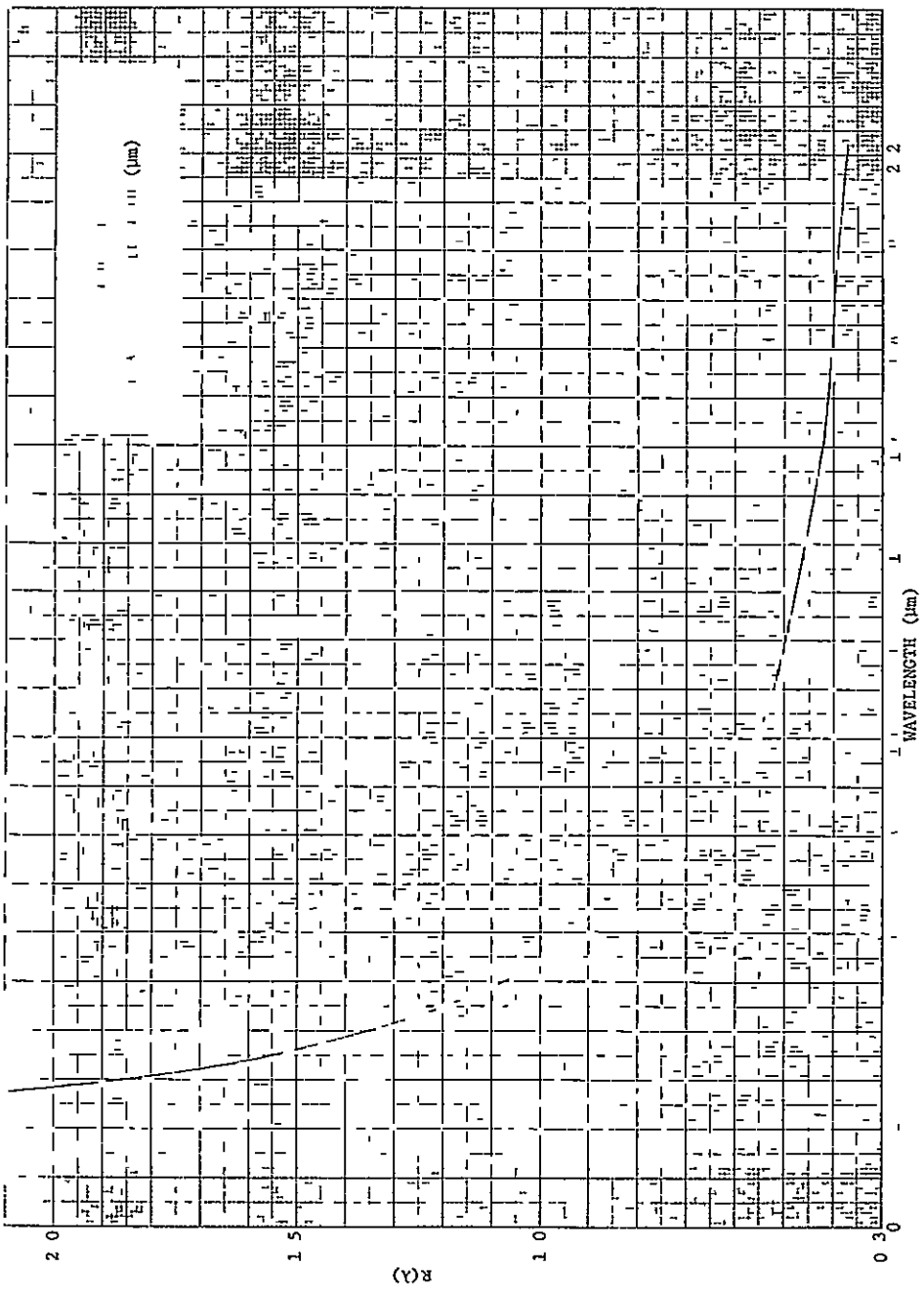

where

$$e^{x} = \frac{\frac{\ell n\ 50}{V} - \kappa_R(\lambda_o,o) - \kappa_G(\lambda_o,o)}{\kappa_A(\lambda_o,V,5)} \tag{61}$$

and

$$\gamma = \frac{\tau_{o,A}(\lambda,V) - \tau_{o,U}(\lambda)}{5\ \kappa_A(\lambda_o,V,5)} \frac{\kappa_A(\lambda_o,4,o)}{\kappa_A(\lambda,4,o)} \tag{62}$$

It should be noted that γ is known from the measurement of the optical thickness $\tau_o(\lambda,V)$ and everything in Equation 61 is known except V. Let the root of Equation 60 be x_o The optical depth $\tau_A(\lambda,V,z)$ can then be determined, i e.,

$$\tau_A(\lambda,V,z) = \tau_{o,A}(\lambda,V) - F(\lambda) \frac{e^{x_o}}{x_o} \left[1 - e^{-\frac{x_o z}{5}} \right] \tag{63}$$

where

$$F(\lambda) = 5\ \kappa_A(\lambda_o,V,5) \frac{\kappa_A(\lambda,4,o)}{\kappa_A(\lambda_o,4,o)} \tag{64}$$

Under normal conditions γ cannot be negative as that would mean that the optical depth at 5 km is greater than the optical thickness. However, the universal optical depth may be greater than $\tau_{o,A}(\lambda,V)$ if between the time of measurement of the universal value and the measurement of $\tau_{oA}(\lambda,U)$ the present universal value has decreased. The roots of Equation 60 vs. γ are illustrated in Figure 11.

Hence, Equation 63 gives as the aerosol optical depth at altitude z and wavelength λ for $z \leq 5$ km. For $z > 5$ km we use Equation 56 where the integral can be evaluated using $\kappa_A(\lambda_o,z)$ from Elterman [18].

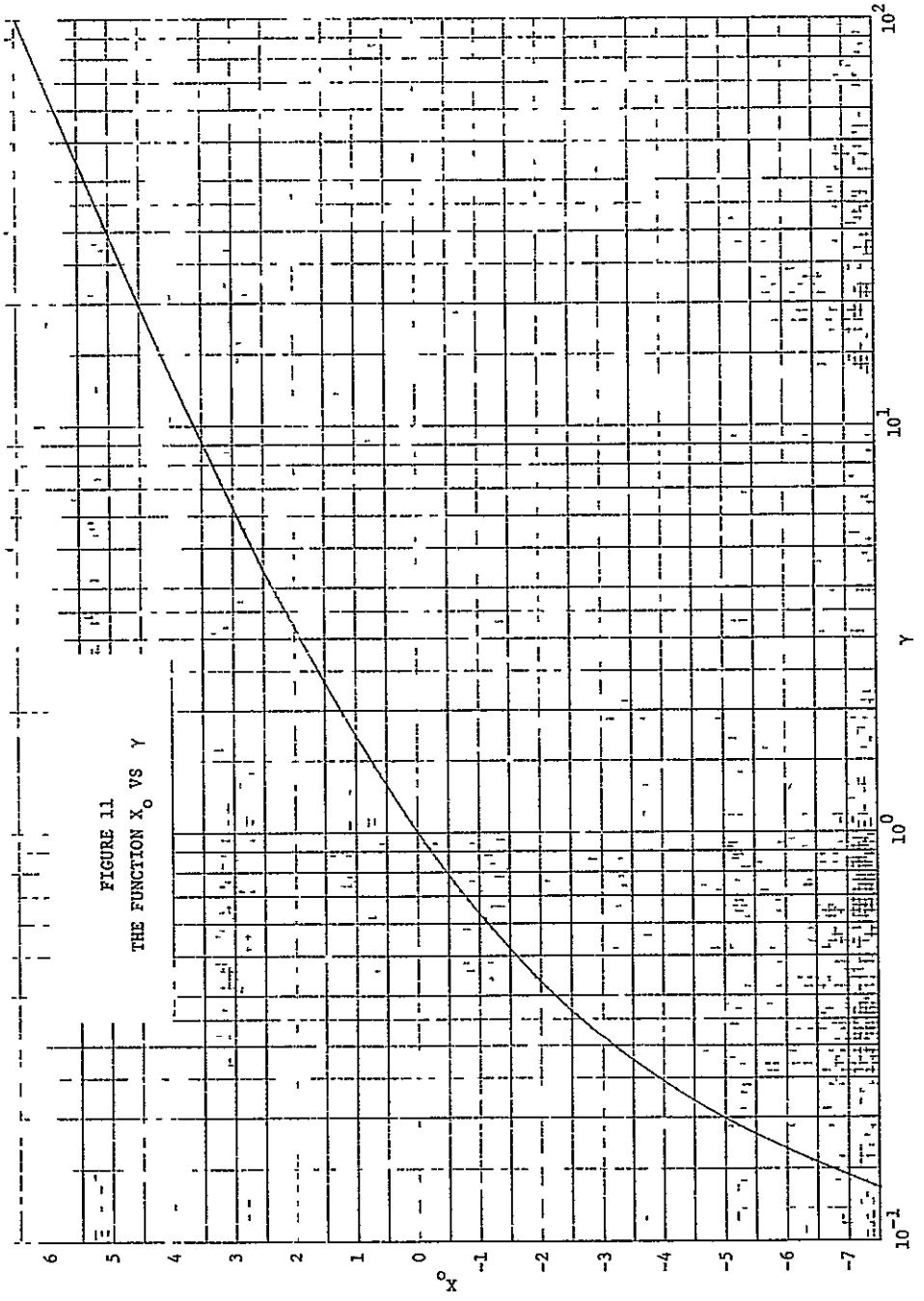
FIGURE 11
THE FUNCTION X_o VS Y
10^{-1}
10^{0}
10^{1}
10^{2}
Y
X_o
6
5
4
3
2
1
0
-1
-2
-3
-4
-5
-6
-7

3.4 RADIATIVE TRANSFER

Having defined the physical properties of the medium we can now describe the process of the transfer of radiant energy through the atmosphere

3 4.1 EQUATION OF TRANSFER

The radiation which is scattered and absorbed by the medium is described by an integro-differential equation [19] For a plane-parallel medium the radiative-transfer equation is

$$\mu \frac{dL}{dt} = L(\tau,\mu,\phi) - \frac{\omega_o(\tau)}{4\pi} \int_0^{2\pi} \int_{-1}^{1} p(\tau,\mu,\phi,\mu',\phi')L(\tau,\mu',\phi')d\mu'd\phi' \quad (65)$$

where $L(\tau,\mu,\phi)$ is the spectral radiance, i.e , the amount of energy arriving at a point on a surface per unit area per unit time per unit solid angle per wavelength interval The units we use here will be milliwatts per square centimeter per steradian per micrometer. It should be noted that radiance is independent of distance if one neglects the effect of interaction with the medium. For example, the spectral radiance of a star is the same regardless of one's distance from the star. The quantity $\omega_o(\tau)$ is the single-scattering albedo and is defined as the ratio of the volume scattering coefficient to the volume extinction coefficient, i.e ,

$$\omega_o(\tau) = \frac{\beta(\lambda,z)}{\kappa(\lambda,z)} \quad (66)$$

thus $\omega_o(\tau)$ is a fraction between zero and one The quantity $p(\tau,\mu,\phi,\mu',\phi')$ is the single-scattering phase function which describes the angular dependence of the scattering at a given optical depth τ in the medium The relationship between the angular coordinates is illustrated in Figure 12.

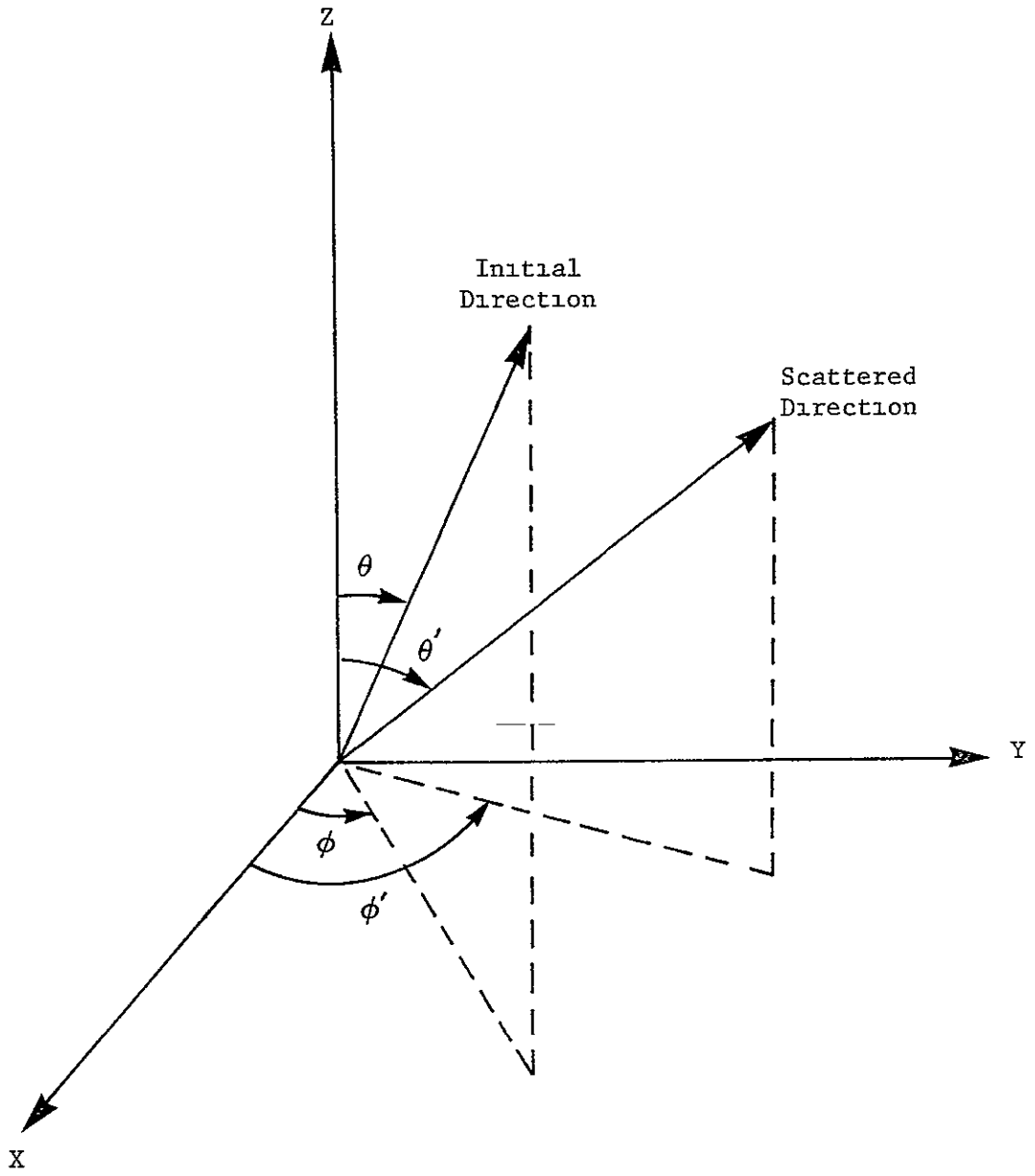

FIGURE 12. RELATIONSHIP BETWEEN THE ANGULAR COORDINATES IN THE SCATTERING PHASE FUNCTION

Much effort has been spent in the last forty years by many investigators to solve Equation 65 for various media and boundary conditions. Mathematically exact formulations of solutions to this equation are beyond the scope of this investigation and considering the limitations of the data and the measurement errors such a solution is not warranted For the purposes of the remote sensing of the Earth's surface an approximate solution is quite adequate A simplified two-stream approximate solution of the radiative-transfer equation has been developed by Turner [20,21] especially for hazy atmospheric conditions Comparisons of the model calculations with mathematically exact formulations and with experiments have demonstrated the utility of the model.

3.4 2 BOUNDARY CONDITIONS

Since the Sun has a angular size of only about one-half degree and constitutes only $\sim 10^{-3}$ per cent of the sky we may consider it to be a point source. The radiance due to the Sun at any optical depth is then given by

$$L_{Sun}(\tau,\mu,\phi) = E_{Sun}(\tau)\delta(\mu + \mu_o)\delta(\phi - \phi_o) \qquad (67)$$

where $E_{Sun}(\tau)$ is the solar irradiance or the amount of energy incident on a surface per unit time per unit area per unit wavelength interval and the δ's are the Dirac delta functions which specify the Sun's location at the spherical coordinates $\theta_o (= \cos^{-1}\mu_o), \phi_o$. It should be noted that irradiance does not depend upon solid angle and refers to the power density regardless of the direction of the incident radiation. Hence, irradiance does depend upon the distance from the source For example, the irradiance from a point source such as a star decreases as the inverse square of the distance to the star.

Since the radiative-transfer equation is linear the direct solar radiation field can be added to the diffuse scattered radiation field

to get the total radiation field in the medium, i e ,

$$L(\tau,\mu,\phi) = L_D(\tau,\mu,\phi) + L_{Sun}(\tau,\mu,\phi) \tag{68}$$

where the radiative-transfer equation can be solved for the diffuse field $L_D(\tau,\mu,\phi)$. The complete solution can then be formed by allowing the diffuse field to satisfy the boundary conditions These are the following:

$$L_D(o,-\mu,\phi) = 0 \tag{69}$$

$$L_D(\tau_o,\mu,\phi) = \int_o^{2\pi} \int_o^1 \mu' \rho(\mu,\phi,\mu',\phi') L(\tau_o,-\mu',\phi') d\mu' d\phi' \tag{70}$$

Equation 69 indicates that the downwelling diffuse radiation field at the top of the atmosphere is zero. In Equation 70 the quantity $\rho(\mu,\phi,\mu',\phi')$ is called the bidirectional reflectance of the surface, a general concept of reflectance which depends upon the direction of the incident radiation and the direction of the reflected radiation.

3 4.3 REMOTE SENSING EQUATION

If we consider a homogeneous atmosphere, that is, one in which the single-scattering albedo and the phase function are independent of optical depth then Equation 65 can be integrated to give the formal solution

$$L(\tau,\mu,\phi) = L(\tau_o,\mu,\phi) e^{-(\tau_o-\tau)/\mu}$$

$$+ \frac{\omega_o}{4\pi\mu} \int_o^{2\pi} \int_{-1}^{1} p(\mu,\phi,\mu',\phi') \int_\tau^{\tau_o} e^{-(\tau'-\tau)/\mu} L(\tau',\mu',\phi') d\tau' d\mu' d\phi'$$

$$+ \frac{\omega_o \mu_o E_o p(\mu,\phi,-\mu_o,\phi_o)}{4\pi(\mu + \mu_o)} \left[e^{-\tau/\mu_o} - e^{-\tau_o/\mu_o} e^{-(\tau_o-\tau)/\mu} \right] \tag{71}$$

where the first term on the right-hand side of the equation represents the radiation attenuated along the path from the target to the sensor. The second term accounts for the multiply scattered radiation along the path and the third term represents the singly scattered solar radiation. Equation 71 can be written in a more compact form as

$$L(\tau,\mu,\phi) = L(\tau_o,\mu,\phi)T(\tau,\mu) + L_p(\tau,\mu,\phi). \tag{72}$$

Equation 72 is called the remote sensing equation in which the quantity $L(\tau_o,\mu,\phi)$ is the surface radiance, $T(\tau,\mu)$ is the transmittance along the path, and $L_p(\tau,\mu,\phi)$ is the so-called path radiance. The product of the surface radiance and transmittance is sometimes called beam radiance, i.e.,

$$L_B(\tau,\mu,\phi) = L(\tau_o,\mu,\phi)T(\tau,\mu) \tag{73}$$

Given the optical depth τ, single-scattering albedo ω_o, and the scattering phase function one can calculate all of the quantities on the right-hand side of Equation 72 to determine the total radiance $L(\tau,\mu,\phi)$ at a sensor.

4
THE INVERSION ALGORITHM

We can now derive the expressions for "inverting" the remote sensing equation to extract radiometric quantities which are independent of the atmosphere. In a strict sense this is impossible to do completely because the atmosphere and surface are coupled, that is, the surface conditions partially determine the radiation field in the atmosphere and likewise the radiation field in the atmosphere partially determines the reflectance characteristics of the surface. One is always limited by the inability to measure enough of the environmental parameters to specify the complete state of the medium. Nevertheless, we will derive approximate expressions which are useful for the analysis of remotely sensed data from the Earth's surface.

4.1 REFLECTANCE

Since reflectance is an important parameter in our investigation we will define carefully the various concepts of reflectance In all of the work considered we will neglect the effects of polarization Also, because almost all quantities are spectral, i.e , we are dealing with parameters specified at a given wavelength we will not specifically refer to these quantities as "spectral".

The fundamental quantity called bidirectional reflectance, $\rho(\mu,\phi,\mu',\phi')$ depends upon the spherical coordinates $\theta'(=\cos^{-1}\mu')$, ϕ' of the incoming radiation and the outgoing spherical coordinates $\theta(=\cos^{-1}\mu)$, ϕ. Thus, according to Equation 70 if one knows the upwelling radiance at the surface and the total (solar plus sky) radiance at the surface one can "invert" the integral equation to extract the bidirectional reflectance of the surface. In practice, this is quite difficult because it means the spectroradiometers must be placed at each site to be investigated and "scanned" in angular patterns. The cost in time and money to perform a detailed investigation of even

one square mile of the Earth's surface in this manner would be enormous. Hence, one employs a less detailed but also a much less costly method of collecting data, that is, remote sensing. It is natural to expect that in a less detailed measurement one would lose a certain amount of information In this case we must be willing to sacrifice some knowledge of the goniometric properties of the surface because of the limitations on the number of directions of observations which are available to us for a given pixel of data Thus, we must define more general but important concepts of reflectance.

The directional-hemispherical reflectance is given by

$$\rho(\mu',\phi') = \int_0^{2\pi} \int_0^1 \mu\rho(\mu,\phi,\mu',\phi')d\mu d\phi \tag{74}$$

This reflectance defines how much of the radiant power incident from one direction will be reflected into all directions Another reflectance is the hemispherical-directional reflectance, given by

$$\rho(\mu,\phi) = \frac{\int_0^{2\pi} \int_0^1 \mu'\rho(\mu,\phi,\mu',\phi')L(\tau_o,-\mu',\phi')d\mu'd\phi'}{\frac{1}{\pi}\int_0^{2\pi} \int_0^1 \mu'L(\tau_o,-\mu',\phi')d\mu'd\phi'}, \tag{75}$$

a more complicated expression, but one which describes the radiant power reflected into a given direction (θ,ϕ) as a result of incident radiant power over all incoming directions. The hemispherical reflectance or albedo ρ is defined as

$$\rho = \frac{\int_0^{2\pi}\int_0^1 \mu'\rho(\mu',\phi')L(\tau_o,-\mu',\phi')d\mu'd\phi'}{\int_0^{2\pi}\int_0^1 \mu'L(\tau_o,-\mu',\phi')d\mu'd\phi'} \tag{76}$$

which is the ratio of the power output to the power input to the surface. This quantity ρ is the reflectance most commonly given in tables or graphs and ranges in value from zero to one or from zero per cent to 100 per cent.

It will be useful to consider the effects of solar and sky radiation separately. We therefore use Equation 75 as

$$\rho(\mu,\phi) = \frac{\int_0^{2\pi}\int_0^1 \mu'\rho(\mu,\phi,\mu',\phi')E_o e^{-\tau_o/\mu'}\delta(\mu'-\mu_o)\delta(\phi'-\phi_o)d\mu'd\phi'}{E/\pi}$$

$$+ \frac{\int_0^{2\pi}\int_0^1 \mu'\rho(\mu,\phi,\mu',\phi')L_D(\tau_o,-\mu',\phi')d\mu'd\phi'}{E/\pi} \tag{77}$$

where E is the total irradiance at the surface, i e.,

$$E = \int_0^{2\pi}\int_0^1 \mu'L(\tau_o,-\mu',\phi')d\mu'd\phi' \tag{78}$$

The first term on the right-hand side of Equation 77 represents the solar radiation and the second term represents the diffuse sky radiation. Performing the first integration we get

$$\rho(\mu,\phi) = (1-f)\pi\rho(\mu,\phi,\mu_o,\phi_o)$$

$$+ \pi f \int_0^{2\pi} \int_0^1 \mu'\rho(\mu,\phi,\mu',\phi') \frac{L_D(\tau_o,-\mu',\phi')}{E_D} d\mu' d\phi' \qquad (79)$$

where f is the ratio of the diffuse sky irradiance to the total (solar plus sky) irradiance. Jerlov [22] gives the amount of reflected energy for various f values and thus one can estimate the reflected properties in terms of haze level or cloud cover.

For water studies one tends to avoid the specular angle but it can be of importance particularly if the glitter pattern on the water surface is large. The bidirectional reflectance of a specular surface is

$$\rho(\mu,\phi,\mu',\phi') = \rho_s(\mu',\phi')\delta(\mu'-\mu)\delta(\phi'-\phi-\pi) \qquad (80)$$

where $\rho_s(\mu',\phi')$ depends only on the incoming zenith angle θ' and not the azimuth angle ϕ'. Thus, it can be given by Fresnel's law for unpolarized radiation, i.e ,

$$\rho_s(\mu') = \frac{1}{2} \frac{\sin^2(\theta' - \chi)}{\sin^2(\theta' + \chi)} + \frac{\tan^2(\theta' - \chi)}{\tan^2(\theta' + \chi)} \qquad (81)$$

where

$$\sin\theta' = n_r \sin\chi, \quad \mu' = \cos\theta' \qquad (82)$$

in which χ is the angle of refraction and n_r is the refractive index This formula can be used with Equations 74 and 75 to determine the reflectance properties of water surface with various atmospheric conditions. A plot of the specular reflectance for a refractive index

of 4/3 is given in Figure 13 The diffuse or Lambertian reflectance (Equation 76) has been calculated by various investigators [23,24] for different sky radiances and they obtain values of 0.066 and 0 052. Since our primary interest in this investigation is on the removal of atmospheric effects from multispectral data over water rather than in the physics of the water medium we will not consider these detailed properties of water any further. Interesting reflectance studies can be found in Siegel and Howell [25] and Wezernak et al [26].

4.2 INTRINSIC RADIANCE

We will now develop the expressions for the actual quantities which will be evaluated and used with the multispectral image data

Separating the solar and sky radiation fields the surface radiance can be written as

$$L(\tau_o,\mu,\phi) = \mu_o E_o e^{-\tau_o/\mu_o} \rho(\mu,\phi,\mu_o,\phi_o) + \int_0^{2\pi}\int_0^1 \mu'\rho(\mu,\phi,\mu',\phi')L_S(\tau_o,-\mu',\phi')d\mu'd\phi' \qquad (83)$$

If the atmosphere were to disappear the only component which remains is the extraterrestrial component and the sky radiance $L_S(\tau_o,-\mu,\phi)$ vanishes Thus, as $\tau_o \to 0$ Equation 83 gives us the radiance for the case of no atmosphere at all, or the "intrinsic" radiance,

$$L_I(\mu,\phi) = \mu_o E_o \rho(\mu,\phi,\mu_o,\phi_o) \qquad (84)$$

This radiance is what would be measured if one were doing remote sensing of the lunar surface from a spacecraft We would like to have the same radiance for the Earth's surface Equation 83 can be written as

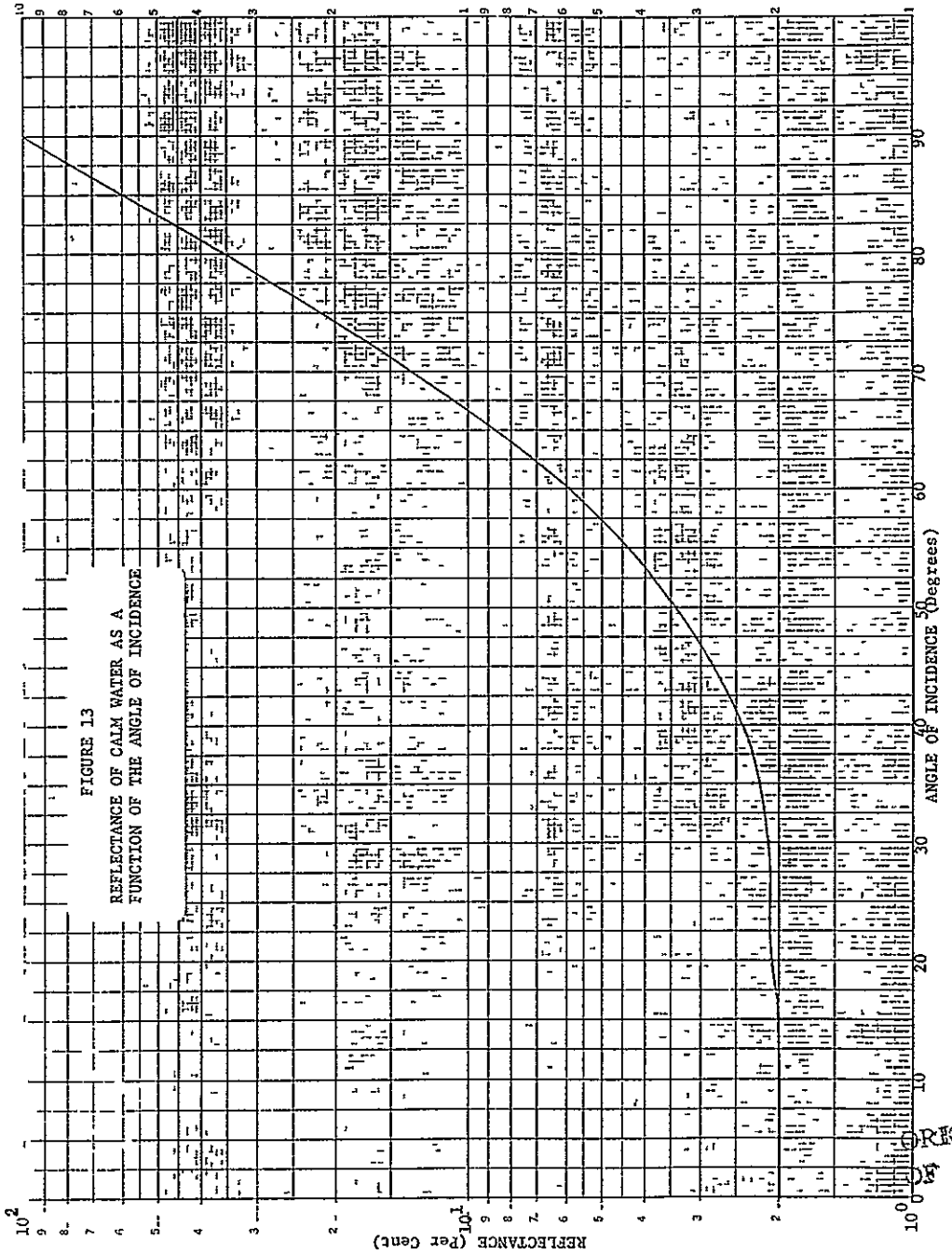

FIGURE 13

REFLECTANCE OF CALM WATER AS A FUNCTION OF THE ANGLE OF INCIDENCE

$$L(\tau_o,\mu,\phi) = L_I(\mu,\phi)e^{-\tau_o/\mu_o}$$

$$+ \int_0^{2\pi} \int_0^1 \mu'\rho(\mu,\phi,\mu',\phi')L_S(\tau_o,-\mu',\phi')d\mu'd\phi' \qquad (85)$$

or, using the equation for the hemispherical-directional reflectance we have,

$$L(\tau_o,\mu,\phi) = L_I(\mu,\phi)e^{-\tau_o/\mu_o} + \frac{E_s(\tau_o)}{\pi}\rho(\mu,\phi) \qquad (86)$$

It should be noted that up to this point there have been no approximations in the formalism Equation 86 is exact and if the intrinsic radiance and the surface radiance were known the reflectance $\rho(\mu,\phi)$ could then be found. The problem is that one usually does not have enough information regarding the sky radiance, $L_s(\tau_o,-\mu,\phi)$ in Equation 85 in order to evaluate the integral. Therefore, we must make some approximations in order to arrive at a meaningful solution If we make the assumption that the surface is perfectly diffuse for the sky radiation then the bidirectional reflectance is a constant and Equation 85 becomes

$$L(\tau_o,\mu,\phi) = L_I(\mu,\phi)e^{-\tau_o/\mu_o} + \frac{L_I(\mu,\phi)}{\mu_o E_o}E_s(\tau_o) \qquad (87)$$

or

$$L(\tau_o,\mu,\phi) = \frac{E(\tau_o)}{\mu_o E_o}L_I(\mu,\phi) \qquad (88)$$

where $E_s(\tau_o)$ is the diffuse sky irradiance and $E(\tau_o)$ is the total (solar plus sky) irradiance at the surface. Now, using the remote sensing equation we get

$$L(\tau,\mu,\phi) = \frac{E(\tau_o)}{\mu_o E_o} L_I(\mu,\phi)T(\tau,\mu) + L_p(\tau,\mu,\phi) \tag{89}$$

Inverting this equation we finally obtain the intrinsic radiance for the surface, i.e.,

$$L_I(\mu,\phi) = F(\tau,\mu,\phi)L(\tau,\mu,\phi) - G(\tau,\mu,\phi) \tag{90}$$

where

$$F(\tau,\mu,\phi) = \frac{\mu_o E_o}{E(\tau_o)T(\tau,\mu)} \tag{91}$$

and

$$G(\tau,\mu,\phi) = F(\tau,\mu,\phi)L_p(\tau,\mu,\phi) \tag{92}$$

Equation 90 then is the basic algorithm for the determination of the radiance characteristic of the Earth's surface free of any atmospheric effects. The functions $F(\tau,\mu,\phi)$ and $G(\tau,\mu,\phi)$ can be calculated according to the atmospheric radiative-transfer model and in some cases can be determined experimentally. Thus, we see that the multiplicative and additive (or subtractive) operators act upon the multispectral image data $L(\tau,\mu,\phi)$ to produce the intrinsic multispectral image data $L_I(\mu,\phi)$.

We can now find the bidirectional reflectance of the surface from Equations 90 and 84, i.e.,

$$\rho(\mu,\phi,\mu_o,\phi_o) = L_I(\mu,\phi)/\mu_o E_o \tag{93}$$

where it must be realized that the surface is considered to be diffuse for the sky radiation only, not for the solar part If one assumes that the surface is diffuse for the solar and the sky radiation then the diffuse reflectance is given by

$$\rho = \pi\rho(\mu,\phi,\mu_o,\phi_o) \tag{94}$$

4.3 FLIGHT CONFIGURATION

Having defined the basic mathematical algorithm to be used we will now describe the procedure for specifying of the input image data, the geometry of the sensor and the environment which is to be investigated The description of the computer program employed will, however, be general enough so that its use is not limited to a particular sensor

The geometrical arrangement of the sensor with respect to the environment can be defined by using a right-handed coordinate system as illustrated in Figure 14 A sensor is located at point Q viewing radiation along the vertical scan plane P_1QP_n where the scan line across the surface is P_1P_n The important point for the user to remember is the location of the first pixel in a given scan line That point defines the critical angle ϕ with respect to the Earth's coordinate system. In Figure 14 the aircraft (or spacecraft) is moving in a Northeasterly direction with a right-handed scan We call this a system with positive helicity. If the craft were moving in a Southwesterly direction P_1 and P_n would be interchanged but the helicity would still be positive. The helicity is inherent in the scanning system. If the direction of flight is denoted by the vector $\vec{F}$ and the spin vector of the scanner by $\vec{S}$ then the helicity H is defined as the outer or

$$H = \frac{\vec{F} \times \vec{S}}{|\vec{F}||\vec{S}|} \tag{95}$$

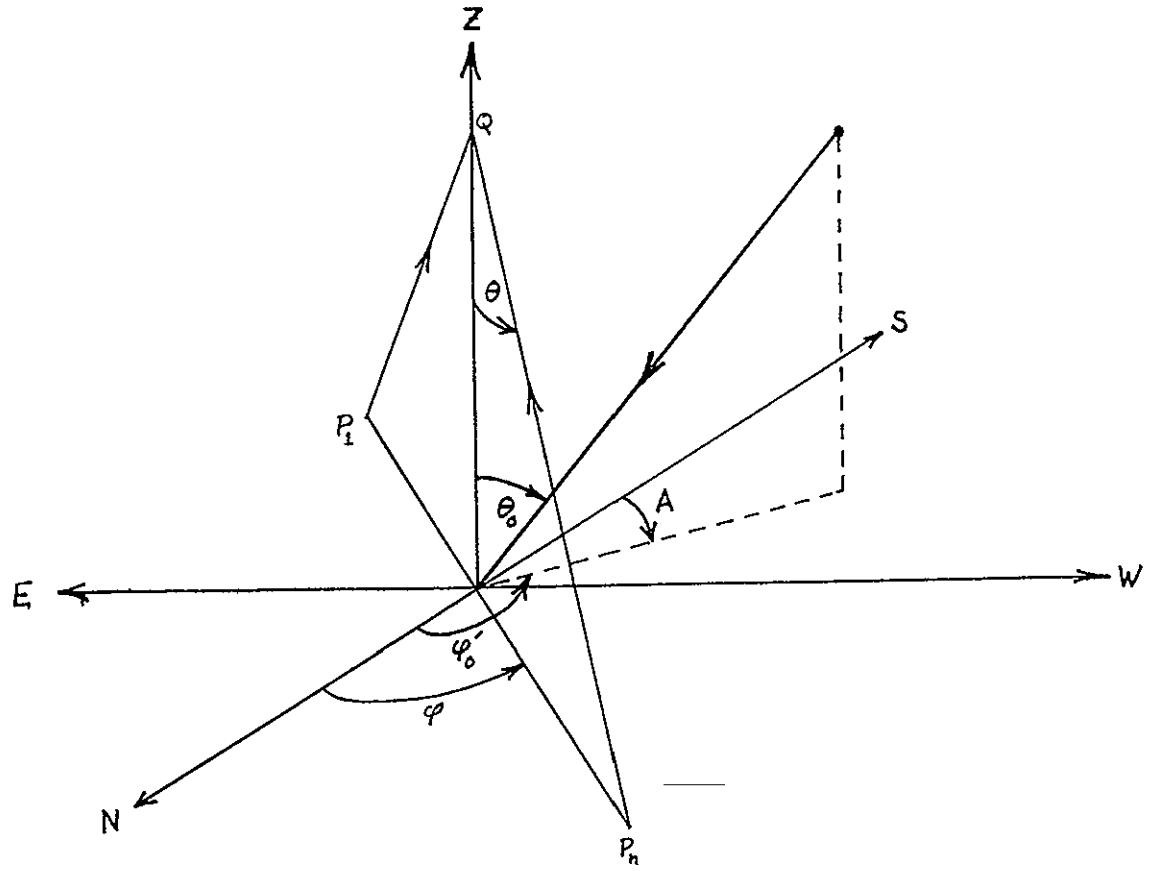

$L(\tau_o,\mu,\phi)$ ∿ Radiation Northward (Projected)

$L(\tau_o,\mu,\phi+\pi)$ ∿ Radiation Southward (Projected)

$\mu = \cos\theta$

θ_o ∿ Solar Zenith Angle

ϕ_o' ∿ Complementary Solar Azimuth Angle

A ∿ Solar Azimuth Angle

ϕ ∿ Relative Azimuth Angle

FIGURE 14. COORDINATE SYSTEM FOR THE MULTISPECTRAL SCANNER

cross product of the corresponding unit vectors. Thus,

$$H = \begin{cases} +1 \text{ for a right-handed scanner} \\ -1 \text{ for a left-handed scanner} \end{cases} \quad (96)$$

The user need not be concerned with deriving the solar zenith angle θ_o or the solar azimuth angle A (or ϕ_o') as these are computed automatically once the latitude, longitude, date, time of day (Standard time), and zone number are specified. For convenience, the international time zones are given in Figure 15 and the time zones for the United States are given in Figure 16. As an example, Cleveland, Ohio is in the Eastern time zone with zone number +5. The subroutine for the computation is quite accurate and it has been checked against the Nautical Almanac. The maximum error is only a fraction of the angular size of the Sun itself.

The extraterrestrial solar irradiance, $E_o(\lambda)$ is calculated using the NASA Standard Values by Thekaekara and Drummond [27] and are illustrated in Figure 17 for a mean Earth-Sun distance. We correct for the variation with distance on a day by day basis.

4.4 ALGORITHM INPUT PARAMETERS

Besides the geometric parameters as defined in the previous section we must now specify those parameters which are characteristic of the medium and the measurement system.

4.4.1 ALTITUDE

There are several "altitudes" which must be specified. First one must know the actual altitude (km) of the sensor above the surface. Second, one must know the pressure (millibars) of the atmosphere at the surface, and third, one must know the atmospheric pressure (millibars) at flight altitude. If only the altitudes are known one can use the tables relating pressure to altitude as given by the U.S. Standard

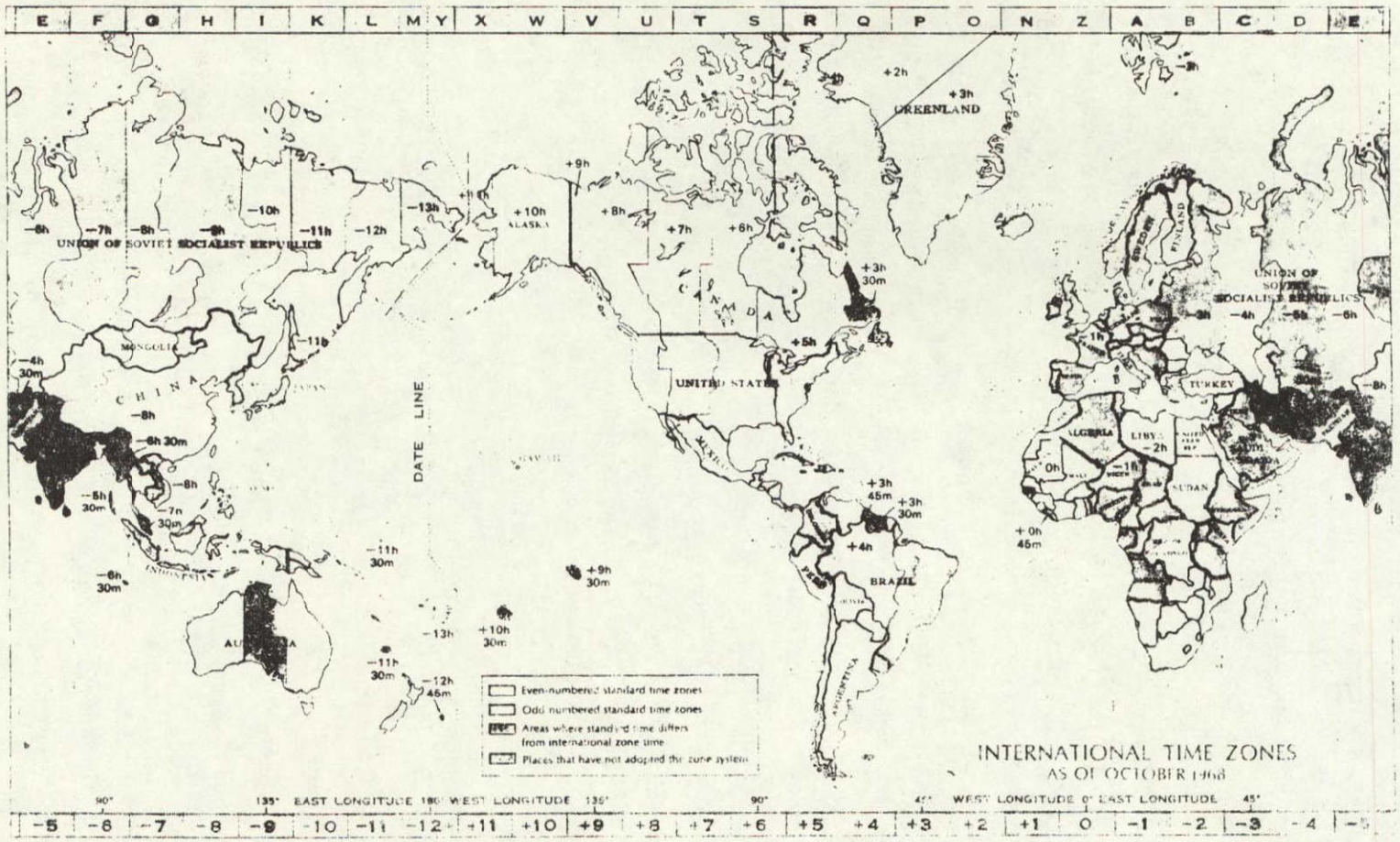

FIGURE 15. INTERNATIONAL TIME ZONES

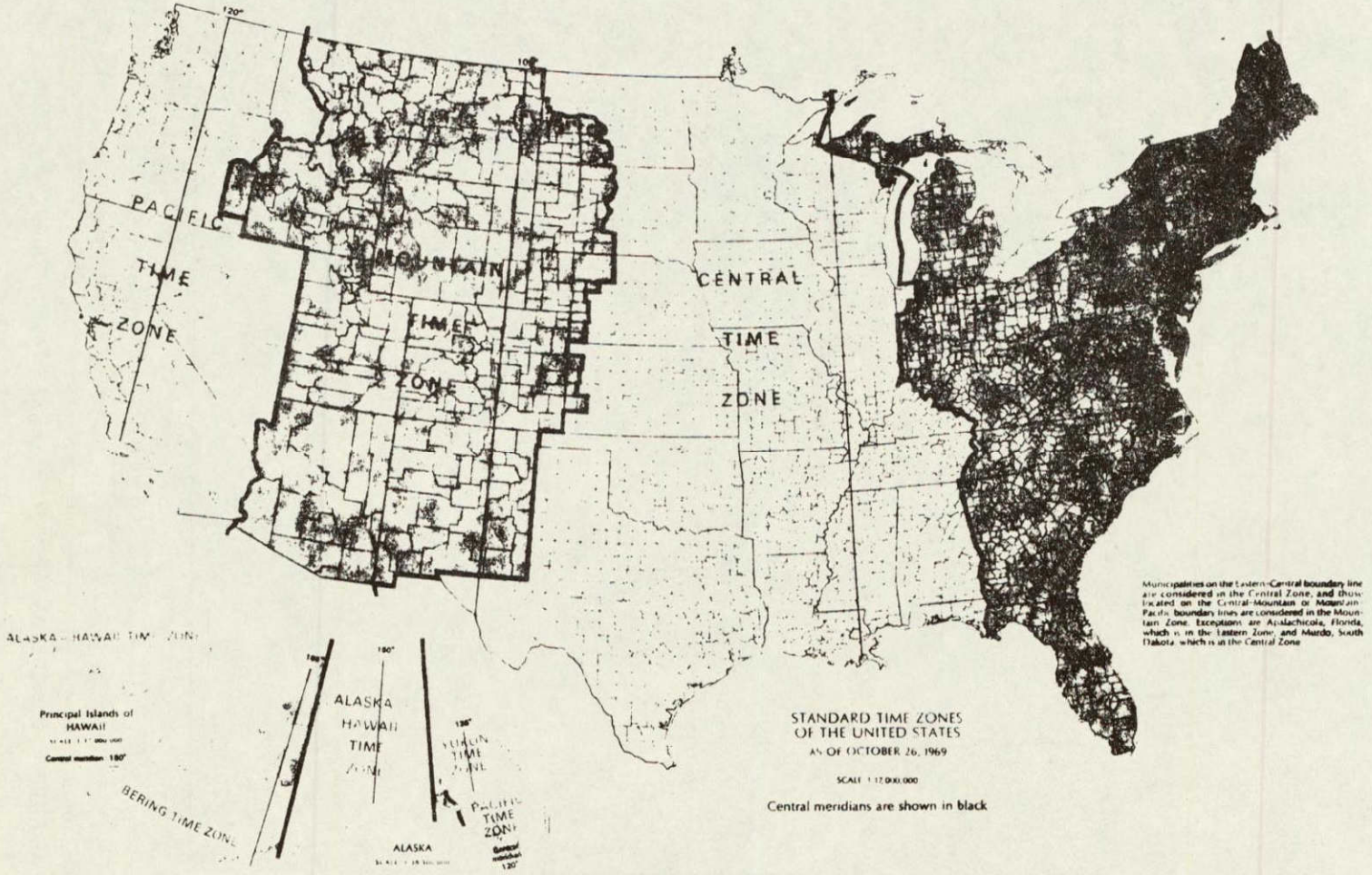

FIGURE 16. STANDARD TIME ZONES OF THE UNITED STATES

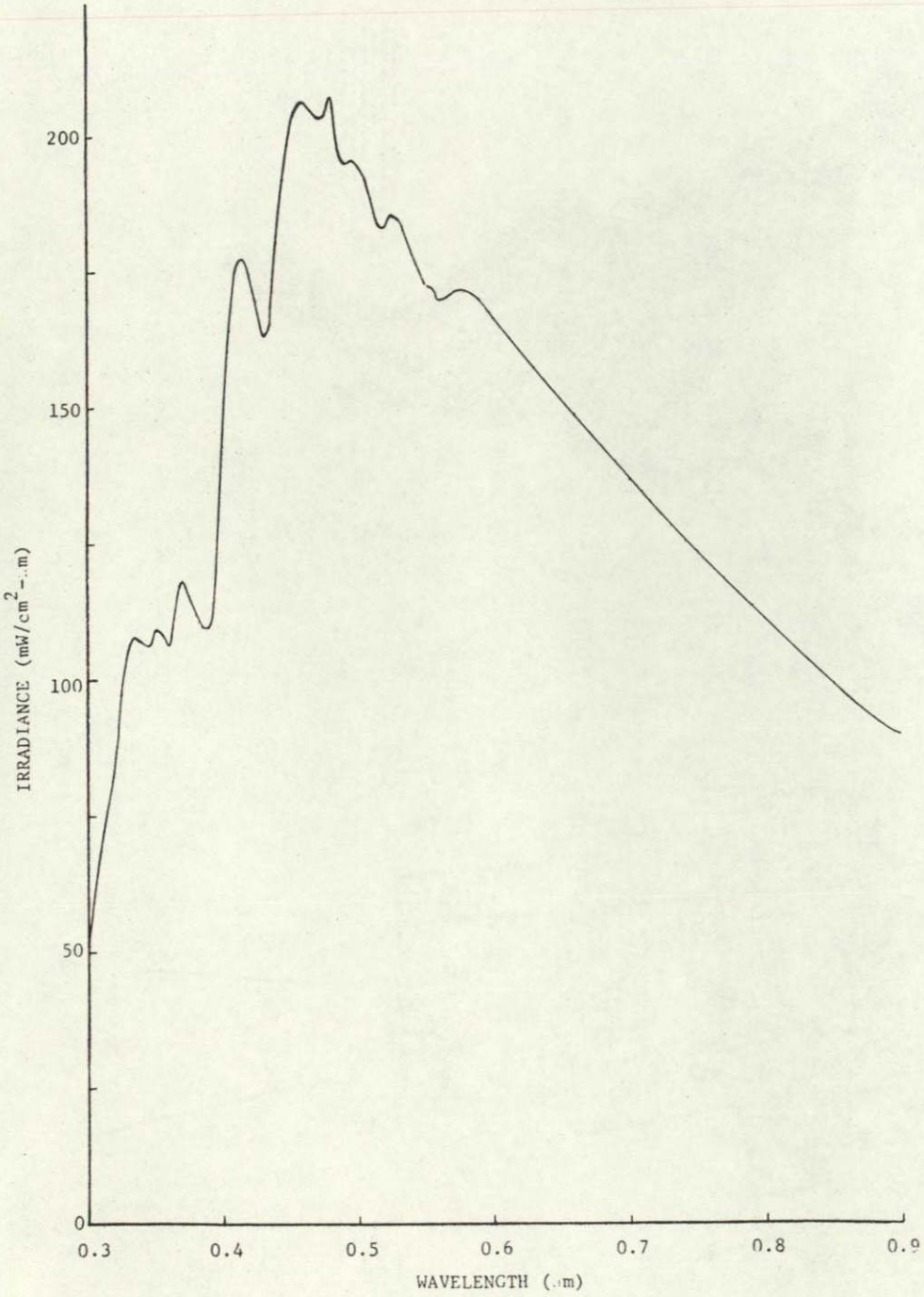

FIGURE 17. NASA STANDARD EXTRATERRESTRIAL SOLAR SPECTRUM

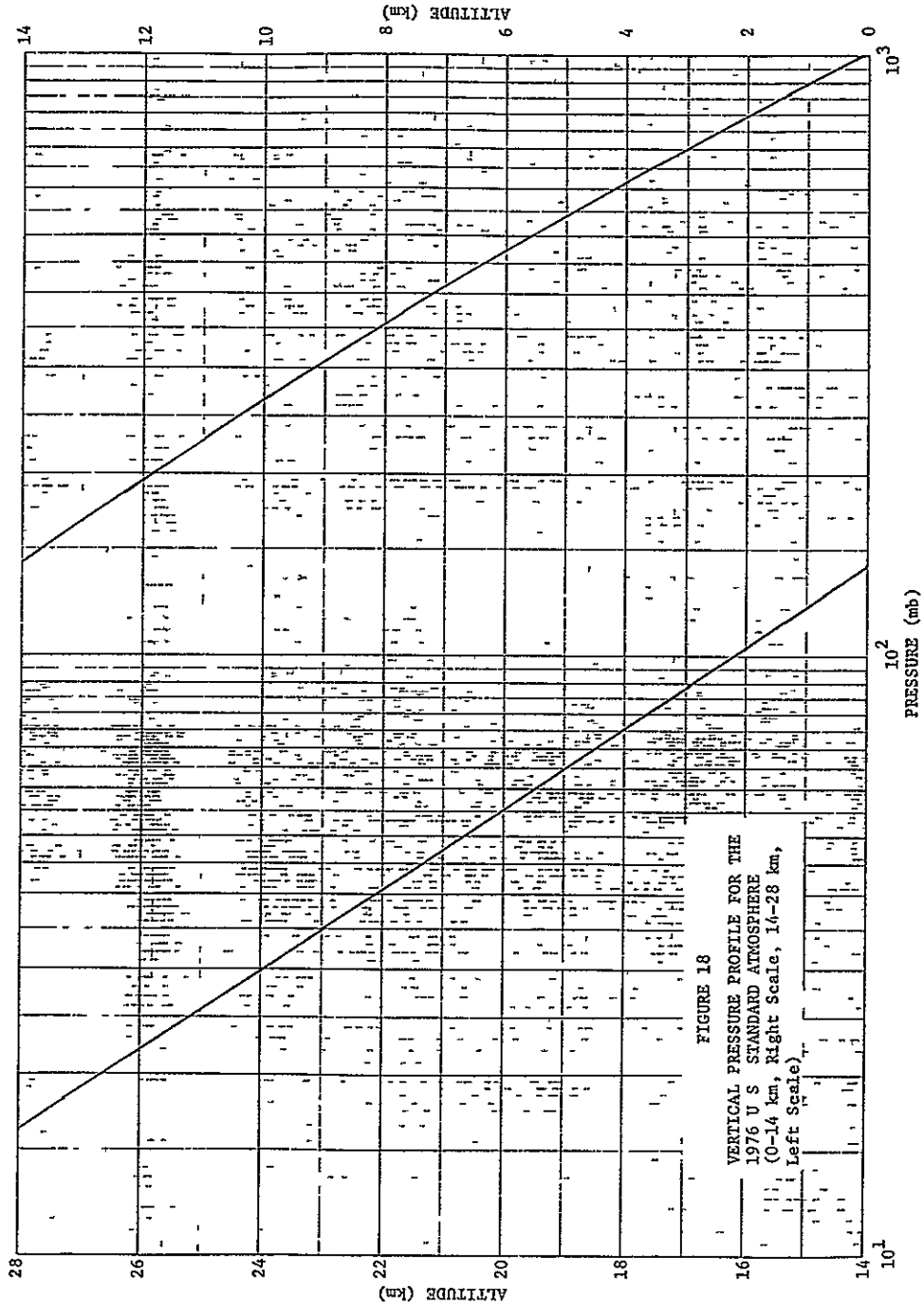

FIGURE 18

TABLE 1

OCS-2-NASA/LEWIS

CONVERSION FACTORS

Channel	λ_o (μm)	F(G = 1)	F(G = 1 5)	F(G = 2.0)	F(G = 3 0)
1	0 428	5.520617	3.680411	4 907215	7.360822
2	0.466	5 349853	3.566569	4 755425	7.1331373
3	0 508	4 643580	3.095720	4 127626	6.191439
4	0 549	4 301303	2 867535	3 823380	5.735070
5	0.592	4.022688	2.681792	3.575723	5.363584
6	0.632	3.680411	2 453607	3.271477	4.907215
7	0.674	3 123931	2.082620	2 776827	4 165241
8	0 714	2.353995	1 569330	2 092440	3 138660
9	0 756	26 812927	17 875285	23.833713	35 750569
10	0 794	1.241034	0.8273560	1 103141	1 654712

Note

$$L(mW/cm^2\text{-}sr\text{-}\mu m) = \frac{FC}{100}$$

where C is the count value from 0 to 255

G is the gain setting

of completeness because they are actually part of the input data.

A number of single scattering phase functions are included with the program. The user may use any phase functions he wants as long as they are realistic for the conditions and satisfy the following normalization relation:

$$\int_{-1}^{1} p(\mu)d\mu = 2 \tag{98}$$

where $p(\mu)$ is the phase function for an angle $\theta(= \cos^{-1}\mu)$. The phase functions which we have made available with the program are of two sets, one corresponding to a maritime haze and one corresponding to a continental haze. Previous work has shown that there is not much difference in the results between the two particulate distributions especially when the visual range is large. The maritime haze is that one characteristic of conditions over large bodies of water such as oceans and seas The continental haze is characteristic of conditions over the land. In either case we have a phase function for the following complex refractive indices of the particulates

$$m = \begin{cases} 1.5 - 0.0i \\ 1.5 - 0.01i \\ 1.5 - 0.10i \\ 1.5 - 1.0i \end{cases} \tag{99}$$

The first of these corresponds to a "clean" haze, i e , one which does not absorb radiation, the second has a slight amount of absorption, and so on. A general, worldwide refractive index would probably be $m = 1.5 - 0.04i$ but there can be considerable local variation about this value. A user can easily determine the sensitivity of the results by simply running the program with different phase functions.

Another quantity which can be changed to correspond with the phase functions is the scattering fraction, f_s, defined as

$$f_s = \frac{\tau^s_{o,A}}{\tau_{o,A}} \tag{100}$$

(called FSCAT in the program) It is the ratio of the scattering part of the aerosol optical thickness to the total aerosol optical thickness and is related to the refractive index. If $f_s = 0$ the particles are absorbing all radiation (and re-radiating it in the thermal region) whereas if $f_s = 1$ the particles scatter all the incident energy Unfortunately the exact relation between f_s and the phase functions involves a more detailed mathematical investigation in radiative-transfer theory and Mie scattering theory than we can present here One should note however, that it would be inconsistent to use an f_s value of zero with the phase function with a refractive index of 1 5 - 0 0i or an $f_s = 1$ with m = 1.5 - 1.0i. The quantity f_s is used to compute the forward scattering fraction η given by

$$\eta = \frac{0\ 96\ f_s\ \tau_{o,A} + 0\ 5\ \tau_{o,R}}{f_s\ \tau_{o,A} + \tau_{o,R}} \tag{101}$$

and the single-scattering albedo ω_o

$$\omega_o = \frac{\tau_{o,R} + f_s\ \tau_{o,A}}{\tau_o} \tag{102}$$

where

$$\tau_o = \tau_{o,R} + \tau_{o,G} + \tau_{o,A} \tag{103}$$

Another quantity which one should change depending upon the season or latitude is the ozone column density. The difference in the results for different densities should be slight for the visible and near infrared parts of the spectrum unless one has extremely clear atmospheric conditions in which case the ozone makes up a larger percentage contribution to the total optical thickness. We have included with the program five ozone integrals, those corresponding to tropical, mid-latitude summer, mid-latitude winter, sub-arctic summer, and sub-arctic winter. To obtain these column densities we integrated the corresponding ozone density profiles as given by McClatchey et al. [9] for these conditions A switch is in the program so the user can select a given condition by simply changing the switch value. Other parameters related to the ozone integrals are, the number of altitudes in the integral and the number of integrals to be read The ozone absorption function $A(\lambda)$ in Equation 13 is also included as data but the values used in this program have been the accepted values for about 25 years and will probably not change much in future measurements The "cutoff" wavelengths of 0 362 μm and 0 439 are also included as "constant" data.

Finally, there are data values for the aerosol model atmospheres Measurements of the stratospheric aerosol distribution are infrequent and only in recent years has there been the impetus to perform satellite measurements of this component. Hence, we consider the input data for the stratospheric aerosol to include the number of wavelengths in the "R" function (Equation 57), the number of profiles (currently one), and the number of altitudes in each profile If additional modeling of the stratospheric component were desired then more profiles could be included. For this reason we have included a switch for the number of the profile desired

The "gamma" function, although included with the input data should not be altered

4.4 4 SPECIFICATION OF IMAGE AREA

Everything described so far has concerned the input data for implementing the atmospheric correction algorithm. We must also describe the subset of MSS data to be processed and the input tape format The first input data card (NSA card) specifies the initial scan line, final scan line, and scan line increments for processing followed by the starting pixel, final pixel and pixel increments for processing points on those lines. For example, if one wants to analyze every line from the second through the fiftieth and each of the 344 pixels per line the entry would be 2, 50, 1, 1, 344, 1. The second input data card specifies the number of pixels available, the maximum scan angle (radians), and the angular scan interval (radians). For the OCS sensor these values would be 344, 770035, and .00449 respectively The third input data card defines the subset of the scan line data buffer which is to be processed by the atmospheric routine Input values of 3, 344, 5 specify that beginning with the third pixel brought into the scan line data buffer according to the NSA card, the atmospheric program should process every 5th pixel (i.e , pixel 4, 9, 14, ..., 344 of the original data tape.

4 4.5 SAMPLE DATA

For ease of application we present here a listing of input data which were used on an actual data set Table 2 includes all inputs including those corresponding to the selection of data points which was just described in the preceding section. A single asterisk denotes those quantities which will change with almost every data collection, the double asterisk denotes quantities which change only a few times, and the remaining quantities rarely change.

4 5 ALGORITHM OUTPUT PARAMETERS

The program is designed to produce an image tape in exactly the same format as the original data set except that atmospheric effects

TABLE 2. SAMPLE INPUT DATA

```
 1    DFBUG,LINE,ATM,IAL,PACK,SPE,IAC,OZONE,AEROSOL,THICKNESS,FSR,PF,RAYLEIGH,SOLAR,PARAMS,DFCAL,DFSR,032UBU,MONITOR,SG64,SPRAY
 3    1,0,1,1,382,1
 4    382,.877665, .0045689   } IMAGE DATA FORMAT (SEE TEXT)
 5    5,30,5
 * 6      6   51976 <-------- DATE   MONTH, DAY  YEAR
 * 7      8   23 0 0 <-------- TIME   STANDARD TIME, 24 HR SYSTEM
 ** 8     5 <-------- TIME ZONE NUMBER
 * 9     41   47 0 0     112   45 0 0 <-------- LATITUDE AND LONGITUDE OF TEST SITE (DEGREES MINUTES, SECONDS)
 *10  12 323   0.0       6 <-------- SENSOR ALTITUDE (km)  BASE ALTITUDE (km), SWITCH FOR DESIRED OUTPUT
 **11    428      466      .508      .549      .592      632      674      714      756      794 <-- CENTER WAVELENGTHS (µm) FOR SENSOR
 *12    .02       02       02        02        02       02       02       02       02      .02 <-- ALBEDO OF BACKGROUND FOR SENSOR WAVELENGTHS
 **-1   1.5,.01, <-------- PARTICULATE REFRACTIVE INDEX (Real, Imaginary)
  1   13,38, <-------- NUMBER OF WAVELENGTHS FOR PHASE FUNCTION, NUMBER OF ANGLES FOR PHASE FUNCTION
  3   1.0       .999391  .997564  .994522  .990268  .984808  .978148  .970296  .961262  .951057 }
  4   .939693  .866025  .766044  .642788  .50      .342020  .173648  .0       -.173648 -.342020 } COSINES OF ANGLES FOR PHASE FUNCTION
  5   -.50     -.642788 -.766044 -.866025 -.939693 -.984808 -.996954 -.999391 -.997564 -.994522 }
  6   -.970296 -.978148 -.984808 -.990268 -.994522 -.997564 -.999391 -1 0
  7   0 40 <-------- WAVELENGTH (µm)
  8    90.7202 82.3252 62.1350 40.5396 24.9011 16.1030 11.0784  8.7039  6.8880  5.5912
  9     4.7005  2.4603  1.4890  0.9554  0.6458  0.4414  0.2849  0.2032  0.1513  0.1206
 10     0.1063  0.1109  0.1212  0.1460  0.2005  0.2668  0.4269  0.5648  0.6393  0.6849
 11     0.6959  0.7237  0.7793  0.7820  0.7164  0.7180  0.8456  0.9320
 12   0,45
 13    81.3277 74.2287 57.0479 38.4010 24.5189 16.3427 11.8080  9.0073  7.1147  5.8181
 14     4.8822  2.5293  1.5180  0.9677  0.6523  0.4455  0.2880  0.2062  0.1546  0.1243
 15     0.1105  0.1159  0.1301  0.1522  0.2070  0.2721  0.4255  0.5542  0.6201  0.6597
 16     0.6694  0.6907  0.7331  0.7361  0.6941  0.7162  0.8404  0.9191
 17   0,50
 18    73.1068 67.1017 52.4761 36.3692 24.0512 16.4799 12.0743  9.2768  7.3627  6.0277
 19     5.0604  2.5995  1.5471  0.9796  0.6282  0.4191  0.2907  0.2088  0.1574  0.1275
 20     0.1141  0.1203  0.1353  0.1577  0.2125  0.2761  0.4225  0.5417  0.5997  0.6338
 21     0.6419  0.6577  0.6992  0.6948  0.6724  0.7105  0.8305  0.9021
 22   0,55
 23    65.9416 60.8556 48.3897 34.4608 23.5266 16.5328 12.2832  9.5125  7.5904  6.2297
 24     5.2324  2.6700  1.5760  0.9911  0.6337  0.4221  0.2928  0.2109  0.1598  0.1302
 25     0.1174  0.1242  0.1398  0.1623  0.2169  0.2788  0.4180  0.5279  0.5788  0.6078
 26     0.6141  0.6255  0.6506  0.6576  0.6515  0.7015  0.9167  0.8820
 27   0,60
 28    59.5664 55.2826 44.7030 32.6833 22.9784 16.5212 12.4806  9.7165  7.7994  6.4214
 29     5.3989  2.7401  1.6042  1.0021  0.6388  0.4248  0.2946  0.2126  0.1619  0.1326
 30     0.1202  0.1276  0.1437  0.1663  0.2204  0.2804  0.4123  0.5133  0.5577  0.5821
 31     0.5867  0.5948  0.6144  0.6236  0.6307  0.6898  0.8001  0.8598
 32   0,65
 33    54.3080 50.6364 41.5213 31.0407 22.3937 16.4894 12.5550  9.8881  7.9820  6.5931
 34     5.5518  2.8085  1.6325  1.0126  0.6432  0.4270  0.2960  0.2140  0.1635  0.1346
 35     0.1226  0.1305  0.1470  0.1695  0.2228  0.2809  0.4056  0.4978  0.5366  0.5572
 36     0.5602  0.5653  0.5814  0.5938  0.6115  0.6762  0.7807  0.8352
 37   0,70
 38    49.7002 46.5483 38.6822 29.5281 21.8118 16.3304 12.6310 10.0315  8.1450  6.7517
 39     5.6960  2.8753  1.6598  1.0228  0.6474  0.4289  0.2971  0.2151  0.1619  0.1363
 40     0.1247  0.1330  0.1498  0.1721  0.2245  0.2805  0.3982  0.4822  0.5159  0.5331
 41     0.5349  0.5379  0.5513  0.5668  0.5927  0.6611  0.7602  0.8105
 42   0,80
 43    42.0527 39.7363 33.8800 26.8719 20.6901 16.0347 12.6906 10.2456  8.4172  7.0302
 44     5.9564  3.0024  1.7122  1.0421  0.6553  0.4322  0.2988  0.2168  0.1670  0.1390
 45     0.1282  0.1370  0.1540  0.1758  0.2261  0.2779  0.3818  0.4512  0.4765  0.4880
 46     0.4877  0.4881  0.4997  0.5193  0.5564  0.6279  0.7161  0.7581
 47   0,90
 48    36.2598 34.5289 30.0074 24.6506 19.0411 15.0644 12.0691 10.3708  8.6207  7.2530
 49     6.1761  3.1193  1.7614  1.0604  0.6625  0.4350  0.3001  0.2179  0.1684  0.1410
```

PHASE FUNCTIONS FOR WAVELENGTHS 0.40 µm TO 2.17 µm

TABLE 2. SAMPLE INPUT DATA (Cont'd)

```
 50      0 1347  0 1398  0 1569  0 1779  0 2057  0 2732  0 3646  0 4214  0 4403  0 4477
 51      0 1461  0 1461  0 1566  0 1799  0 2229  0 5933  0 6712  0 7067
 52    1 06
 53     29 6370 28  143 25 5817 21 8260 18 1551 15 0221 12 4882 10 4590  8 8300  7 5185
 54      6 4549  3 3841  1 8339  1 0804  0 6738  0 4394  0 3020  0 2194  0.1703  0.1433
 55      0 1335  0 1426  0.1593  0 1789  0.2223  0 2634  0 3371  0 3783  0 3899  0 3932
 56      0 3910  0 3916  0 4029  0 4292  0 4749  0 5395  0 6078  0 6301
 57    1 26
 58     24 2957 23 5951 21 7244 19.2216 16 6175 14 2292 12 1624 10 4129  8 9444  7 7146
 59      6 6824  3 4539  1 9148  1 1221  0 6883  0 4455  0 3047  0 2212  0.1721  0 1454
 60      0 1359  0 1445  0 1602  0.1779  0 2158  0 2496  0 3058  0 3332  0 3595  0 3404
 61      0 3390  0 3413  0 3540  0 3812  0 4245  0 4790  0 5281  0 5482
 62    1 67
 63     18.3815 17 9755 17 0733 15 7806 14 3042 12.8036 11 3727 10 0563  8 0707  7.8165
 64      6 8862  3 6998  2.0542  1.1904  0 7224  0 4626  0 3140  0 2270  0 1766  0 1493
 65      0 1394  0 1462  0.1592  0.1730  0 2009  0 2235  0 2559  0 2684  0 2706  0 2710
 66      0 2722  0 2779  0 2918  0 3158  0 3489  0 3853  0 1148  0 4263
 67    2 17
 68     14 6515 14 4827 14.0020 13.2763 12 3891 11 4181 10 4239  9 4486  8.5189  7 6503
 69      6 8505  3 8686  2.1885  1 2731  0.7713  0.4911  0 3316  0.2386  0 1849  0 1558
 70      0.1443  0 1482  0.1580  0.1679  0.1869  0 2009  0 2186  0 2279  0 2265  0.2284
 71      0 2328  0 2394  0 2521  0.2704  0 2928  0 3151  0 3370  0 3384
*14      992       17  431 <------ ATMOS  PRESSURE (MILLIBARS) AT TEST SITE, PRESSURE (MILLIBARS) AT SENSOR ALTITUDE
**15      71    1    7    8 <------ NO  OF OZONE ALTITUDES, NO  OF OZONE INTEGRALS  NO  OF OZONE WAVELENGTHS BEFORE AND AFTER CUTOFF
 16       362      439 <------ FIRST AND SECOND OZONE CUTOFF WAVELENGTHS (μm)
  1         1  6 0134E-05
  2         2  1 2040E-04
  3         3  1 8090E-04
  4         4  2 4393E-04
  5         5  3 0892E-04
  6         6  5 7617E-04
  7         7  8 4820E-04
  8         8  5 2507E-04
  9         9  6 0781E-04
 10        10  6 9497E-04
 11        11  7 9485E-04
 12        12  9 0956E-04
 13        13  1 0431E-03
 14        14  1 2096E-03
 15        15  1 3951E-03
 16        16  1 5939E-03
 17        17  1 8187E-03
 18        18  2 0774E-03
 19        19  2 3787E-03
 20        20  2 7095E-03
 21        21  3 0600E-03
 22        22  3 4222E-03
 23        23  3 7729E-03
 24        24  4 1027E-03
 25        25  4 4129E-03
 26        30  5 6857E-03
 27        35  6 3996E-03
 28        40  6 7126E-03
 29        45  6 8418E-03
 30        50  6 8747E-03
 31        51  6 8787E-03
 32        52  6 8822E-03
 33        53  6 8854E-03
 34        54  6.8883E-03
 35        55  6 8912E-03
```

** OZONE EQUIVALENT THICKNESS (cm/km)

TABLE 2. SAMPLE INPUT DATA (Cont'd)

```
36        56  6 8939E-03
37        57  6 8967E-03
38        58  6 8996E-03
39        59  6 9026E-03
40        60  6 9057E-03
41        61  6 9092E-03
42        62  6 9129E-03
43        63  6 9169E-03
44        64  6 9214E-03
45        65  6 9264E-03
46        66  6 9319E-03
47        67  6 9381E-03
48        68  6.9449E-03
49        69  6 9524E-03
50        70  6 9606E-03
51        71  6 9696E-03
52        72  6 9792E-03
53        73  6.9894E-03
54        74  7 0000E-03
55        75  7 0108E-03
56        76  7 0218E-03
57        77  7 0325E-03
58        78  7 0427E-03
59        79  7 0523E-03
60        80  7 0609E-03
61        81  7 0685E-03
62        82  7 0750E-03
63        83  7 0803E-03
64        84  7 0844E-03
65        85  7 0876E-03
66        86  7 0898E-03
67        87  7 0914E-03
68        88  7 0925E-03
69        89  7 0931E-03
70        90  7 0935E-03
71       100  7 1010E-03
**10   7 1010  E-03 <-- MAXIMUM OZONE EQUIVALENT THICKNESS (cm/km)
1         27 2 10  E 02 \
2         28 1 06  E 02  |
3         30 1 01  E 01  |
4         32 8 98  E -1  |
5         34 6 80  E -2  |
6         36 1 80  E -3  |
7        362 1 00  E -3  |  OZONE ABSORPTION FUNCTION (cm^-1) IN TERMS OF WAVELENGTH
8        439 1 00  E -3  |
9         45 3 50  E -3  |
10        50 3 45  E -2  |
11        55 9 20  E -2  |
12        60 1 32  E -1  |
13        65 6 20  E -2  |
14        70 2 30  E -2  |
15        80 1 00  E -2 /
**20      1 <-- NO OF OZONE INTEGRAL
**21    6 <-- NO OF EXPERIMENTAL OPTICAL THICKNESSES
22        40        6  \
23      0.50       .38  |
24      0 61       30   |  EXPERIMENTAL WAVELENGTHS AND OPTICAL THICKNESSES
25        7017      21  |
26        8730      19  |
27      1 04        23 /
```

TABLE 2 SAMPLE INPUT DATA (Cont'd)

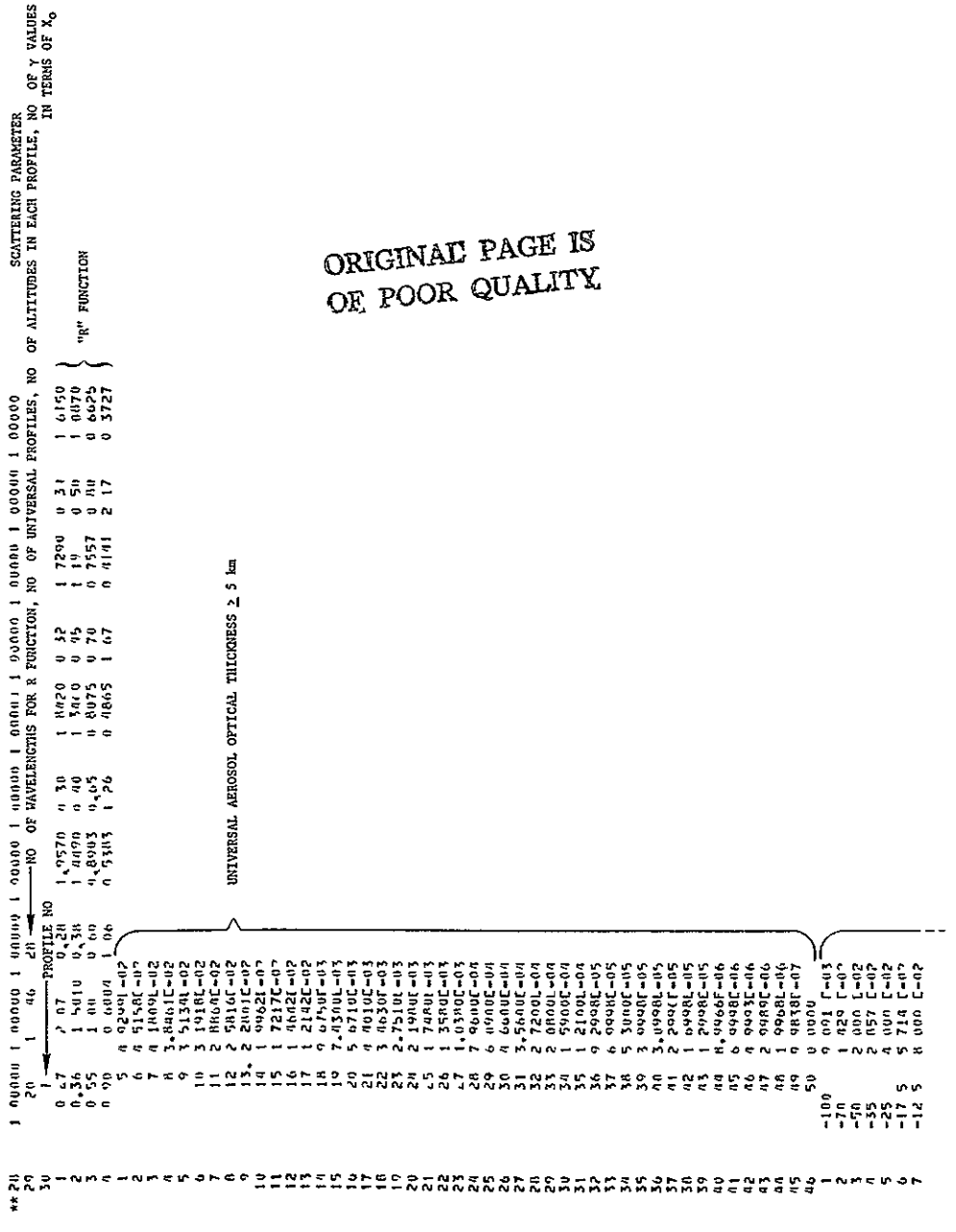

ORIGINAL PAGE IS
OF POOR QUALITY

TABLE 2 SAMPLE INPUT DATA (Cont'd)

```
  8      -8 75   1.143 E-01
  9      -6 25   1 597 E-01
 10      -4 38   2 256 E-01
 11      -3 13   3 055 E-01
 12      -2      4 323 E-01
 13      -1 5    5 173 E-01
 14      -1      6 321 E-01
 15      -  5    7 869 E-01
 16       0      1 000 E 00
 17       1      1 718 E 00
 18       1 5    2 321 E 00
 19       2      3.195 E 00
 20       2 5    4 473 E 00
 21       3      6 352 E 00
 22       3 5    9 176 E 00
 23       4      1 340 E 01
 24       4 5    1 978 E 01
 25       5      2 948 E 01
 26       5 5    4 431 E 01
 27       6      6 707 E 01
 28       6 475  1 0048  2
*30       2 50 0.0
END OF FILE
```

GAMMA" FUNCTION

AZIMUTH ANGLE (DEGREES MINUTES, SECONDS)

have been removed. An option switch has therefore been included so that one can produce various output data sets. If the switch (LSW) is set equal to 1 the output is the digitized path radiance. If LSW=2 the output consists of beam radiance (digitized), if LSW=3 one gets surface radiance (digitized), if LSW=4 the digitized intrinsic radiance results, and if LSW=5 the (digitized) reflectance is produced If LSW=6 all of these quantities (non-digitized) are printed out including the input data in radiometric units In addition, much of the input data is also printed and the direct solar and the total irradiance is printed The optical thicknesses interpolated from the measured values are printed A flow chart of ATCOR-1 is depicted in Figure 19 Figure 20 illustrates a flow diagram of the computations in terms of subroutines This overall procedure is carried out under a LINE11 system structure.

LINE11

LINE11 is the name of a software structure developed over a period of years at ERIM. It has grown in response to a need for a flexible testbed for algorithms which operate on multispectral scanner data. The key concept is to regard a computational run involving multispectral scanner data as composed of a series of logical steps (QSTEP=1,2, ,11) At each logical step all of the modules are given an opportunity in turn, to communicate their requirements, to have access to the labeled common area, and to manipulate the data which is available for processing during that step. In a very real sense, every subroutine is called during each QSTEP This logical structure is best illustrated by the following chart. Basically, LINE11 provides a software setting in which multispectral scanner data is made available for processing by a user specified algorithm. During QSTEP=8 a single scan line is the unit of multispectral scanner data available. These scan lines are handled in a group corresponding to the "region" specified at QSTEP=6 The set of "regions" to be processed are specified at QSTEP=4

SCENARIO FOR LINE11

QSTEP Number	Activity	Comments
1	Linking of modules	The individual modules are brought together in the order in which the user has indicated they are to be exercised so that each module knows the address of the module which precedes it (i.e , the module which supplies data for it to manipulate).
2	Specify default control parameters	
3	Initialize and read the control variables	During this step the monitor and all modules involved will identify themselves by printing out their name, version, and the date of their last programming update.
4	Specify set of regions to be processed	
5	Read the title (file header) for a specific region	
6	Initiate processing of a region	
7	Determine and pass along addresses of any dynamically allocated arrays	
8	Buffer up a single scan line and process it	Any program modules which manipulate the data a scan line at a time are executed once per scan line during this step.
9	End processing of a region	Summarize results for this region, e.g., a given polygon.
10	End processing of a set of regions	Summarize results for all regions, e.g., tabulate an entire flight line
11	End of all processing	Close files, terminate activity

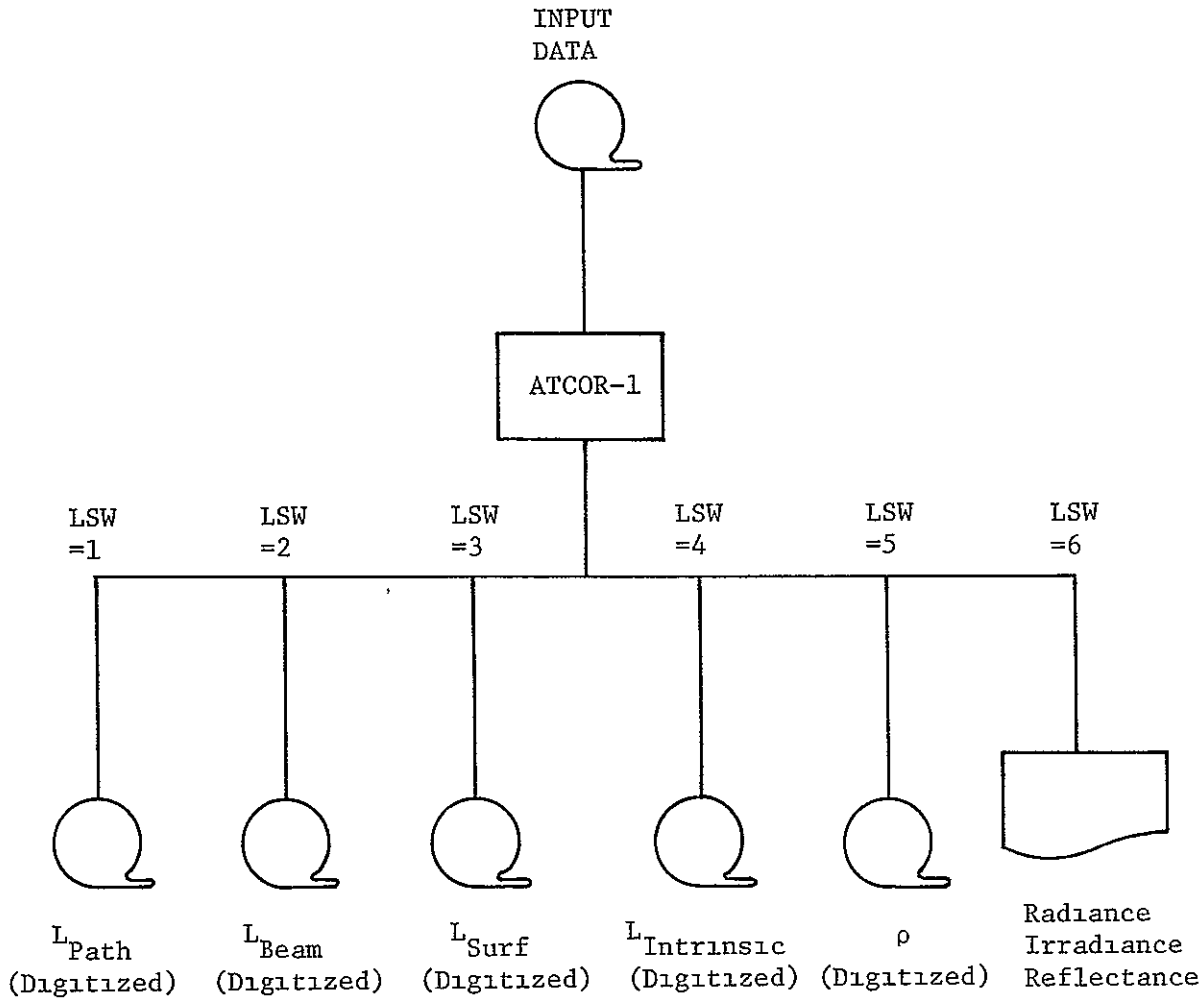

FIGURE 19. OPTIONS FOR OUTPUT FROM ATMOSPHERIC CORRECTION PROGRAM ATCOR-1

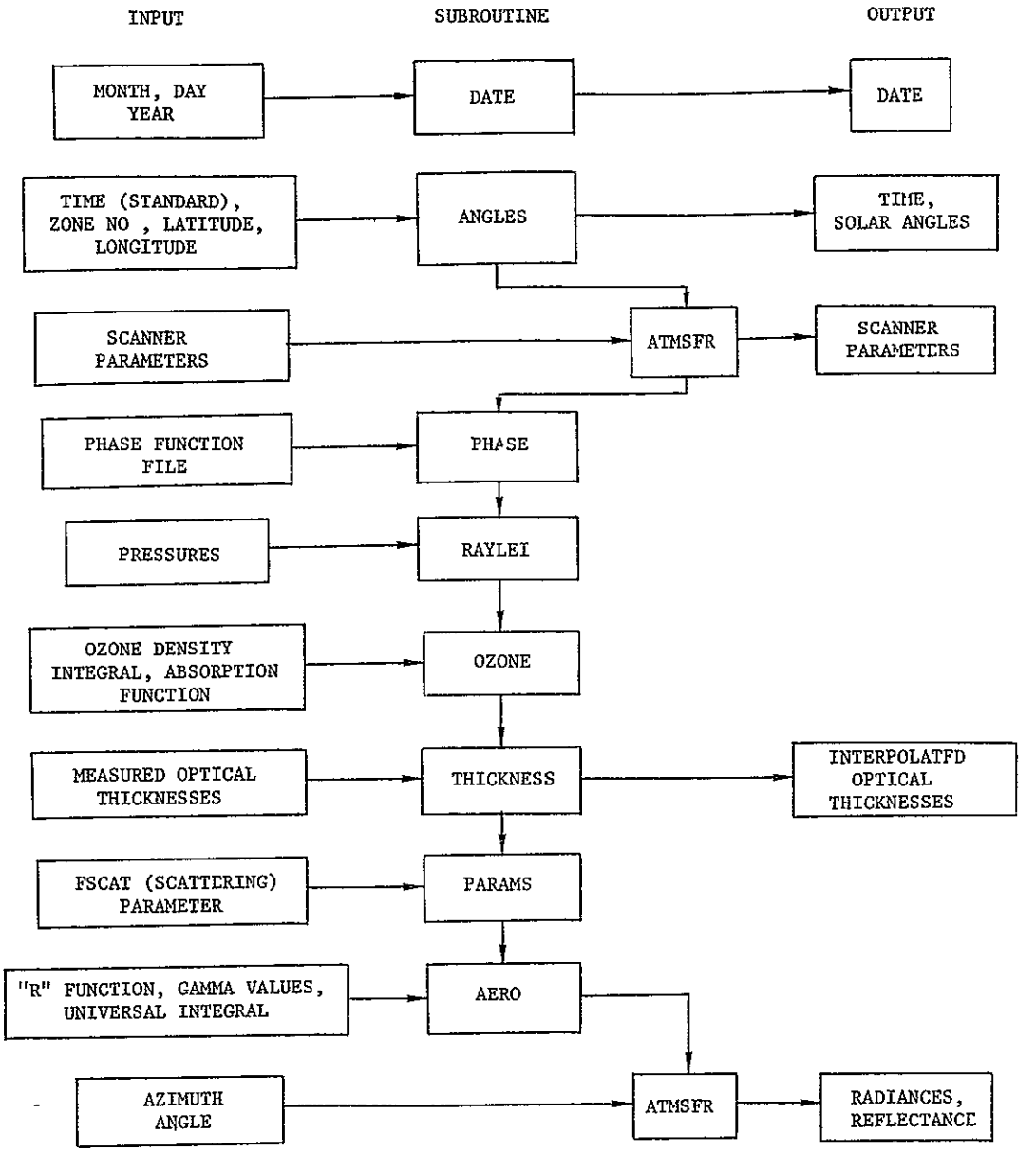

FIGURE 20 ATCOR-1 MATHEMATICAL FLOW CHART

5
ANALYSIS OF MULTISPECTRAL DATA

In this section we will analyze portions of the actual multispectral remote sensor data in order to determine the effectiveness of the correction algorithm

5 1 LAKE ERIE DATA

The object of this program is to eliminate atmospheric effects from multispectral remote sensor data Hence, it would be desirable to have data for situations of widely varying atmospheric conditions For the purposes of this investigation we have analyzed two data sets which were obtained by the Sponsor using high-altitude aircraft The first set was for June 5, 1976, a hazy day over the western part of Lake Erie The second set of data was for the same area but for clear conditions on September 24, 1976 The actual flight lines are indicated on the map in Figure 21 Optical thickness data were obtained using a small radiometer with filters to monitor the direct sunlight at several wavelengths Table 3 presents measured values at the time of overflight along with "standard" values for various visibility conditions. As can be seen from the table, conditions on June 5, 1976 were similar to those for an atmosphere with a visual range approximately 30 km and for September 24, 1976 it is extremely clear with a very high visibility

From the many lines of data we selected a few representative examples to verify the algorithm * Figure 22 illustrates the data for Channel 1 (λ = 0 428 μm) and Channel 7 (λ = 0 674 μm) for a scan line through Pelee Island, on the hazy day A similar scan is shown in Figure 23 for the extremely clear day In the first case every fifth pixel is given and in the second case every eighth pixel is presented. In both cases it is obvious where the island land area begins by noting the sharp increase of reflectance as a result of vegetation especially for the longer wavelength It should be noted that the scan planes for

*Unfortunately, revised calibration values for the sensor which took this data were received as this document was being prepared thereby calling into question the specific results presented in this section See Appendix A for details

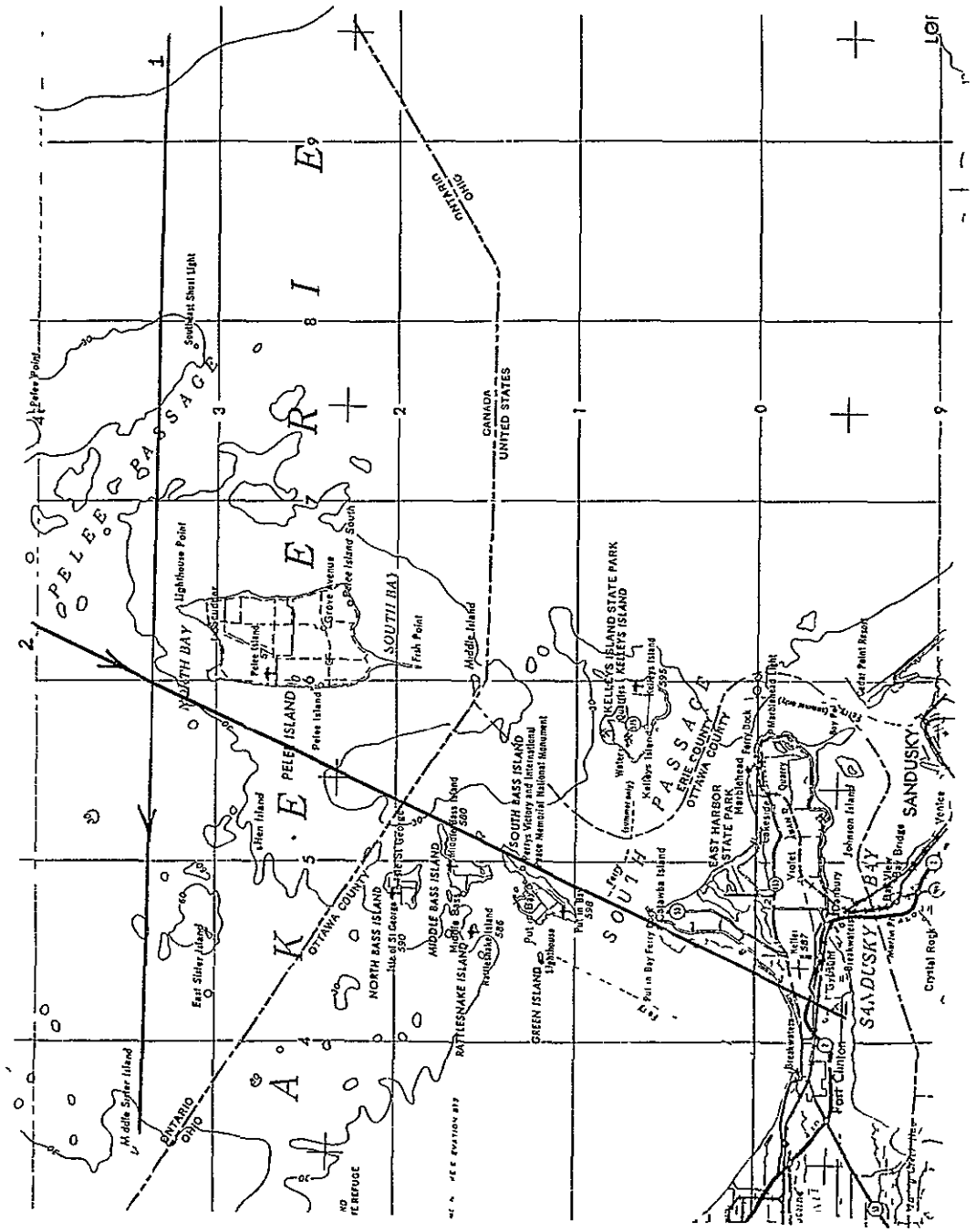

FIGURE 21 FLIGHT LINES

TABLE 3

SPECTRAL OPTICAL THICKNESS ACCORDING TO ELTERMAN'S MODEL

Wavelength (μm)	Clear (23 KM)	Moderately Hazy (10 KM)	Hazy (4 KM)	Very Hazy (2 KM)
0 40	0.682	1 00	1.64	2 59
0.45	0.508	0.792	1.36	2.20
0 50	0.422	0.679	1.19	1.97
0.55	0.374	0.600	1.07	1.78
0.60	0.334	0.540	0.960	1.62
0.65	0.300	0.476	0 860	1.46
0.70	0.262	0.425	0.790	1.33
0.75	0.241	0 390	0 740	1.25
0.80	0.226	0.364	0.695	1.17
0.90	0.204	0.326	0.625	1.07
1.00	0.191	0.300	0.580	0.991
1 10	0.183	0.288	0.550	0 959

SPECTRAL OPTICAL THICKNESS AT TIME OF OVERFLIGHTS

Wavelength (μm)	6/5/76	9/24/76
0.3800	0 63	0 4
0 5000	0 38	0.2
0.6100	0.30	0.19
0 7487	0.21	0 18
0 8730	0 19	0 18
1 0400	0 23	0 21

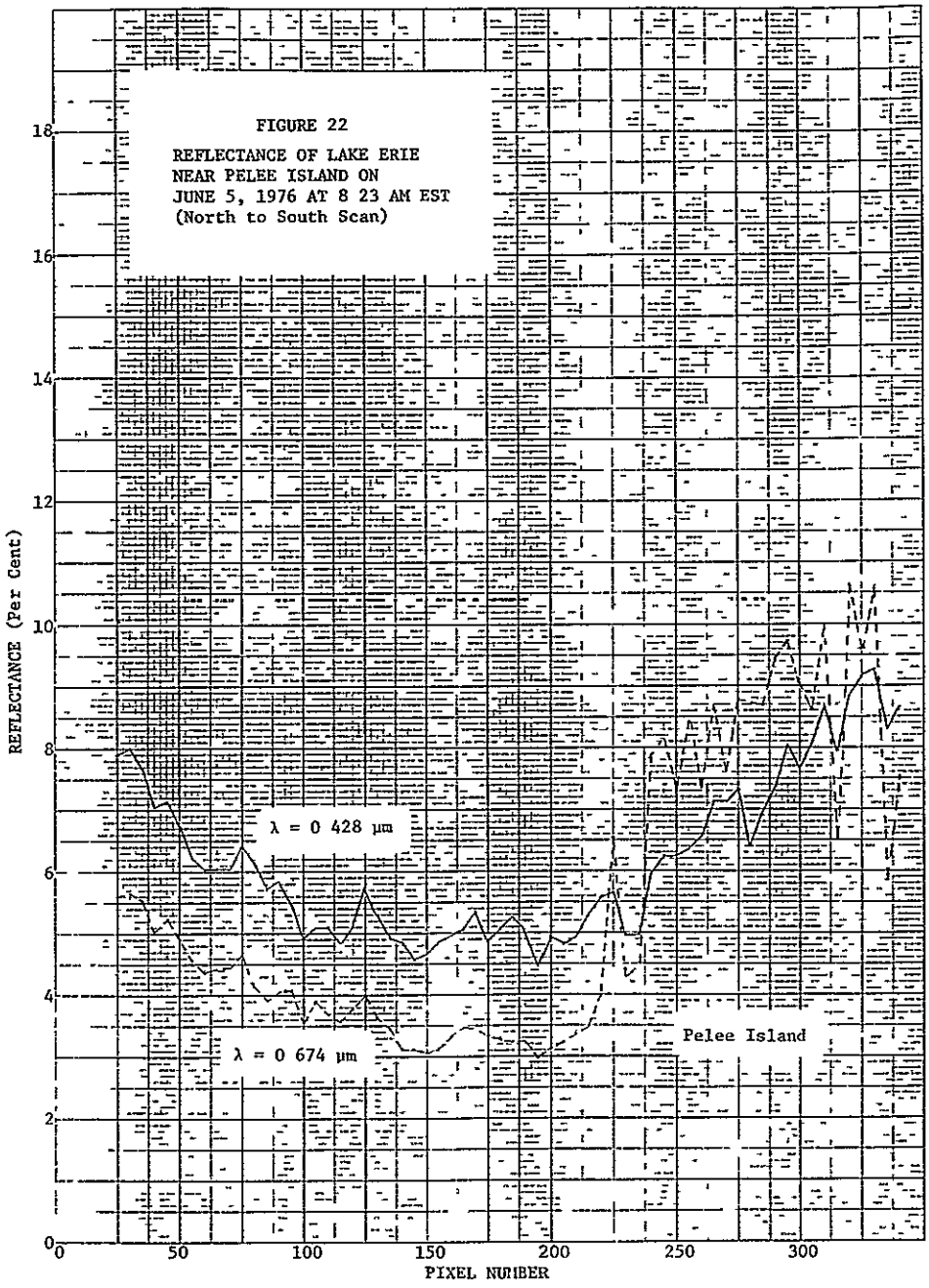

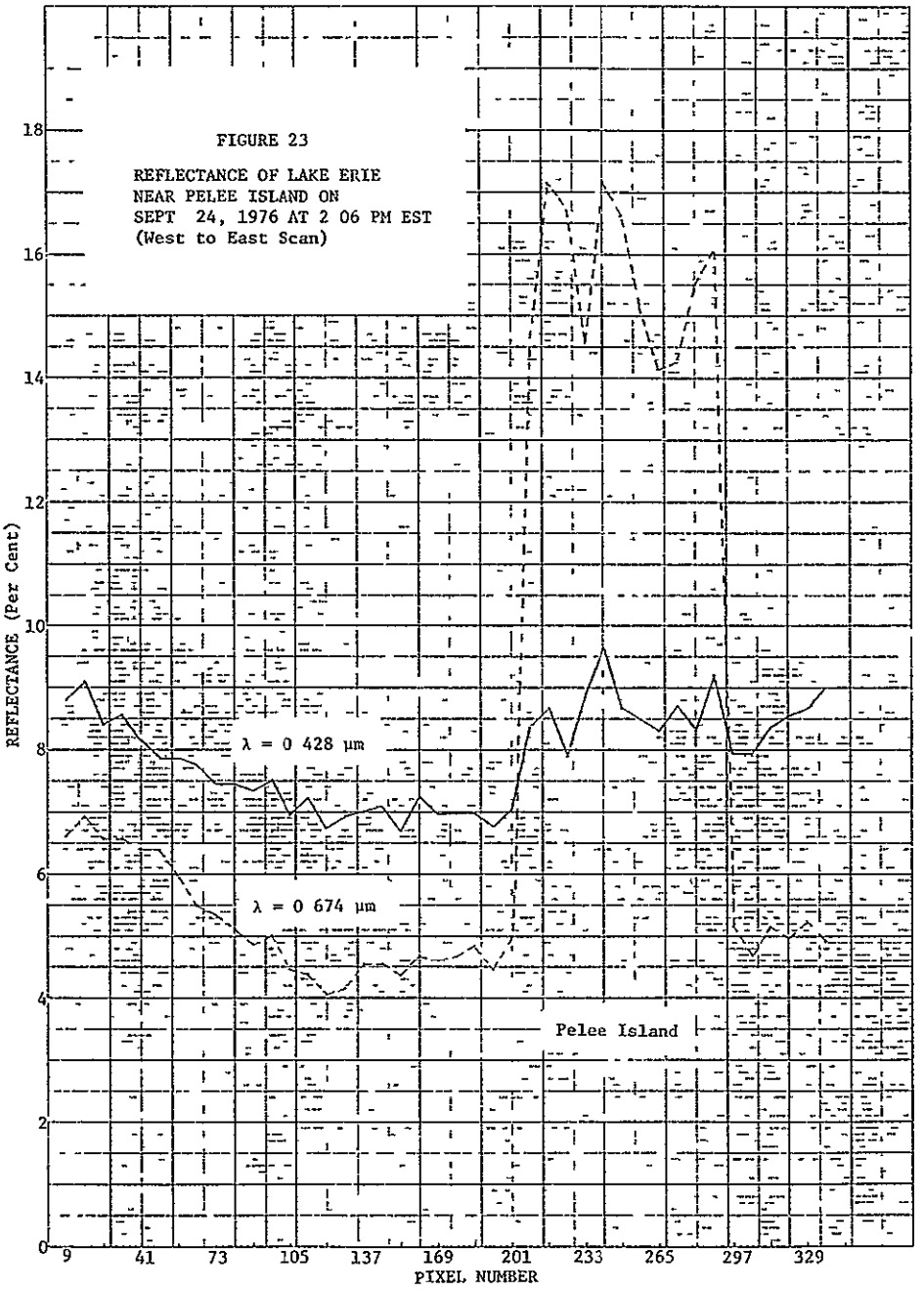

the two days are not coincident but instead are almost perpendicular to one another. The slight variation of reflectance with angle may be due to an incorrect value being chosen for the input atmospheric parameters or it could be a real effect of the water This can be determined by varying the input parameters throughout their normal range of values.

It is interesting to look at the spectral variation in the reflectance for these two situations They are presented in Figures 24 and 25. The reflectances for the water in either case are quite similar but there seems to be an unusual change in the land reflectances It should be pointed out however that there can easily be larger variations in the land reflectances as the result of looking at wet soil, crops, and roadways

5.2 REFLECTANCE DATA

For the purpose of someone who is unfamiliar with reflectances of natural materials such as vegetation, soil, and water we present in this section a set of reflectance curves for a variety of these materials. Figure 26, taken from Kumar [28], illustrates the reflectance of a green leaf in the spectral range 0.4 μm to 2.6 μm. It is interesting to note the large increase in reflectance near the chlorophyll absorption band and the similar increase in the reflectance curves for Pelee Island as depicted in Figures 24 and 25 Figures 27, 28, 29, and 30 illustrate the spectral reflectance of various soils and forms of vegetation most common to the United States. These figures, taken from Leeman et al. [29] are only a small part of the entire compilation but they serve as representative examples for the understanding of the results of our analysis. More important to our study, however, is the spectral reflectance of water. Figures 31, 32, 33, and 34 taken from Wezernak et al [30] illustrate the reflectance of water bodies Figure 31 depicts Atlantic Ocean water with low chlorophyll levels where the level is indicated in mg/m^3. Figure 32 shows water from the Pacific Ocean

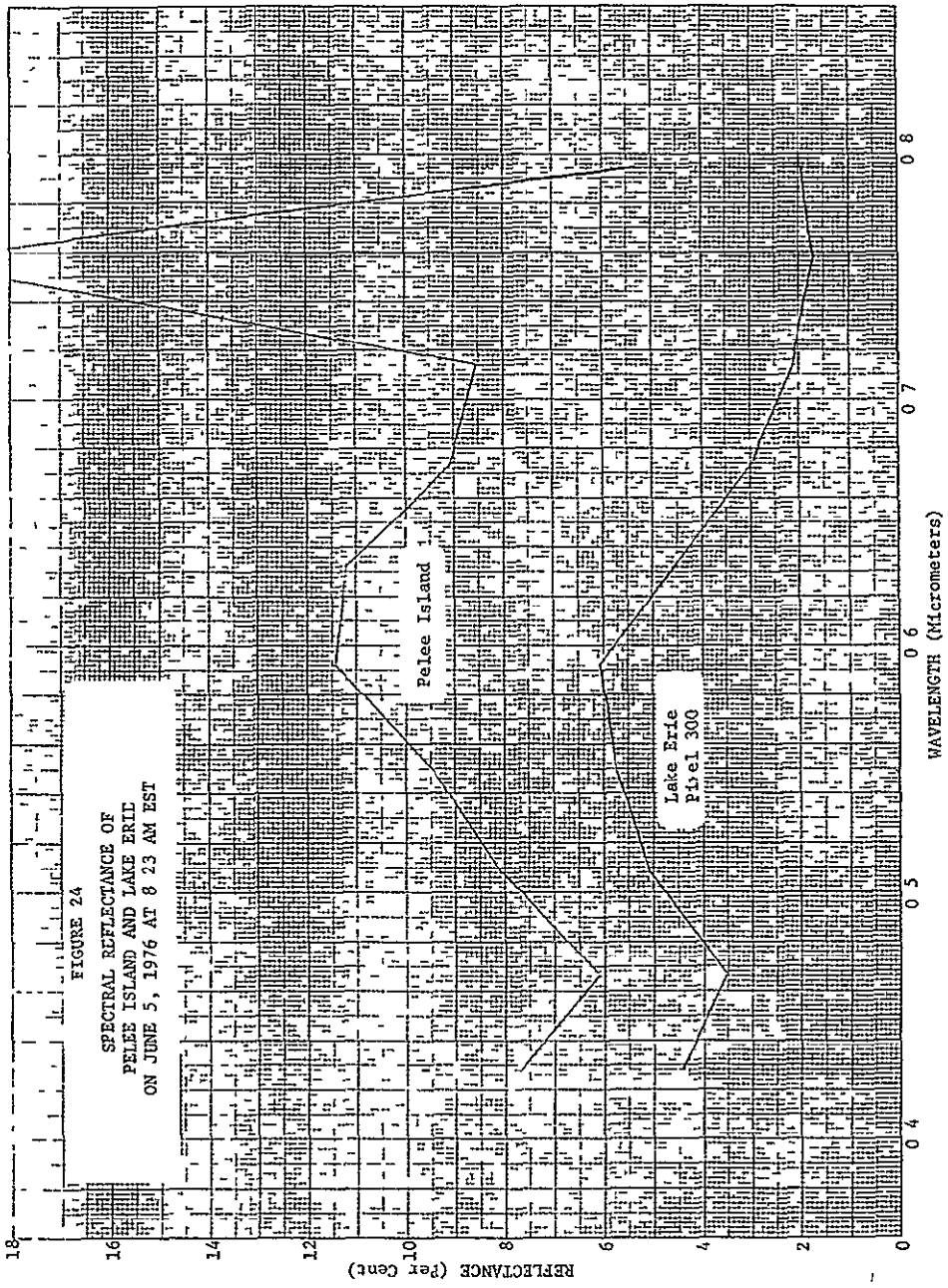

FIGURE 24
SPECTRAL REFLECTANCE OF
PELEE ISLAND AND LAKE ERIE
ON JUNE 5, 1976 AT 8 23 AM EST

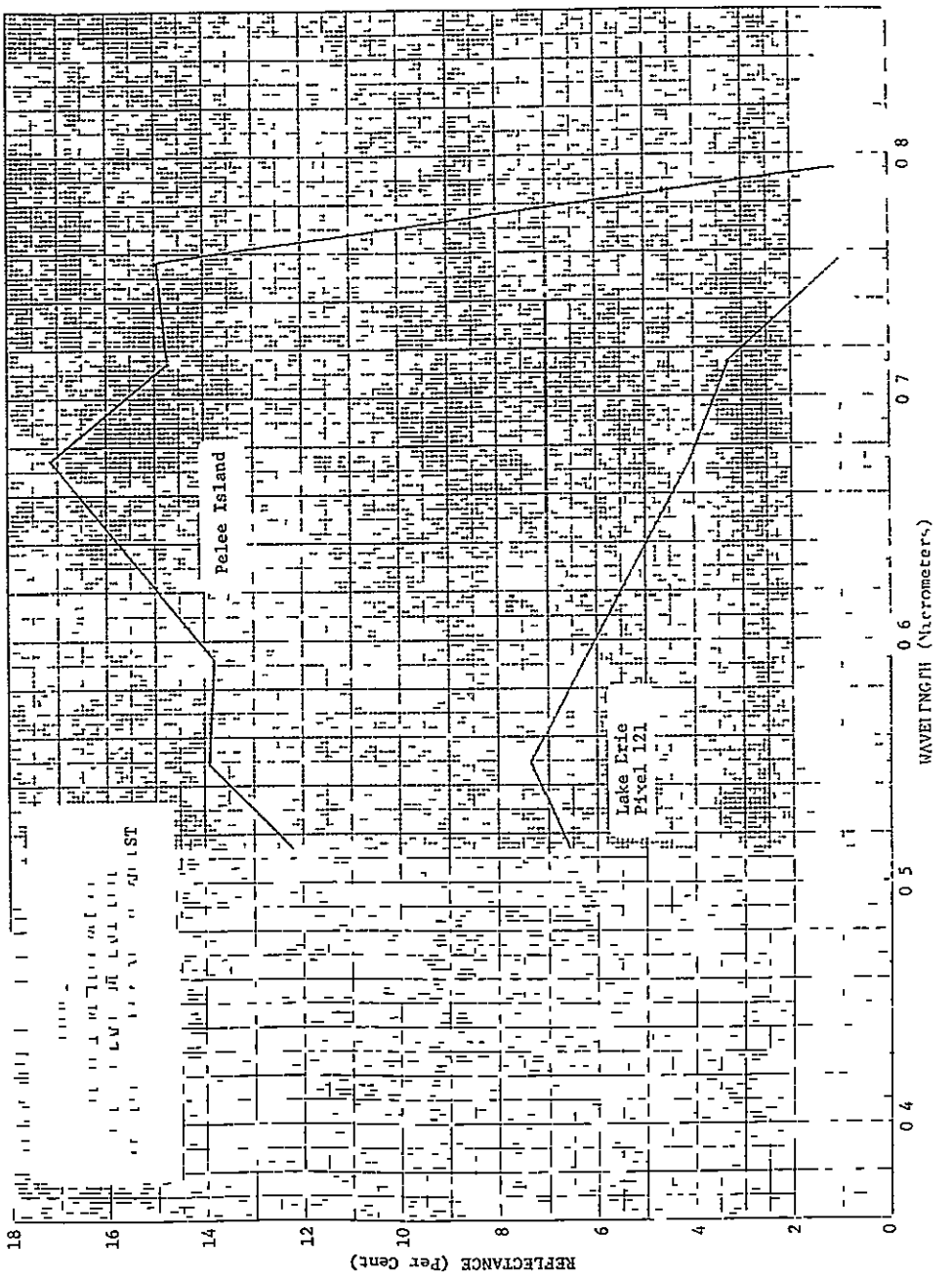

ORIGINAL PAGE IS
OF POOR QUALITY

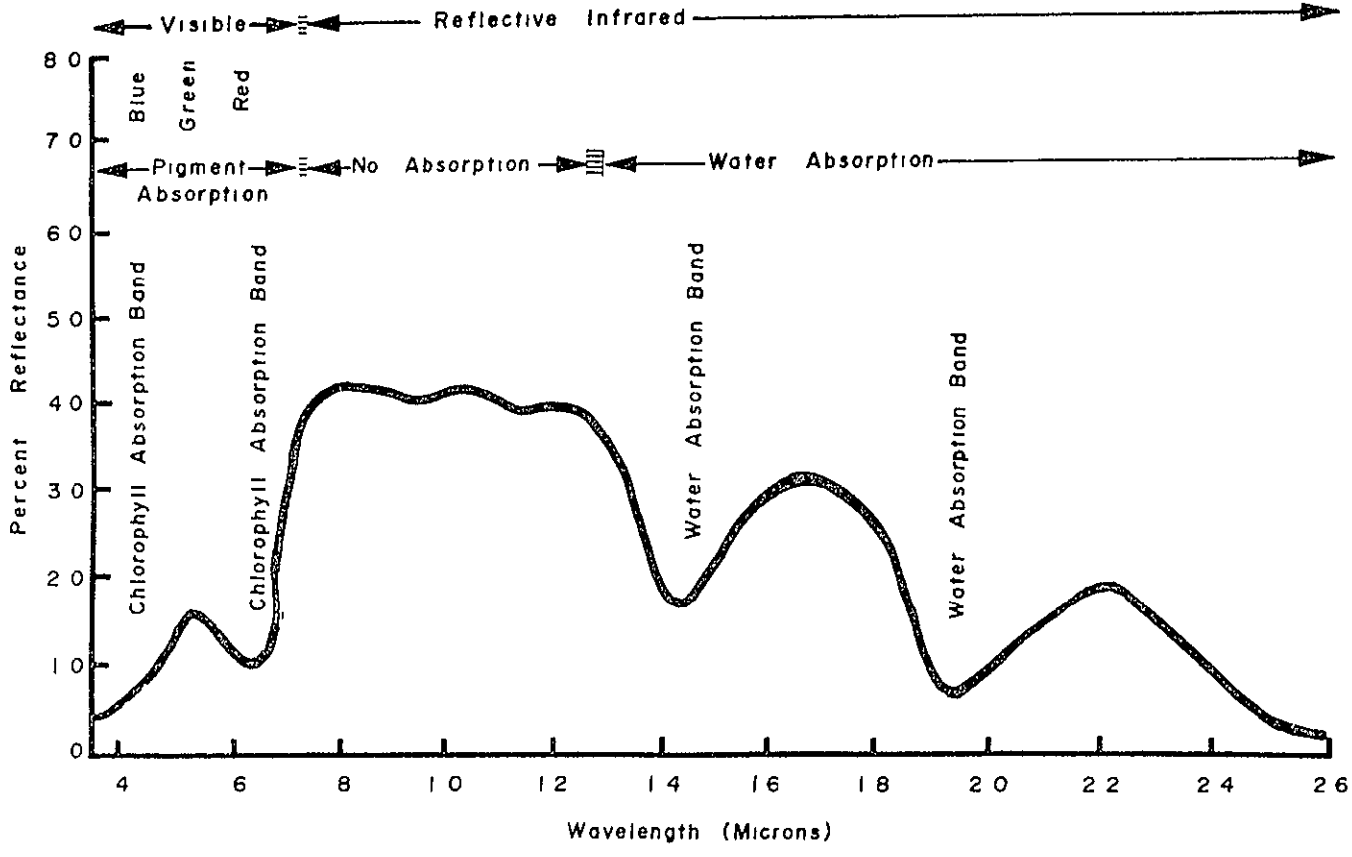

FIGURE 26. CHARACTERISTIC SPECTRAL REFLECTANCE CURVE OF A GREEN LEAF
(Taken from Ref 28, Fig. 80)

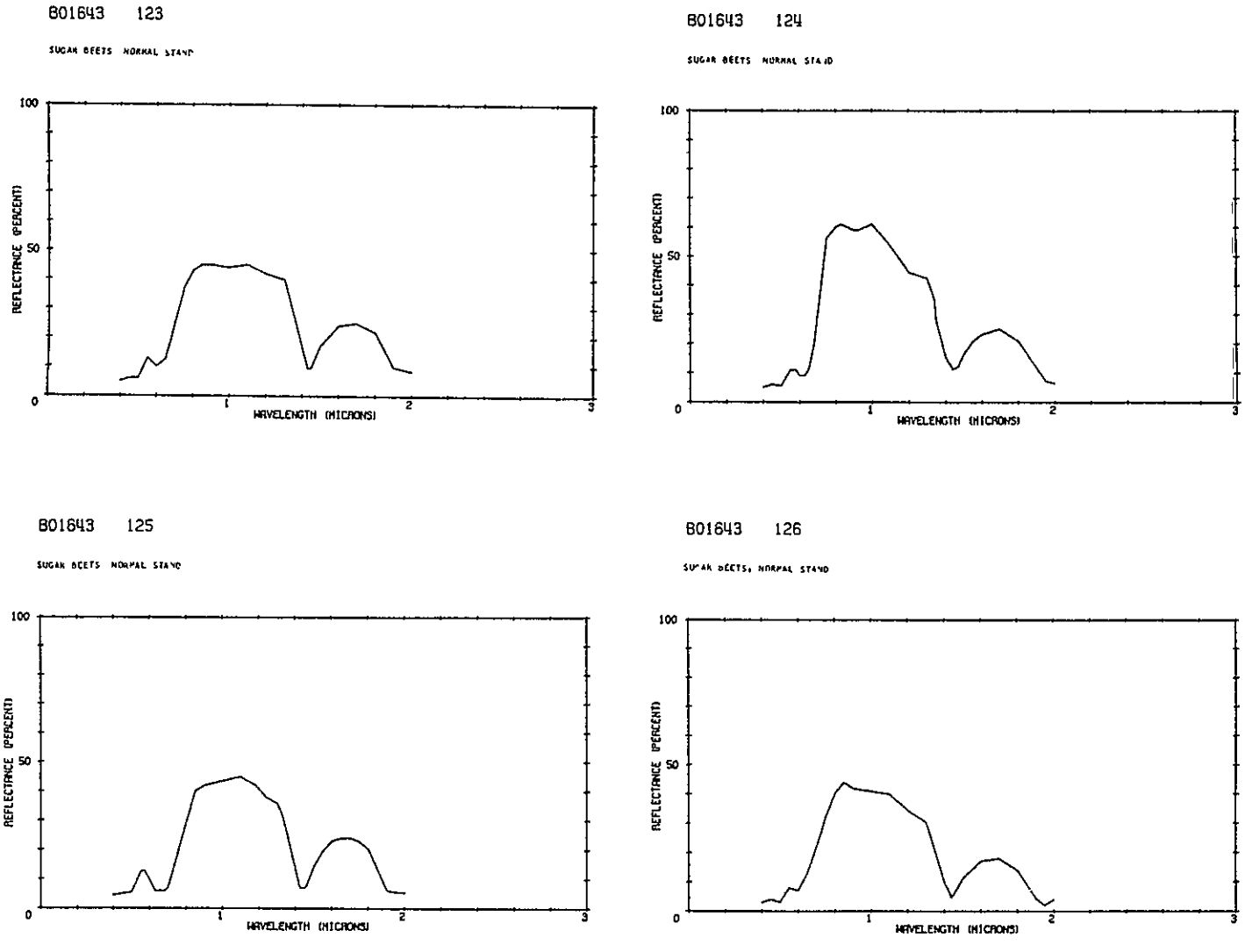

FIGURE 27 SPECTRAL REFLECTANCE OF SUGAR BEETS

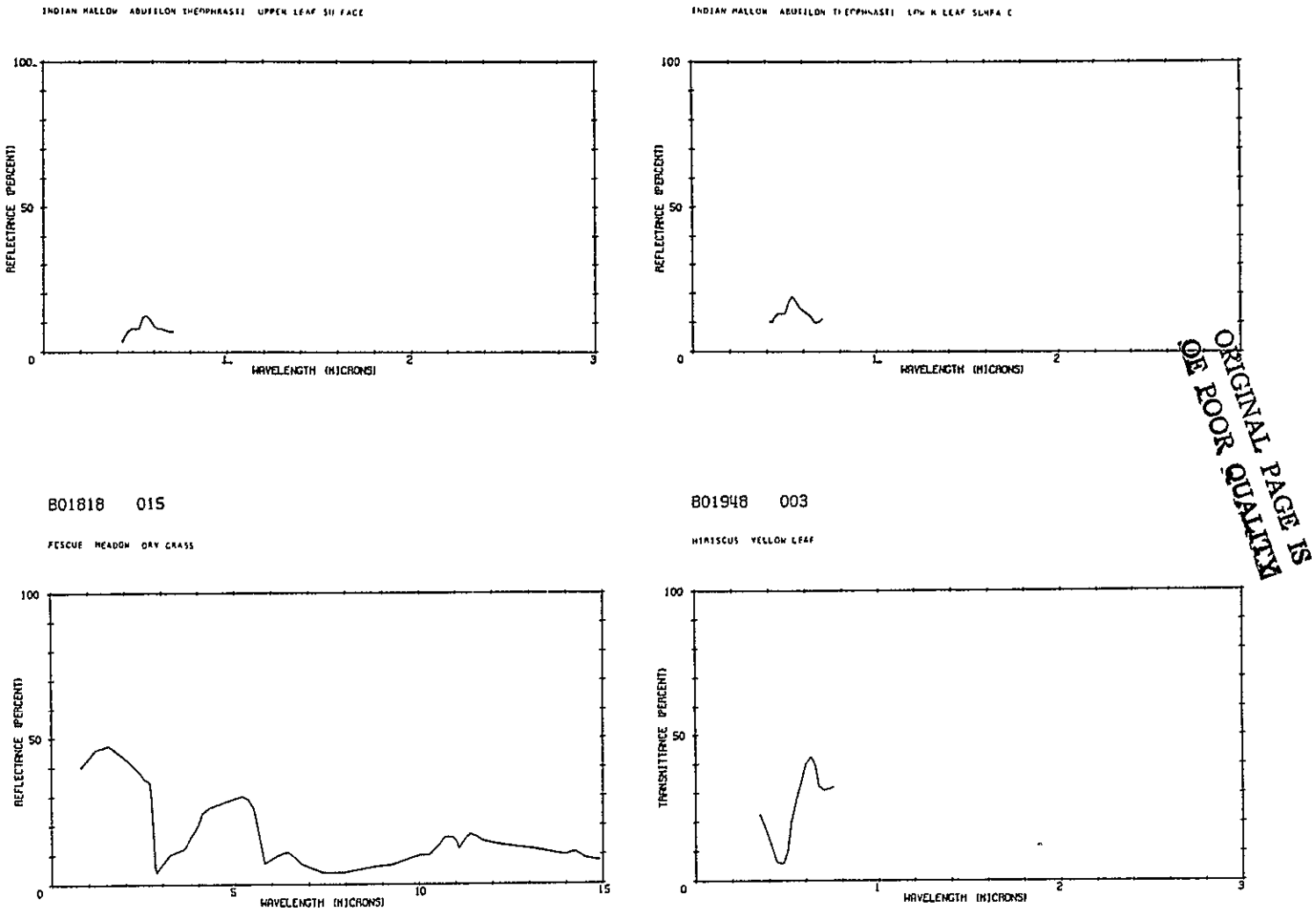

FIGURE 28 SPECTRAL REFLECTANCE OF VEGETATION

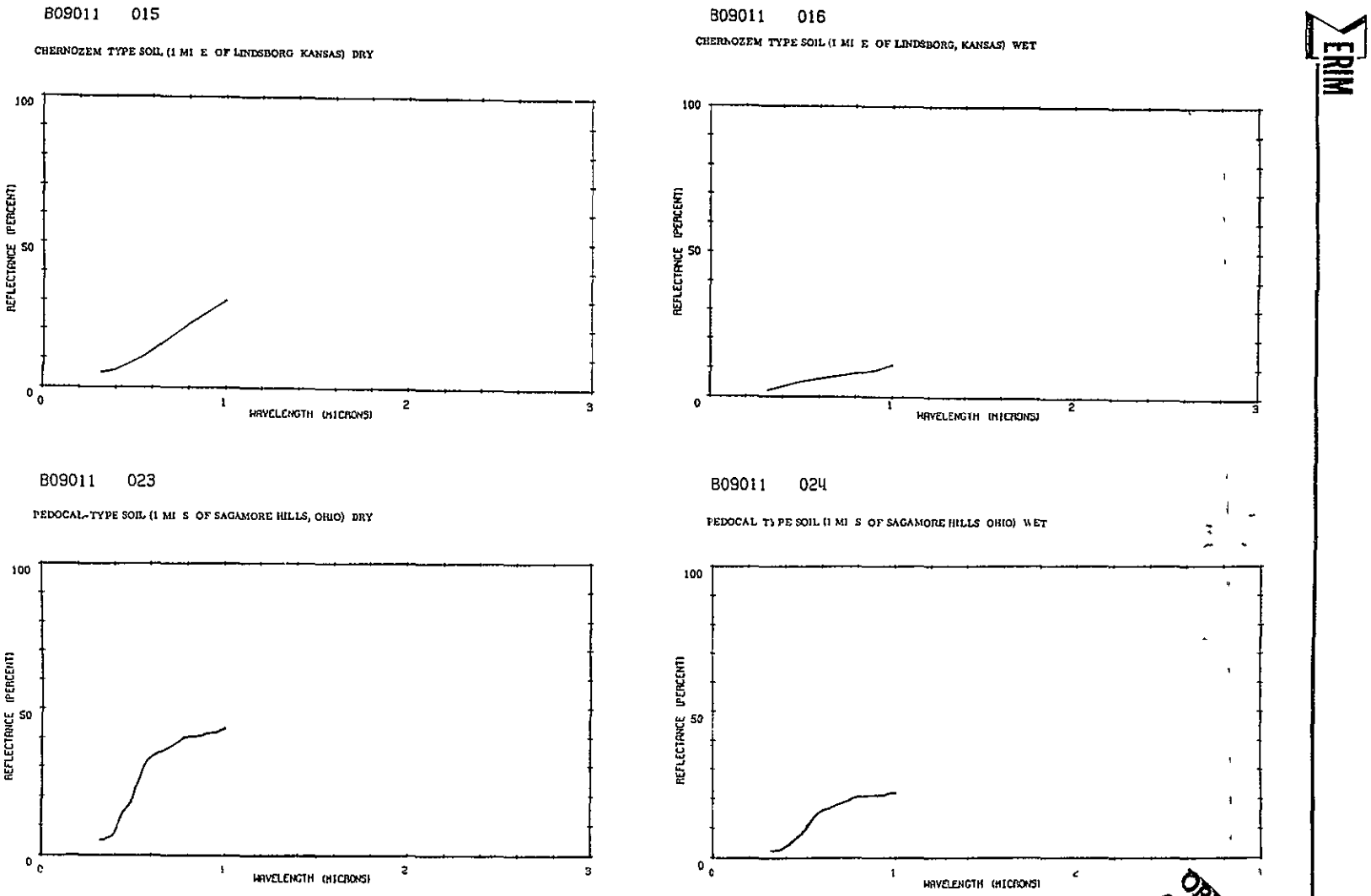

FIGURE 29 SPECTRAL REFLECTANCE OF SOIL

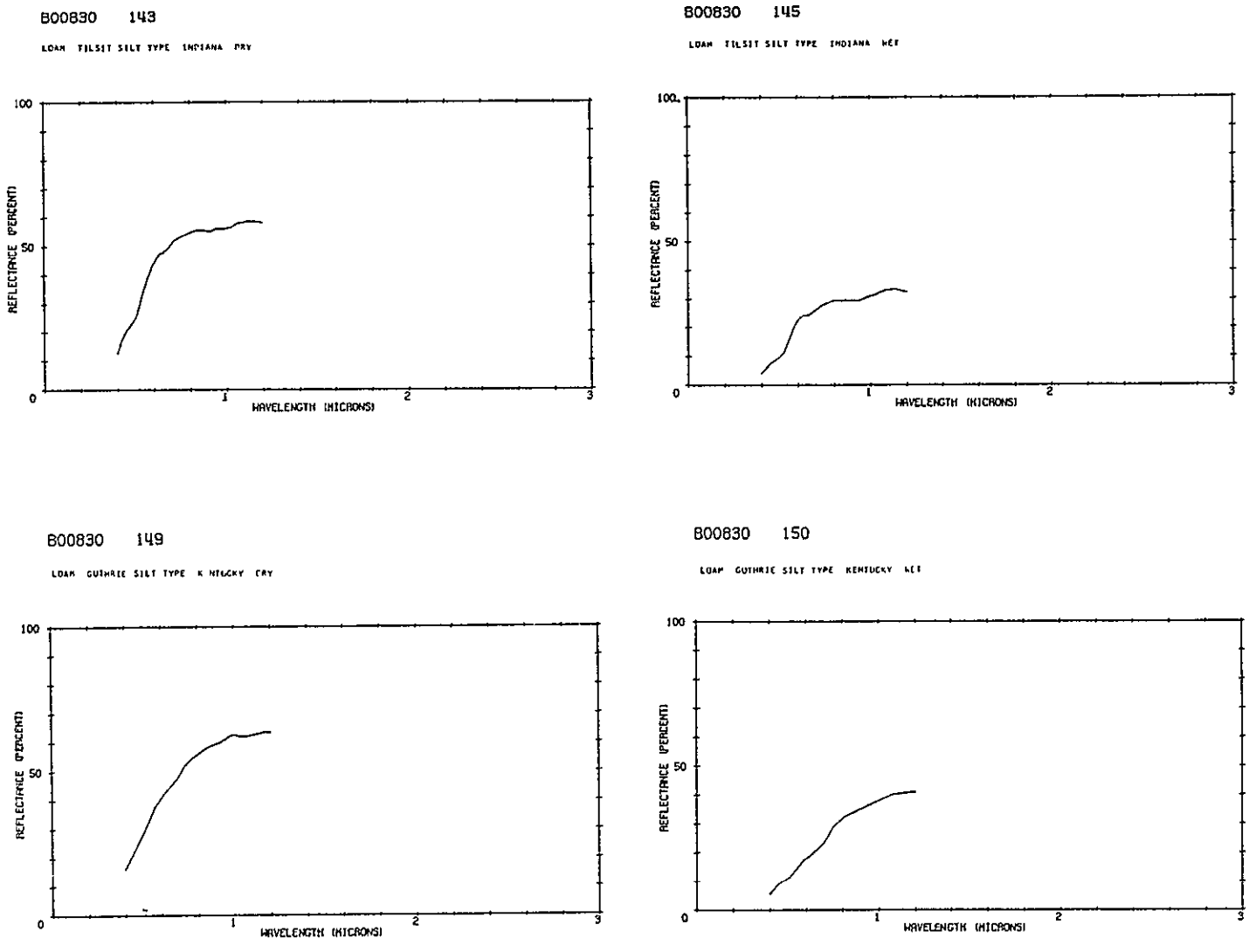

FIGURE 30 SPECTRAL REFLECTANCE OF SOIL

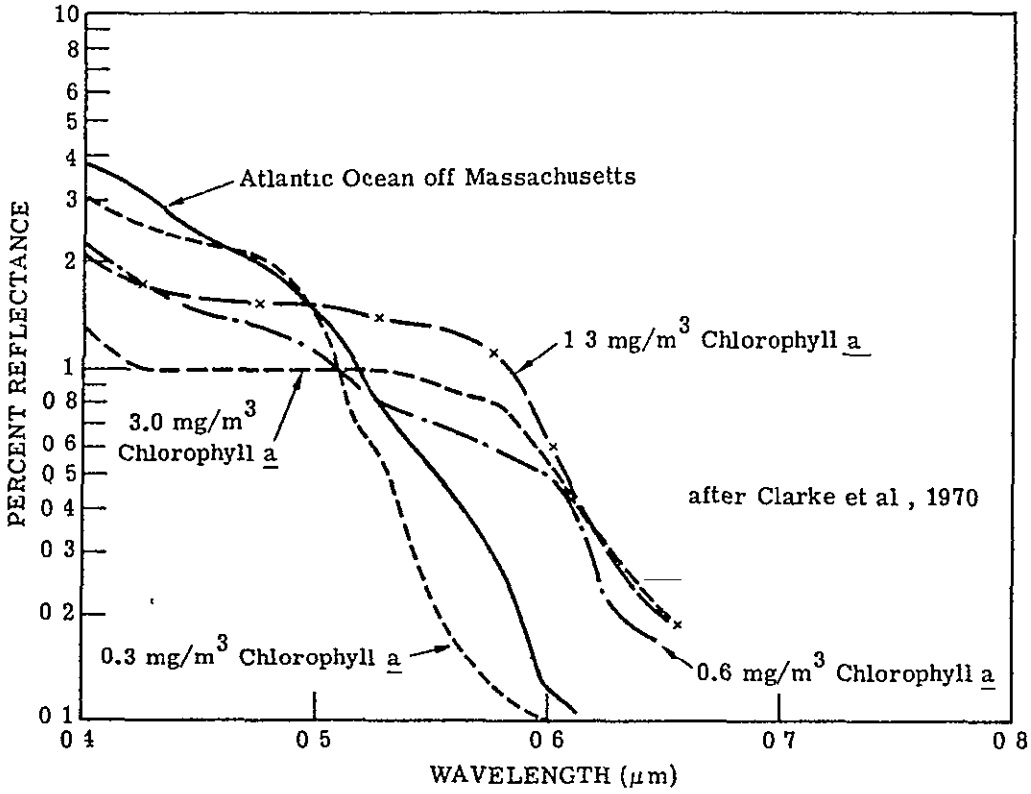

FIGURE 31. LOW CHLOROPHYLL LEVELS - ATLANTIC OCEAN

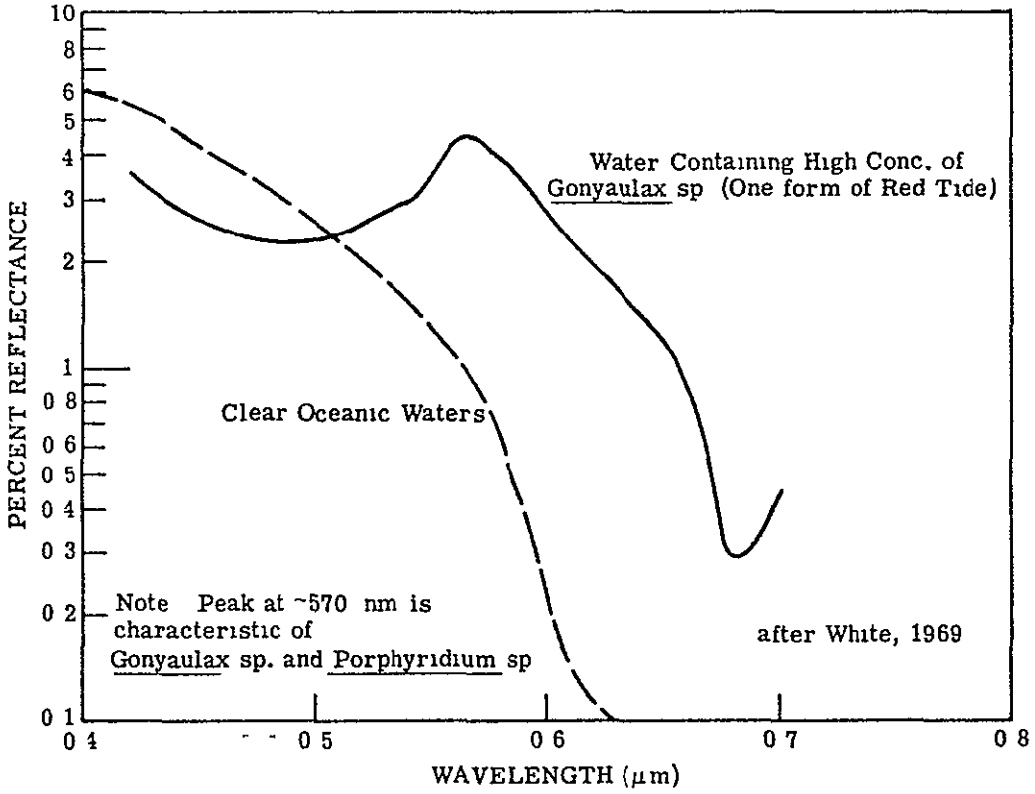

FIGURE 32. GONYAULAX sp Pacific Coastal Waters

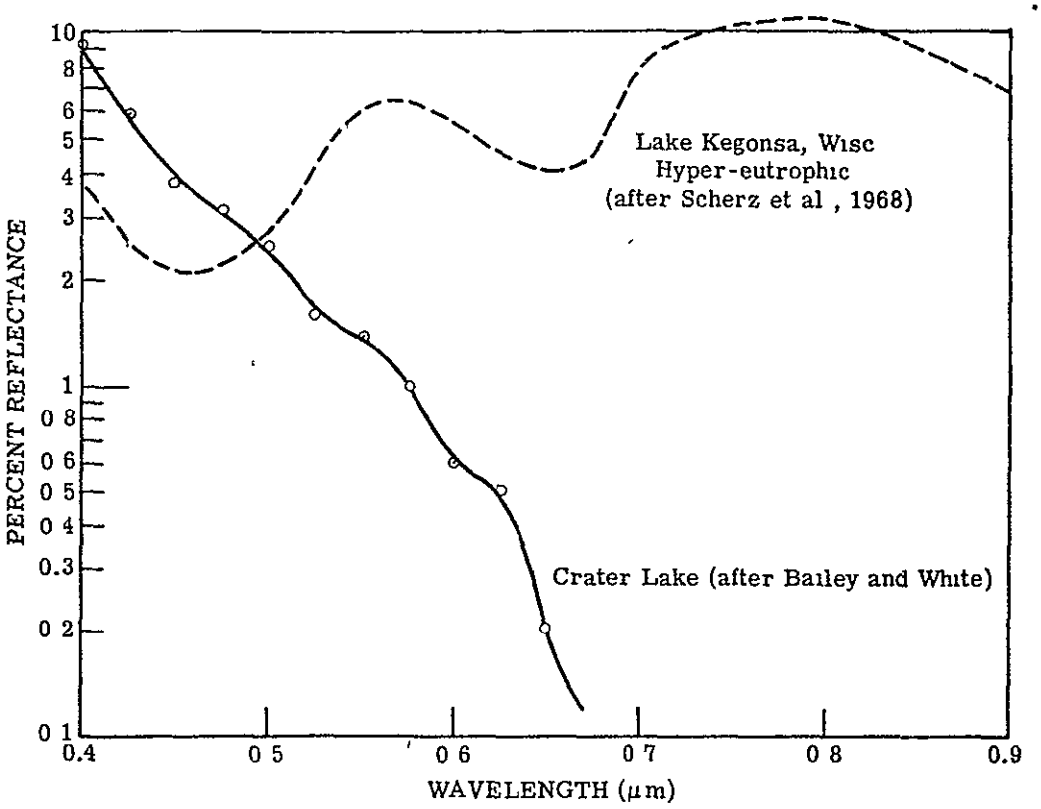

FIGURE 33 LAKES OLIGOTROPHIC-EUTROPHIC

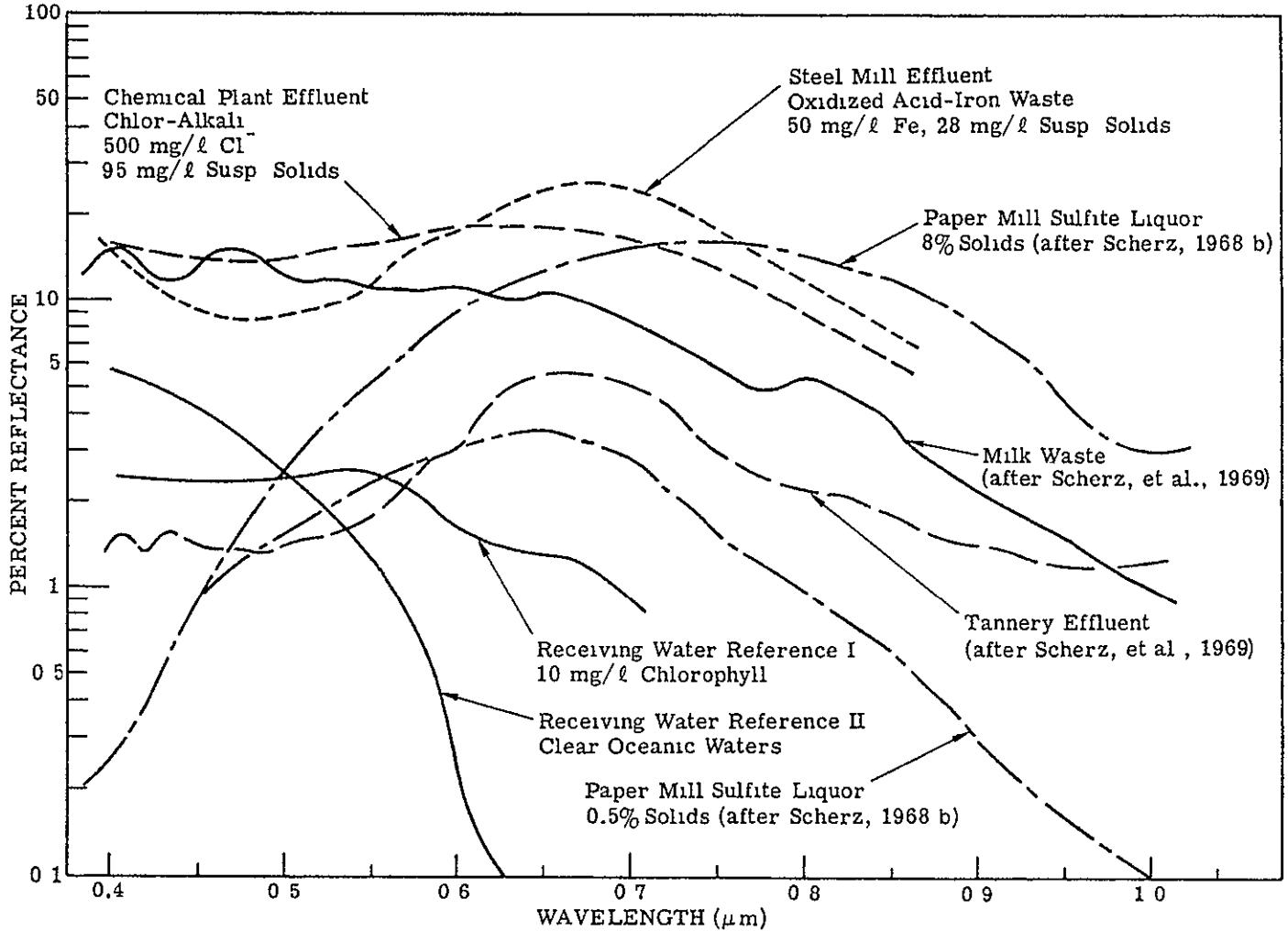

FIGURE 34 INDUSTRIAL EFFLUENTS

with a high concentration of Gonyaulex sp., one form of Red Tide. In Figure 33 the reflectance of oligotrophic-eutrophic lakes is depicted and the large degree of variability should be noted. Finally, Figure 34 illustrates the reflectance of water with the presence of industrial effluents. If one compares these curves with those corresponding to Lake Erie it will be noticed that they are similar not only spectrally but in absolute value It seems likely that Lake Erie contains similar effluents and the reflectance curve is some combination of those in Figure 34.

5.3 DISCUSSION OF RESULTS

The results of our analysis of the multispectral remote sensor data indicate that the atmospheric-radiative-transfer model can be used to extract meaningful information on the radiance and reflectance characteristics of surface materials. The reflectance curves obtained from a sample of the data certainly are reasonable and consistent with what one believes to be the actual reflectance of Lake Erie water. Unfortunately, in our case we had no data from a "very hazy" day on which to verify the algorithm's effectiveness but the formulas used in the program have been used in other radiative-transfer programs for a wide range of atmospheric conditions.

One can determine the overall sensitivity of the results to changes in the environmental parameters which define the scene by altering the input parameters. In a sense, the model's results can only be as reliable as the input data. For our flight, the optical thickness data were collected at only one point in the overall flight path but it is entirely possible that there was considerable fluctuation throughout the region covered The ideal situation would be to have a number of well-calibrated devices at various points in the flight path to determine the degree of aerosol variability.

6
RECOMMENDATIONS AND CONCLUSIONS

In any project involving a number of measurements by many people over a period of time it is important to point out the probable sources of error Perhaps the major source of error in the entire experiment is in the measurement of the spectral optical thickness In discussions with the NASA/Houston personnel who have been involved with the radiometric devices we learned that the calibration procedures are very difficult to perform and once the instruments are calibrated it is likely that they may "drift" from their calibrated values over a period of time. For example, in this particular experiment the optical thickness in the first channel of the radiometer was less than that for a pure Rayleigh atmosphere, clearly an impossibility Certainly one should place great emphasis on reliable measurements of the spectral optical thickness. Also, in some cases the measured optical thickness increase at the longer wavelengths indicating poor band selection or a problem with the filters A recommendation for partially eliminating this difficulty is to perform the measurements with a large aperture device ($\sim 5^{\circ}$ opening angle) and simultaneously photograph the Sun to account for the solar aureole This should also be easier to do from an aircraft and would provide the advantage that the optical depth at flight altitude would be known.

Another source of possible error lies in the calibration of the multispectral scanner Calibration procedures can be difficult for this type of device and should be verified carefully. For this experiment we did not have the details on the scanner characteristics but we were presented with the calibration values.

Users of the ATCOR-1 program are assumed to be somewhat familiar with the basic ideas of radiometry and atmospheric structure. As was stated earlier one should be consistent in the application of input

data and multispectral imagery. For example, the surface albedo must be consistent with the region of observation. If one is over water the albedo input should be similar to that of water Fortunately, we have found that the results of the calculations are relatively insensitive to albedo changes for the usual conditions encountered

Care should also be taken to specify ozone concentrations which are appropriate for the latitude and season. The results do not depend critically on the ozone optical thicknesses unless the atmosphere is clear of haze.

The reflectances we obtained as a result of applying the algorithm to multispectral aircraft imagery compared well with other published reflectance data. A further check on the model's accuracy would be to make measurements of the reflectance at the water surface at various points in the region of interest and compare these values with those obtained by remote sensing.

From the user's point of view, it would be desirable to eliminate the necessity of having to obtain ancillary information from field measurements One possibility is to use a "sky" sensor, i.e., one which is responsive to the upper hemispherical radiation of the Sun plus sky. Simultaneously, photographs of the upper hemisphere could be taken and digitized to determine the fraction of direct solar radiation Such a measurement would then allow one to measure the optical thickness of the atmospheric layer above the aircraft. By flying the aircraft at various altitudes a profile of the aerosol properties could even be generated to improve the algorithm's input parameters.

Finally, it should be pointed out that the radiative-transfer model used in this investigation can be used for any semi-transparent medium such as glass or water The only change involves the parameters which define the medium and perhaps the boundary conditions. Additional work can be done on the subject of water studies by taking into consideration the actual sky radiance distribution in the calculations for

APPENDIX A

Research calibration values for the Ocean Color Scanner were received as this document was being prepared for publication For completeness, the results obtained using the revised set of "F-Values" are presented in this section Unfortunately, the limited amount of effort which could be spent was not adequate to resolve the issue of correct sensor/model calibration

On March 29, 1978 revised values for the OCS-2 radiometric conversion factors were received from our NASA sponsor. These revised values are.

Channel	New F-Value	(Original F-Value from Table 1)
1	5 504	(5 520617)
2	4 920	(5 349853)
3	4 908	(4 643580)
4	5.383	(4 301303)
5	4 638	(4 022688)
6	3 968	(3 680411)
7	4.529	(3 123931)
8	3.541	(2 353995)
9	2.095	(26 812927)
10	1 849	(1.241034)

Figure A-1 lists the command file used to process OCS data collected on September 24, 1976 using the "revised" OCS-2 radiometric conversion factors. Specific details of the input data format was described

A-2

reflectance Most investigators neglect the angular distribution in the modeling of the diffuse reflectance from the water surface but with an atmospheric-radiative-transfer model this effect can easily be treated. In this way it might be possible to extract detailed properties of the water medium by multispectral remote sensing

earlier in conjunction with Table 2. Figure A-2 gives the resulting program outputs for selected pixels on scan line number 4. The pixels chosen were observed over a range of scan angles from +45° (Pixel #1) to -43° (Pixel #337). For comparison the program outputs on these same data values with the original OCS-2 radiometric conversion factors are given in Figure A-3. The improper values of intrinsic reflectance which are predicted in Channel 9 are due to the incorrect scanner calibration.

```
1     DEBUG LINF+ATM+CAL+PACK+SPLINE+OZONE+AEROSOL+THICKNESS+FSR+PF+RAYLEIGH+SOLAR+PARAMS+DECAL+OFSR+O32U8U+MONITOR+SG64;SPRAY,
2     4,4,1,1,344,1,,,***** REPEAT OF REPORT
2.2   344,,.7836,.0045689
2.4   1,344,8
3        9  241976
4        14   06 0.0
5         5
6        41   47 0 0      82   45 0.0
7     12.323    0.0,        6
8       .428      .466      .508      .549      .592      .632      .674      .714      .756      .794
9       .02       .02       .02       .02       .02       .02       .02       .02       .02       .02
-1     1.5,.01,
1     13,38,
3     1.0       .999391 .997564 .994522 .990268 .984808 .978148 .970296 .961262 .951057
4      .939693 .866025 .766044 .642788 .50      .342020 .173648 .0       -.173648-.342020
5     -.50     -.642788-.719340-.766044-.829038- 866025-.913545-.939693-.951057-.961262
6     -.970296-.978148-.984808-.990268-.994522-.997564-.999391-1.0
7     0,40
8      90 7202 82 3252 62.1350 40 5396 24.9011 16.1030 11.4784  8.7039  6.8480  5.5912
9       4 7005  2.4603  1.4890  0.9554  0.6158  0.4113  0 2849  0.2037  0.1513  0.1206
10      0 1067  0 1109  0.1242  0 1460  0 2005  0.2668  0.4269  0.5648  0.6393  0.6849
11      0.6959  0 7237  0 7793  0.7820  0.7164  0.7180  0.8456  0.9320
12    0,45
13     81.3277 74.2287 57.0479 38 4010 24.5189 16.3427 11 8860  9.0073  7.1147  5.8141
14      4.8822  2.5293  1.5180  0.9677  0.6223  0.4155  0.2880  0.2062  0.1546  0.1243
15      0 1105  0.1159  0.1301  0 1522  0.2070  0.2721  0 4255  0.5542  0.6201  0.6597
16      0.6694  0.6907  0 7331  0.7361  0.6941  0.7162  0.8404  0.9191
17    0,50
18     71 1068 67.1017 52.4761 36 3692 24 0512 16.4799 12.0743  9.2768  7.3627  6.0277
19      5.0404  2.5995  1.5471  0.9796  0.6282  0.4191  0.2907  0.2088  0.1574  0.1275
20      0.1141  0.1203  0.1353  0.1577  0 2125  0.2761  0 4225  0.5417  0.5997  0.6338
21      0.6419  0.6577  0 6902  0.6948  0.6724  0.7105  0.8305  0.9021
22    0,55
23     65.9416 60.8556 48 3897 34.4608 23.5266 16.5328 12.2832  9.5125  7.5904  6.2297
24      5.2324  2.6700  1.5760  0.9911  0 6337  0.4221  0 2928  0.2109  0.1598  0.1302
25      0 1174  0 1242  0 1398  0.1623  0.2169  0.2788  0.4180  0.5279  0.5788  0.6078
26      0.6141  0.6255  0 6506  0.6576  0.6515  0.7015  0.8167  0.8820
27    0,60
28     59.5664 55.2226 44.7030 32 6833 22.9784 16.5212 12 4006  9.7165  7.7994  6.4214
29      5 3989  2.7401  1.6042  1 0021  0.6308  0.4248  0 2946  0.2126  0.1619  0.1326
30      0.1202  0.1276  0.1437  0.1663  0 2204  0 2804  0.4123  0 5133  0.5577  0.5821
31      0.5867  0.5948  0 6144  0.6236  0.6307  0.6898  0 8001  0.8598
32    0,65
33     54.3080 50.6364 41.5213 31.0407 22.3937 16 4494 12.5550  9 8861  7.9820  6.5931
34      5 5518  2.8085  1.6325  1.0126  0.6432  0 4270  0 2960  0.2140  0.1635  0.1346
35      0 1226  0 1305  0.1470  0.1695  0.2228  0.2809  0.4056  0.4978  0.5366  0.5572
36      0 5602  0 5653  0 5814  0 5938  0 6115  0.6762  0.7807  0.8352
37    0,70
38     49.7002 46 5483 38.6822 29.5281 21.8118 16.3384 12 6310 10.0315  8.1450  6.7517
39      5 6960  2 8753  1.6598  1.0228  0.6474  0.4289  0 2971  0.2151  0.1649  0.1363
40      0 1247  0.1330  0 1498  0.1721  0.2245  0.2805  0.3982  0.4822  0.5159  0.5331
41      0.5349  0.5379  0 5513  0 5668  0 5927  0.6611  0.7602  0.8103
42    0,80
43     42.0527 39.7363 33.8800 26.8719 20.6901 16.0347 12.6906 10.2456  8.4172  7.0302
44      5.9564  3.0024  1.7122  1.0421  0.6553  0.4322  0.2988  0.2168  0.1670  0.1390
45      0.1282  0 1370  0.1540  0 1758  0.2261  0.2779  0.3818  0.4512  0.4765  0.4880
46      0 4877  0 4884  0.4994  0 5193  0.5564  0.6279  0.7161  0.7581
47    0,90
48     36.2598 34.4289 30.0974 24.6506 19.6411 15.6643 12.6591 10.3768  8.6207  7.2550
49      6 1761  3.1193  1.7614  1.0604  0.6625  0.4350  0.3001  0.2179  0.1686  0.1410
```

FIGURE A-1

Command File Used to Process September 24, 1976 Data

```
 50      0.1307  0.1398  0.1569  0.1779  0.2257  0.2732  0 3646  0.4214  0.4403  0.4477
 51      0.4461  0.4461  0.4566  0.4799  0.5229  0.5933  0 6717  0.7067
 52    1.06
 53     29 6370 28.5143 25.5817 21.8260 18.1551 15.0221 12 4882 10.4590  8.8308  7.5185
 54      6 4509  3 2841  1.8339  1.0884  0.6738  0.4394  0 3020  0.2194  0.1703  0.1433
 55      0 1335  0 1426  0.1593  0.1789  0.2223  0.2634  0.3371  0.3783  0.3899  0.3932
 56      0.3910  0.3916  0.4029  0.4292  0.4749  0.5393  0.6028  0.6301
 57    1.26
 58     24.2957 23.5951 21.7244 19.2216 16.6175 14.2292 12 1624 10.4129  8.9444  7.7146
 59      6 6824  3.4539  1.9148  1.1221  0.6883  0.4455  0.3047  0.2212  0.1721  0.1454
 60      0.1359  0.1445  0.1602  0.1779  0.2158  0.2496  0.3058  0.3332  0.3395  0.3404
 61      0.3390  0 3413  0.3540    3812  0.4245  0.4790  0.5201  0.5482
 62    1.67
 63     18 3015 17.9755 17.0733 15.7806 14 3042 12.6036 11.3727 10.0563  8.8707  7.8165
 64      6 8862  3.6998  2.0542  1.1904  0.7224  0.4626  0 3140  0.2270  0.1766  0.1493
 65      0.1394  0.1462  0.1592  0.1730  0.2009  0.2235  0 2559  0.2684  0.2706  0.2710
 66      0.2722  0.2779  0.2918  0.3158  0.3489  0.3853  0 4148  0.4263
 67    2.17
 68     14.6515 14 4827 14 0020 13.2763 12.3891 11.4181 10.4239  9.4486  8.5189  7.6503
 69      6 8505  3 8686  2.1885  1.2731  0.7713  0.4915  0.3316  0.2386  0.1849  0.1558
 70      0.1443  0 1482  0.1580  0.1679  0.1869  0.2009  0 2186  0.2249  0.2265  0.2284
 71      0 2320  0 2394  0.2521  0.2704  0.2928  0.3151  0.3320  0.3384
 11     992.      179 431
 12      71    1    7    8
 13      .362    .439
  1        1  6 0134E-05
  2        2. 1.2000E-04
  3        3. 1.0090E-04
  4        4  2 4393E-04
  5        5  3.0892E-04
  6        6  3.7617E-04
  7        7. 4 4820E-04
  8        8  5 2507E-04
  9        9. 6 0781E-04
 10       10  6.9497E-04
 11       11  7 9485E-04
 12       12. 9 0965E-04
 13       13  1.0431E-03
 14       14  1.2096E-03
 15       15  1.3951E-03
 16       16. 1 5919E-03
 17       17  1 8182E-03
 18       18  2.0774E-03
 19       19  2.3787E-03
 20       20  2.7095E-03
 21       21. 3.0600E-03
 22       22  3.4222E-03
 23       23. 3.7729E-03
 24       24. 4.1027E-03
 25       25  4.4129E-03
 26       30. 5.6857E-03
 27       35  6.3996E-03
 28       40  6.7126E-03
 29       45. 6 8418E-03
 30       50  6.8707E-03
 31       51  6.8787E-03
 32       52  6 8822E-03
 33       53  6 8850E-03
 34       54. 6.8883E-03
 35       55. 6.8912E-03
```

```
36          56.  6.8939E-03
37          57.  6.8967E-03
38          58.  6.8996E-03
39          59.  6.9026E-03
40          60.  6.9057E-03
41          61   6.9092E-03
42          62.  6.9129E-03
43          63   6.9169E-03
44          64.  6.9214E-03
45          65.  6.9264E-03
46          66   6.9319E-03
47          67   6.9381E-03
48          68.  6.9449E-03
49          69.  6.9524E-03
50          70.  6.9606E-03
51          71   6.9696E-03
52          72   6.9792E-03
53          73.  6.9898E-03
54          74.  7.0000E-03
55          75.  7.0108E-03
56          76.  7.0218E-03
57          77   7.0325E-03
58          78.  7.0427E-03
59          79.  7.0523E-03
60          80.  7.0609E-03
61          81.  7.0685E-03
62          82.  7.0750E-03
63          83   7.0803E-03
64          84.  7.0844E-03
65          85.  7.0876E-03
66          86.  7.0898E-03
67          87.  7.0914E-03
68          88.  7.0925E-03
69          89.  7 0931E-03
70          90.  7.0935E-03
71         100.  7.1010E-03
15      7.1010   E-03
 1          .27 2.10  E 02
 2          .28 1.06  E 02
 3          .30 1 01  E 01
 4          .32 8 98  E -1
 5          .34 6.40  E -2
 6          .36 1.80  E -3
 7          362 1.00  E -3
 8         .439 1 00  E -3
 9          .45 3.50  E -3
10          .50 3.45  E -2
11          .55 9.20  E -2
12          .60 1.32  E -1
13          .65 6.20  E -2
14          .70 2.30  E -2
15          .80 1.00  E -2
17          1
18      6
19          .40       .4
20         0,50       .20
21         0,61       .19
22          .7487     .18
23          .8730     .18
24         1.04       .21
```

```
 1.00000 1.00000 1.00000 1.00000 1.00000 1.00000 1.00000 1.00000 1.00000 1.00000
    20    1   46   28
     1
  0.27    2.07    0.28    1.9570  0.30    1.8420  0.32    1.7290  0.34    1.6150
  0.36    1 5010  0.38    1.4490  0.40    1.3460  0.45    1.19    0.50    1.0870
  0.55    1 00    0 60    0.8903  0.65    0.8075  0.70    0.7557  0.80    0.6625
  0.90    0.6000  1.06    0.5383  1.26    0.4865  1.67    0.4141  2.17    0.3727
     5. 4.9299E-02
     6. 4.5158E-02
     7. 4.1809E-02
     8. 1 8861E-02
     9. 3.5130E-02
    10. 3.1918E-02
    11. 2.8864E-02
    12  2.5816E-02
    13. 2.2801E-02
    14. 1.9962E-02
    15. 1.7217E-02
    16. 1.4642E-02
    17. 1.2142E-02
    18. 9.6750E-03
    19. 7.4300E-03
    20. 5.6710E-03
    21. 4.4010E-03
    22. 3.4430E-03
    23. 2.7510E-03
    24. 2.1980E-03
    25. 1.7480E-03
    26. 1.3580E-03
    27. 1.0380E-03
    28  7.9600E-04
    29. 6 0000E-04
    30  4.6600E-04
    31. 3.5600E-04
    32  2.7200E-04
    33  2.0800E-04
    34. 1 5900E-04
    35. 1 2100E-04
    36. 9.2998E-05
    37. 6.9998E-05
    38. 5.3000E-05
    39  3.9998E-05
    40. 3.0998E-05
    41. 2 2996E-05
    42. 1.6998E-05
    43. 1 2998E-05
    44  8 9966E-06
    45. 6.9998E-06
    46. 4.9993E-06
    47  2.9989E-06
    48. 1.9968E-06
    49. 9 9839E-07
    50. 0.0000
-100.    9 091 E-03
-70.     1.429 E-02
-50.     2.000 E-02
-35.     2.857 E-02
-25      4 000 E-02
-17.5    5.714 E-02
-12.5    8.000 E-02
```

```
      8      -8.75   1.143 E-01
      9      -6.25   1.597 E-01
     10      -4.38   2 255 E-01
     11      -3 13   3.055 E-01
     12      -2.     4.323 E-01
     13      -1.5    5.179 E-01
     14      -1.     6.321 E-01
     15      - .5    7.869 E-01
     16       0.     1.000 E 00
     17       1.     1.718 E 00
     18       1.5    2.321 E 00
     19       2.     3.195 E 00
     20       2.5    4 473 E 00
     21       3.     6 352 E 00
     22       3.5    9.176 E 00
     23       4.     1.340 F 01
     24       4.5    1.978 E 01
     25       5.     2.948 E 01
     26       5.5    4.431 E 01
     27       6.     6.707 E 01
     28       6.475  1.000E  2
     31     295   0 0.0
END OF FILE
```

SIMULATION DATE IS: SEPTEMBER 24, 1976

LATITUDE= 41DEG 47MIN 0.0 SEC LONGITUDE= 82DEG 45MIN 0.0 SEC
TIME IS 14: 61 0.0 TIME ZONE 5
SOLAR ZENITH ANGLE= 48 DEGREES 39 MINUTES 17.172 SECONDS
SOLAR AZIMUTH ANGLE= 323 DEGREES 23 MINUTES 51.738 SECONDS
PARTICULATE REFRACTIVE INDEX=1.50-0.01I

FIGURE A-2

Results of Using the Command File With Revised OCS-2 Calibration Factors

INPUT OPTICAL THICKNESSES

	1	2	3	4	5	6
WAVELENGTH	0.4000000	0.5000000	0.6100000	0.7487000	0.8730000	1.0400000
OPTICAL THICKNESS (MEASURED)	0.4000000	0.2000000	0 1900000	0.1800000	0.1800000	0.2100000

AZIMUTH ANGLE FROM SUN TO SCAN PLANE=295 DEGREES, 0 MINUTES, 0.0 SECONDS
MAXIMUM SCAN ANGLE=0.7836000 RADIANS. ANGULAR RESOLUTION OF SCANNER IS 0.0045689 RADIANS.

CHANNEL	1	2	3	4	5	6	7	8	9	10
WAVELENGTH	0.42800	0.46600	0.50800	0.54900	0.59200	0.63200	0.67400	0.71400	0.75600	0.79400
INTERPOLATED OPTICAL THICKNESS	0.31271	0.23619	0.19497	0.18410	0.18781	0.19106	0.18884	0.18405	0.17934	0.17731
BACKGROUND ALBEDO	0.02000	0.02000	0.02000	0.02000	0.02000	0.02000	0.02000	0.02000	0.02000	0.02000
SINGLE SCATTERING ALBEDO	1.00000	0.98385	0.93054	0.83695	0.76230	0.84666	0.93333	0.96748	0.98024	0.98181
SCATTERING PARAMETER (FSCAT)	1.00000	1.00000	1.00000	1.00000	1.00000	1.00000	1.00000	1.00000	1.00000	1.00000

LINE NUMBER 4 PIXEL NUMBER 1 SCAN ANGLE= 44.897 DEGREES

	1	2	3	4	5	6	7	8	9	10
LTOT	31.67413	33.62744	31.35635	32.55060	30.37640	0.0	18.86238	14.57091	163 45493	0.0
LPATH	2.67908	2.24081	1.46501	0.94981	0.72285	0.74029	0.74419	0.67832	0 59518	0.52614
LBEAM	28.99504	31.38663	29.89134	31.60078	29.65355	0.0	18.11819	13.89259	162.85974	0.0
LSURF	40.30391	39.89513	36.04190	37.20776	34.81749	0.0	22.42094	17.27614	202.42769	0.0
LINTR	48.40654	45.83755	40.50633	41.85716	39.37375	0.0	23.74289	18.01074	209 27748	0.0
RHOS	0.44491	0.34144	0.32457	0.36868	0.35415	0.0	0.25041	0.20587	2 61015	0.0

LINE NUMBER 4 PIXEL NUMBER 9 SCAN ANGLE= 42.803 DEGREES

	1	2	3	4	5	6	7	8	9	10
LTOT	16.27180	17.40715	16.23152	17.10501	13.93741	0.0	6.73128	4.91411	2.56400	0.0
LPATH	2.60044	2.16785	1.41363	0.91371	0.69245	0.70461	0.70441	0.63967	0.55951	0.49340
LBEAM	13.67136	15.23930	14.81789	16.19130	13.24496	0.0	6.02687	4.27444	2.00448	0.0
LSURF	18.78880	19.21078	17 75186	18.95699	15.46554	0.0	7.40351	5.27564	2 47286	0.0
LINTR	22.56607	22.07225	19.95074	21.32581	17.48938	0.0	7.84003	5.49997	2.55653	0.0
RHOS	0.20741	0.16441	0.15986	0.18784	0.15731	0.0	0.08269	0.06287	0.03189	0.0

LINE NUMBER 4 PIXEL NUMBER 17 SCAN ANGLE= 40.709 DEGREES

	1	2	3	4	5	6	7	8	9	10
LTOT	16.39603	17.14340	16.47745	17.10501	14.29478	0.0	7.17510	5.02839	2.56400	0.0
LPATH	2.53424	2.10642	1.37023	0.88310	0.66655	0.67400	0.67013	0.60630	0.52866	0.46505
LBEAM	13.86179	15.03698	15.10721	16.22191	13.62823	0.0	6.50497	4.42209	2.03533	0.0
LSURF	18.85701	18.81531	17.99379	18.89690	15.83407	0.0	7.93820	5.42112	2 49404	0.0
LINTR	22.64798	21.61787	20.22264	21.25821	17.90613	0.0	8.40624	5.65164	2.57843	0.0
RHOS	0.20816	0.16103	0 16204	0.18724	0.16106	0.0	0.08866	0.06460	0.03216	0.0

LINE NUMBER 4 PIXEL NUMBER 25 SCAN ANGLE= 38.614 DEGREES

	1	2	3	4	5	6	7	8	9	10
LTOT	15.89918	16.87965	16.10855	17.10501	13.93741	0.0	6.95319	4.79983	3.84600	0.0
LPATH	2.47928	2.05536	1.33399	0.85738	0.64464	0.64788	0.64070	0.57756	0 50203	0.44053
LBEAM	13.41990	14.82429	14.77457	16.24762	13 29277	0.0	6.31249	4.22227	3.34197	0.0
LSURF	18.08893	18.42545	17 50597	18.84079	15.37530	0.0	7.65765	5.14478	4.07282	0.0
LINTR	21.72549	21.16994	19 67439	21.19508	17.38733	0.0	8.10915	5.36354	4 21063	0.0
RHOS	0.19968	0.15769	0 15765	0.18669	0.15639	0.0	0.08553	0.06131	0.05252	0.0

LINE NUMBER 4 PIXEL NUMBER 33 SCAN ANGLE= 36.520 DEGREES

	1	2	3	4	5	6	7	8	9	10
LTOT	15.77496	16.61591	15.73966	16.46677	13.69916	0.0	6.80525	4.79983	1.28200	0.0
LPATH	2.43454	2.01368	1.30417	0.83605	0.62628	0.62573	0.61556	0.55290	0 47911	0.41939
LBEAM	13.34042	14.60222	14.43550	15.63072	13.07288	0.0	6.18969	4.24693	0.80289	0 0
LSURF	17.83354	18.04033	17 02394	18.05116	15.06007	0.0	7.46857	5.14655	0 97256	0.0
LINTR	21.41876	20.72746	19 13266	20.30679	17 03084	0.0	7.90893	5.36539	1.00547	0.0
RHOS	0.19686	0.15440	0.15331	0.17886	0.15318	0.0	0.08341	0.06133	0 01254	0.0

LINE NUMBER 4 PIXEL NUMBER 41 SCAN ANGLE= 34.426 DEGREES

	1	2	3	4	5	6	7	8	9	10
LTOT	15.65075	16.74779	15.73966	16.59442	13.46092	0.0	6.80525	4.74269	1.92300	0.0
LPATH	2.39913	1.98052	1.98016	0.81867	0.61111	0.60713	0.59427	0.53184	0.45946	0.40121
LBEAM	13.25162	14.76726	14.45950	15.77575	12.84981	0.0	6.21103	4.21085	1.46354	0.0
LSURF	17.58310	18.14529	16.98009	18.15134	14.74932	0.0	7.45821	5.07766	1.76410	0.0
LINTR	21.11797	20.84805	19.88337	20.41948	16.67943	0.0	7.89796	5.29359	1.82379	0.0
RHOS	0.19410	0.15529	0.15291	0.17986	0.15002	0.0	0.08330	0.06051	0.02275	0.0

LINE NUMBER 4 PIXEL NUMBER 49 SCAN ANGLE= 32.332 DEGREES

	1	2	3	4	5	6	7	8	9	10
LTOT	15.27812	16.35216	15.49373	16.33913	13.22267	0.0	6.65731	4.68555	3.20500	0.0
LPATH	2.37227	1.95514	1.96145	0.80486	0.59080	0.59170	0.57628	0.51399	0.44271	0.38567
LBEAM	12.90564	14.39702	14.23228	15.53427	12.62387	0.0	6.08103	4.17155	2.76229	0.0
LSURF	17.00943	17.60385	16.64948	17.81392	14.44252	0.0	7.27038	5.00794	3.31479	0.0
LINTR	20.42897	20.22597	18.71181	20.03990	16.33247	0.0	7.69905	5.22088	3.42695	0.0
RHOS	0.18777	0.15066	0.14994	0.17651	0.14690	0.0	0.08120	0.05968	0.04274	0.0

LINE NUMBER 4 PIXEL NUMBER 57 SCAN ANGLE= 30.237 DEGREES

	1	2	3	4	5	6	7	8	9	10
LTOT	14.90548	16.08842	15.00187	15.82853	13.10355	0.0	6.28746	4.39984	3.20500	0.0
LPATH	2.35326	1.93686	1.94754	0.79429	0.58908	0.57913	0.56137	0.49901	0.42856	0.37247
LBEAM	12.55222	14.15156	13.75432	15.03424	12.51447	0.0	5.72609	3.90083	2.77644	0.0
LSURF	16.44333	17.22745	16.03499	17.10874	14.27508	0.0	6.81921	4.66418	3.31845	0.0
LINTR	19.74905	19.79349	18.02121	19.33669	16.14313	0.0	7.22127	4.86250	3.43674	0.0
RHOS	0.18152	0.14744	0.14440	0.17032	0.14520	0.0	0.07616	0.05558	0.04279	0.0

LINE NUMBER 4 PIXEL NUMBER 65 SCAN ANGLE= 28.143 DEGREES

	1	2	3	4	5	6	7	8	9	10
LTOT	14.78127	15.95655	14.91000	15.19028	12.38881	0.0	5.99158	4.17128	1.92300	0.0
LPATH	2.34149	1.92511	1.93804	0.78668	0.58171	0.56912	0.54919	0.48660	0.41672	0.36137
LBEAM	12.43977	14.03144	13.77196	14.40361	11.80709	0.0	5.44239	3.68468	1.50627	0.0
LSURF	16.20732	17.01348	15.92473	16.42320	13.43240	0.0	6.45850	4.38984	1.79385	0.0
LINTR	19.46561	19.54761	17.33536	18.47540	15.19018	0.0	6.83930	4.57650	1.85455	0.0
RHOS	0.17891	-0.14561	0.13891	0.16273	0.13663	0.0	0.07213	0.05231	0.02313	0.0

LINE NUMBER 4 PIXEL NUMBER 73 SCAN ANGLE= 26.049 DEGREES

	1	2	3	4	5	6	7	8	9	10
LTOT	14.53284	15.29719	14.14110	14.80733	12.26968	0.0	5.62173	4.05700	1.92300	0.0
LPATH	2.33643	1.91938	1.93258	0.78177	0.57649	0.56145	0.53946	0.47650	0.40698	0.35215
LBEAM	12.19641	13.37781	12.90852	14.02557	11.69319	0.0	5.08227	3.58050	1.51602	0.0
LSURF	15.81254	16.16309	14.98061	15.95312	13.27107	0.0	6.01704	4.25190	1.79962	0.0
LINTR	18.99147	18.57059	16.81375	17.94681	15.00774	0.0	6.36651	4.43270	1.86052	0.0
RHOS	0.17455	0.13833	0.13473	0.15808	0.13499	0.0	0.06715	0.05067	0.02320	0.0

LINE NUMBER 4 PIXEL NUMBER 81 SCAN ANGLE= 23.955 DEGREES

	1	2	3	4	5	6	7	8	9	10
LTOT	14.40863	14.90158	13.89517	14.29674	11.43582	0.0	5.39982	3.88558	1.92300	0.0
LPATH	2.33759	1.91922	1.23084	0.77934	0.57323	0.55589	0.53197	0.46849	0.39912	0.34463
LBEAM	12.07104	12.98235	12.66433	13.51740	10.86259	0.0	4.86785	3.41708	1.52388	0.0
LSURF	15.58146	15.63523	14.64104	15.34187	12 30204	0.0	5.74206	4.04607	1.80371	0.0
LINTR	18.71393	17.96411	16.45459	17.25896	13 91190	0.0	6.08062	4.21011	1.86475	0.0
RHOS	0.17200	0.13381	0.13185	0.15202	0.12513	0.0	0.06413	0.04821	0 02326	0.0

LINE NUMBER 4 PIXEL NUMBER 89 SCAN ANGLE= 21.860 DEGREES

	1	2	3	4	5	6	7	8	9	10
LTOT	14.16020	14.90158	13.64924	14.16909	11.19758	0.0	5.17791	3.94272	1 92300	0.0
LPATH	2.34456	1.92425	1.23257	0.77922	0.57178	0.55229	0.52653	0.46241	0.39299	0.33867
LBEAM	11.81565	12.97733	12.41667	13.38987	10 62580	0.0	4.65138	3.48030	1.53001	0.0
LSURF	15.19223	15.58469	14.32285	15.16767	12.01093	0.0	5.47285	4.11026	1 80630	0.0
LINTR	18.24644	17.90605	16.09698	17.06297	13.58269	0.0	5.79553	4.28504	1.86742	0.0
RHOS	0.16771	0.13338	0.12898	0.15029	0.12217	0.0	0.06113	0.04898	0.02329	0.0

LINE NUMBER 4 PIXEL NUMBER 97 SCAN ANGLE= 19.766 DEGREES

	1	2	3	4	5	6	7	8	9	10
LTOT	13.78757	14.50596	13.03441	13.53084	10.95933	0.0	5.17791	3.77129	1.92300	0.0
LPATH	2.35699	1.93415	1.23755	0.78127	0 57205	0.55056	0.52305	0.45819	0 38852	0.33421
LBEAM	11.43058	12.57181	11.79686	12.74957	10.38728	0.0	4.65485	3.31310	1 53448	0.0
LSURF	14.64623	15.05960	13.58109	14.41753	11 72148	0.0	5.46466	3.90383	1 80742	0.0
LINTR	17.59068	17.30273	15.26335	16.21910	13.25537	0.0	5.78686	4.06983	1.86858	0.0
RHOS	0.16168	0.12889	0.12230	0.14286	0.11923	0.0	0.06103	0.04652	0.02331	0.0

LINE NUMBER 4 PIXEL NUMBER 105 SCAN ANGLE= 17.672 DEGREES

	1	2	3	4	5	6	7	8	9	10
LTOT	14.03599	14.24221	12.91144	13.78614	10 60196	0.0	5.02997	3.77129	1.92300	0.0
LPATH	2.37460	1.94868	1.24564	0.78540	0.57398	0.55066	0.52152	0.45580	0.38570	0.33123
LBEAM	11.66140	12.29354	11.66580	13.00074	10.02798	0.0	4.50844	3.31550	1.53730	0.0
LSURF	14.89646	14.69356	13 40695	14.67932	11 29921	0.0	5.28233	3.89877	1 80710	0.0
LINTR	17.89120	16.88219	15.06764	16.51361	12.77784	0.0	5.59379	4.06455	1 86825	0.0
RHOS	0.16444	0.12575	0 12074	0.14545	0 11493	0.0	0.05900	0.04646	0.02330	0.0

LINE NUMBER 4 PIXEL NUMBER 113 - SCAN ANGLE= 15.578 DEGREES

	1	2	3	4	5	6	7	8	9	10
LTOT	13.66335	13.84660	12.54254	13.02024	10 36371	0.0	4.88203	3.65701	1.92300	0.0
LPATH	2.39711	1.96760	1.25668	0.79151	0.57751	0.55253	0.52190	0.45521	0 38450	0.32970
LBEAM	11 26625	11.87900	11.28586	12.22873	9.78621	0.0	4.36012	3.20181	1.53850	0.0
LSURF	14.35349	14.17064	12 95073	13.78944	11.01251	0.0	5.09978	3.75846	1 80534	0.0
LINTR	17.23907	16.28137	14 55491	15.51259	12 45362	0.0	5.40046	3.91827	1.86643	0.0
RHOS	0.15845	0.12128	0 11663	0.13663	0.11201	0.0	0.05696	0.04479	0 02328	0.0

LINE NUMBER 4 PIXEL NUMBER 121 SCAN ANGLE= 13.484 DEGREES

	1	2	3	4	5	6	7	8	9	10
LTOT	13.78757	14.37409	12.54254	13.02024	10.00634	0.0	4.80806	3.54273	1 28200	0.0
LPATH	2.42429	1.99070	1.27055	0.79954	0.58257	0.55614	0.52416	0.45639	0.38490	0.32961
LBEAM	11.36328	12.38338	11.27199	12.22070	9 42377	0.0	4.28390	3.08634	0.89710	0.0
LSURF	14.44408	14.74777	12 91804	13.76480	10 59286	0.0	5.00322	3.61744	1.05111	0.0
LINTR	17.34789	16.94447	14.51817	15.48482	11 97906	0.0	5.29822	3.77126	1 08668	0.0
RHOS	0.15945	0.12622	0.11633	0.13639	0.10775	0.0	0.05588	0.04311	0 01355	0.0

LINE NUMBER 4 PIXEL NUMBER 129 SCAN ANGLE= 11.389 DEGREES

	1	2	3	4	5	6	7	8	9	10
LTOT	13.78757	13.84660	12.05068	13.02024	10.00634	0.0	4.51218	3.37131	1 28200	0.0
LPATH	2.45593	2.01781	1.28713	0.80939	0 58913	0.56146	0.52827	0.45933	0 38688	0.33094
LBEAM	11.33164	11.82879	10 76355	12.21085	9 41722	0.0	3 98391	2.91197	0.89512	0.0
LSURF	14.37614	14.06754	12.32185	13 74056	10.57556	0.0	4.64707	3.40872	1.04746	0.0
LINTR	17.26630	16.16290	13 84814	15.45756	11.95849	0.0	4 92106	3.55367	1.08290	0.0
RHOS	0.15870	0.12040	0.11096	0.13615	0 10757	0.0	0.05190	0.04062	0 01351	0.0

LINE NUMBER 4 PIXEL NUMBER 137 SCAN ANGLE= 9.295 DEGREES

	1	2	3	4	5	6	7	8	9	10
LTOT	13.66335	13 58285	12.54254	13.02024	10.12547	0.0	4.58615	3.54273	1.92300	0.0
LPATH	2.49181	2.04877	1.30629	0.82099	0 59710	0.56839	0.53415	0.46397	0.39038	0.33364
LBEAM	11.17155	11.53414	11.23625	12 19925	9 52837	0.0	4.05200	3.07077	1 53262	0.0
LSURF	14.15064	13.70132	12.85144	13.71674	10 69213	0.0	4.72165	3.60020	1 79157	0.0
LINTR	16.99585	15.74215	14.44332	15.43675	12.09131	0.0	5.00005	3.75328	1.85220	0.0
RHOS	0.15621	0.11726	0.11573	0.13591	0 10876	0.0	0.05274	0.04290	0.02110	0.0

LINE NUMBER 4 PIXEL NUMBER 145 SCAN ANGLE= 7.201 DEGREES

	1	2	3	4	5	6	7	8	9	10
LTOT	14.03599	14.63783	13.03441	13.65849	10 48284	0.0	4.88203	3.65701	2.56400	0.0
LPATH	2.53170	2.08323	1.32789	0.83425	0 60641	0.57686	0.54170	0.47020	0.39533	0.33764
LBEAM	11.50429	12.55460	11 70652	12.82424	9.87642	0.0	4.34032	3.18682	2 16867	0.0
LSURF	14.55392	14.89996	13.37980	14.41055	11 07595	0.0	5 05354	3.72347	2.53301	0.0
LINTR	17.47980	17.11932	15.03713	16.21126	12 52536	0.0	5.35150	3.88179	2.61872	0.0
RHOS	0.16066	0.12752	0.12049	0.14279	0.11766	0.0	0.05644	0.04437	0.03766	0.0

LINE NUMBER 4 PIXEL NUMBER 153 SCAN ANGLE= 5.107 DEGREES

	1	2	3	4	5	6	7	8	9	10
LTOT	13.66335	14.11034	12.91144	13.78614	10.48284	0.0	4.80806	3.65701	1.28200	0.0
LPATH	2.57543	2.12117	1.35181	0.84907	0.61700	0.58678	0.55085	0.47795	0 40166	0.34290
LBEAM	11.08793	11.98917	11.55963	12.93707	9.86584	0.0	4.25720	3.17906	0.88034	0.0
LSURF	14.01421	14.21931	13 20498	14.53066	11.05909	0.0	4.95380	3.71213	1 02761	0.0
LINTR	16.83160	16.33730	14 88065	16.34637	12 50630	0.0	5.24588	3.86998	1.06218	0.0
RHOS	0.15470	0.12169	0.11892	0.14398	0.11249	0.0	0.05533	0.04423	0.01325	0.0

LINE NUMBER 4 PIXEL NUMBER 161 SCAN ANGLE= 3.018 DEGREES

	1	2	3	4	5	6	7	8	9	10
LTOT	14.28442	14.37409	13.15737	13.76614	10.72108	0.0	5.10394	3.71415	0.64100	0.0
LPATH	2.62281	2.16239	1.37795	0.86539	0.62880	0.59809	0.56154	0.48718	0.40933	0.34937
LBEAM	11.66161	12.21169	11.77942	12.92074	10.09228	0.0	4.54248	3.22647	0.23167	0.0
LSURF	14.73035	14.47683	13.45142	14.50796	11.30958	0.0	5.28359	3.76656	0.27032	0.0
LINTR	17.69171	16.63316	15.11762	16.32085	12.78956	0.0	5.59511	3.92672	0.27946	0.0
RHOS	0.16261	0.12398	0.12114	0.14375	0.11504	0.0	0.05901	0.04488	0.00349	0.0

LINE NUMBER 4 PIXEL NUMBER 169 SCAN ANGLE= 0.918 DEGREES

	1	2	3	4	5	6	7	8	9	10
LTOT	14.03599	14.50596	13.28034	14.29674	10.95933	0.0	4.95600	3.71415	1.28200	0.0
LPATH	2.67171	2.20678	1.40622	0.88316	0.64177	0.61073	0.57371	0.49785	0.41831	0.35703
LBEAM	11.36229	12.29916	11.87411	13.41357	10.31756	0.0	4.38229	3.21630	0.86369	0.0
LSURF	14.34806	14.57743	13.55729	15.05914	11.56038	0.0	5.09638	3.75336	1.00757	0.0
LINTR	17.23257	16.74875	15.23661	16.98090	13.07318	0.0	5.19687	3.91298	1.04166	0.0
RHOS	0.15839	0.12476	0.12209	0.14922	0.11759	0.0	0.05692	0.04473	0.01200	0.0

LINE NUMBER 4 PIXEL NUMBER 177 SCAN ANGLE= -1.176 DEGREES

	1	2	3	4	5	6	7	8	9	10
LTOT	14.28442	14.90158	13.52627	14.29674	10.95933	0.0	5.17791	3.77129	1.28200	0.0
LPATH	2.72810	2.25433	1.43669	0.90248	0.66600	0.62487	0.58756	0.51015	0.42879	0.36607
LBEAM	11.55632	12.64725	12.08958	13.39429	10.30333	0.0	4.59035	3.26115	0.85321	0.0
LSURF	14.59336	14.99019	13.80346	15.03764	11.54454	0.0	5.33842	3.80576	0.99536	0.0
LINTR	17.52718	17.22299	15.51326	16.91670	13.05528	0.0	5.65317	3.96759	1.02904	0.0
RHOS	0.16110	0.12829	0.12431	0.14900	0.11743	0.0	0.05962	0.04535	0.01283	0.0

LINE NUMBER 4 PIXEL NUMBER 185 SCAN ANGLE= -3.270 DEGREES

	1	2	3	4	5	6	7	8	9	10
LTOT	14.03599	14.50596	13.40331	14.29674	11.31670	0.0	5.25188	3.94272	1.92300	0.0
LPATH	2.78617	2.30528	1.46956	0.92346	0.67175	0.64094	0.60364	0.52464	0.44129	0.37694
LBEAM	11.24982	12.20068	11.93375	13.37327	10.64095	0.0	4.64824	3.41808	1.48170	0.0
LSURF	14.21102	14.46438	13.62809	15.01651	11.92924	0.0	5.40689	3.98977	1.72894	0.0
LINTR	17.06798	16.61887	15.31617	16.89294	13.49031	0.0	5.72569	4.15943	1.78745	0.0
RHOS	0.15687	0.12379	0.12273	0.14879	0.12134	0.0	0.06039	0.04754	0.02229	0.0

LINE NUMBER 4 PIXEL NUMBER 193 SCAN ANGLE= -5.365 DEGREES

	1	2	3	4	5	6	7	8	9	10
LTOT	14.16020	14.50596	13.40331	14.16909	11.19758	0.0	5.10394	3.82843	3.20500	0.0
LPATH	2.84813	2.35989	1.50513	0.94648	0.68933	0.65941	0.62256	0.54191	0.45636	0.39016
LBEAM	11.31208	12.14607	11.89818	13.22261	10.50825	0.0	4.48138	3.28652	2.74964	0.0
LSURF	14.29890	14.40641	13.59246	14.85209	11.77975	0.0	5.21498	3.83786	3.20865	0.0
LINTR	17.17352	16.55226	15.27613	16.70796	13.32126	0.0	5.52246	4.00105	3.31723	0.0
RHOS	0.15784	0.12330	0.12241	0.14716	0.11982	0.0	0.05825	0.04573	0.04137	0.0

LINE NUMBER 4 PIXEL NUMBER 201 SCAN ANGLE= -7.459 DEGREES

	1	2	3	4	5	6	7	8	9	10
LTOT	14.03599	14.76970	13 77220	14.42439	11.67407	0.0	5.39982	3.94272	3.20500	0.0
LPATH	2.91412	2 41835	1.54357	0.97168	0.70894	0.68061	0.64472	0.56238	0.47437	0.40606
LBEAM	11.12187	12.35135	12.22863	13.45270	10.96512	0.0	4.75510	3.38034	2.73062	0.0
LSURF	14 07204	14.66019	13 97763	15.11777	12.29769	0.0	5.53697	3.94993	3 18965	0.0
LINTR	16.90105	16.84384	15 70901	17.00685	13.90698	0.0	5.86343	4.11789	3.29759	0.0
RHOS	0.15534	0.12547	0.12587	0.14980	0.12509	0.0	0.06184	0.04707	0 04113	0.0

LINE NUMBER 4 PIXEL NUMBER 209 SCAN ANGLE= -9.553 DEGREES

	1	2	3	4	5	6	7	8	9	10
LTOT	14.78127	15.42906	14.63297	16.39442	13.46092	0.0	7.47098	6.74262	6.41000	0.0
LPATH	2.98403	2.48054	1.58477	0.99896	0.73047	0.70435	0.66990	0.58583	0.49515	0.42448
LBEAM	11.79723	12.94853	13.04820	15.59546	12.73045	0.0	6.80108	6.15678	5 91485	0.0
LSURF	14.94581	15.38344	14.92534	17.53694	14.28653	0.0	7.92597	7.20036	6 91505	0.0
LINTR	17.95049	17.67482	16.77411	19.72832	16.15608	0.0	8.39329	7.50653	7.14904	0.0
RHOS	0.16499	0.13166	0.13441	0.17377	0.14532	0.0	0 08852	0.08580	0.08916	0.0

LINE NUMBER 4 PIXEL NUMBER 217 SCAN ANGLE=-11.647 DEGREES

	1	2	3	4	5	6	7	8	9	10
LTOT	15.89918	17.93463	17.70711	20.16859	18.46408	0.0	16.79121	13.59952	22.43498	0.0
LPATH	3.05774	2.54631	1.62860	1.02918	0.75375	0.73041	0.69783	0.61201	0 51843	0.44520
LBEAM	12.84143	15.38832	16.07851	19.14040	17.71033	0.0	16.09338	12.98751	21.91653	0.0
LSURF	16.29514	18.30367	18.40857	21.54054	19 89085	0.0	18.77492	15.20523	25 65010	0.0
LINTR	19.57108	21.03001	20.68880	24.23219	22 49379	0.0	19.88190	15.85178	26 51805	0.0
RHOS	0.17988	0.15665	0.16578	0.21344	0 20232	0.0	0.20969	0.18119	0.33074	0.0

LINE NUMBER 4 PIXEL NUMBER 225 SCAN ANGLE=-13.741 DEGREES

	1	2	3	4	5	6	7	8	9	10
LTOT	15.27812	16.61591	16.60042	18.12621	16.91548	0.0	16.71724	13.54238	19.22998	0.0
LPATH	3.13544	2.61587	1.67524	1.05953	0.77898	0.75905	0.72885	0.64125	0.54453	0.46846
LBEAM	12.14268	14.00003	14.92518	17.06667	16.13649	0.0	15.98839	12.90113	18 68544	0.0
LSURF	15.43883	16.67625	17.10724	19.22554	18.14066	0.0	18.67621	15.12380	21.89703	0.0
LINTR	19.54262	19.16020	19 22627	21.62791	20.51456	0.0	19.77737	15.76689	22.63799	0.0
RHOS	0.17043	0.14272	0.15406	0.19050	0.18452	0.0	0.20859	0.18022	0 20235	0.0

LINE NUMBER 4 PIXEL NUMBER 233 SCAN ANGLE=-15.836 DEGREES

	1	2	3	4	5	6	7	8	9	10
LTOT	16.76866	18.33025	17.83008	18.25386	16.20074	0.0	14.35021	13.02811	13 46099	0.0
LPATH	3.21745	2.68963	1.72508	1.09335	0.80652	0.79084	0.76364	0.67417	0.57401	0.49478
LBEAM	13.55121	15.64061	16.10500	17.16051	15 39422	0.0	13 58657	12.35393	12 88699	0.0
LSURF	17.26988	18.66208	18.48398	19.35349	17.32583	0.0	15.89456	14.50467	15 12521	0.0
LINTR	20.74179	21.84182	20 77354	21.77197	19.59312	0.0	16.83171	15.12143	15 63702	0.0
RHOS	0.19064	0.15972	0.16646	0.19177	0 17623	0.0	0.17752	0.17208	0 19503	0.0

LINE NUMBER 4 PIXEL NUMBER 241 SCAN ANGLE=-17.930 DEGREES

	1	2	3	4	5	6	7	8	9	10
LTOT	17.63814	20.83583	21.39610	23.74278	21.56128	0.0	17.23503	13.59952	20.51198	0.0
LPATH	3.30415	2.76802	1.77850	1.12996	0.83672	0.82628	0.80280	0.71138	0.60737	0.52458
LBEAM	14.33398	18.06781	19.61758	22.61282	20.72455	0.0	16.43222	12.88813	19.90460	0.0
LSURF	18.31694	21.60069	22.55008	25.53694	23.35579	0.0	19.25728	15.15899	23.40343	0.0
LINTR	21.99934	24.81815	25.34331	28.72798	26.41216	0.0	20.39270	15.80357	24.19536	0.0
RHOS	0.20220	0.18487	0.20307	0.25304	0.23756	0.0	0.21508	0.18064	0.30177	0.0

LINE NUMBER 4 PIXEL NUMBER 249 SCAN ANGLE=-20.024 DEGREES

	1	2	3	4	5	6	7	8	9	10
LTOT	15.52654	17.14340	16.23152	18.12621	15.84338	0.0	15.31182	13.54238	18.58899	0.0
LPATH	3.39586	2.85137	1.83581	1.16962	0.86983	0.86976	0.84678	0.75326	0.64494	0.55815
LBEAM	12.13068	14.29203	14.39571	16.95657	14.97355	0.0	14.46504	12.78912	17.94403	0.0
LSURF	15.54957	17.12527	16.57681	19.17876	16.90016	0.0	16.98595	15.07344	21.14149	0.0
LINTR	18.67661	19.67610	18.63014	21.57529	19.11172	0.0	17.98744	15.71439	21.85687	0.0
RHOS	0.17165	0.14656	0.14928	0.19004	0.17190	0.0	0.18971	0.17962	0.27260	0.0

LINE NUMBER 4 PIXEL NUMBER 257 SCAN ANGLE=-22.118 DEGREES

	1	2	3	4	5	6	7	8	9	10
LTOT	15.65075	16.48404	15.73966	16.33913	14.65215	0.0	14.20227	13.14239	14.10199	0.0
LPATH	3.49274	2.93986	1.89714	1.21244	0.90592	0.90931	0.89557	0.79980	0.68669	0.59541
LBEAM	12.15801	13.54418	13.84252	15.12469	13.74622	0.0	13.30670	12.34259	13.41530	0.0
LSURF	15.63959	16.27084	15.97175	17.13898	15.54159	0.0	15.66139	14.58111	15.84259	0.0
LINTR	18.76374	18.69440	17.95013	19.28062	17.57538	0.0	16.58479	15.20112	16.37866	0.0
RHOS	0.17264	0.13925	0.14383	0.16982	0.15808	0.0	0.17492	0.17375	0.20428	0.0

LINE NUMBER 4 PIXEL NUMBER 265 SCAN ANGLE=-24.213 DEGREES

	1	2	3	4	5	6	7	8	9	10
LTOT	15.65075	17.01152	16.47745	17.48796	16.08162	0.0	15.23785	13.42809	17.30699	0.0
LPATH	3.59489	3.03360	1.96253	1.25841	0.94498	0.95682	0.94901	0.85081	0.73241	0.63613
LBEAM	12.05586	13.97792	14.51491	16.22954	15.13664	0.0	14.28883	12.57728	16.57457	0.0
LSURF	15.56987	16.84053	16.78537	18.42477	17.14674	0.0	16.86057	14.89746	19.62486	0.0
LINTR	18.70001	19.34894	18.86453	20.72710	19.39058	0.0	17.85468	15.53092	20.28893	0.0
RHOS	0.17187	0.14413	0.15116	0.18256	0.17441	0.0	0.18831	0.17752	0.25305	0.0

LINE NUMBER 4 PIXEL NUMBER 273 SCAN ANGLE=-26.307 DEGREES

	1	2	3	4	5	6	7	8	9	10
LTOT	16.02338	17.67088	16.72339	18.50916	16.43900	0.0	14.05433	13.54238	24.35799	0.0
LPATH	3.70242	3.13262	2.03195	1.30743	0.98680	1.00795	1.00660	0.90574	0.78153	0.67980
LBEAM	12.32095	14.53826	14.69144	17.20172	15.45220	0.0	13.04773	12.63663	23.57645	0.0
LSURF	15.98321	17.57249	17.03252	19.57161	17.54227	0.0	15.44048	15.01191	27.99750	0.0
LINTR	19.19644	20.18994	19.14229	22.01723	19.83781	0.0	16.35086	15.65024	28.94487	0.0
RHOS	0.17644	0.15039	0.15338	0.19393	0.17843	0.0	0.17245	0.17888	0.36101	0.0

LINE NUMBER 4 PIXEL NUMBER 281 SCAN ANGLE=-28.401 DEGREES

	1	2	3	4	5	6	7	8	9	10
LTOT	15.65075	16.87965	16.35449	17.36032	15.48601	0.0	14.49815	13.48524	18.58899	0.0
LPATH	3.81532	3.23684	2.10521	1.35925	1.03106	1.06709	1.06751	0.96373	0.83324	0.72562
LBEAM	11.83543	13.64282	14.24928	16.00105	14.45495	0.0	13.43064	12.52150	17.75574	0.0
LSURF	15.42984	16.54994	16.56660	18.25044	16.44987	0.0	15.94478	14.92414	21.15459	0.0
LINTR	18.53181	19.01508	18.61867	20.53098	18.60252	0.0	16.88490	15.55873	21.87041	0.0
RHOS	0.17033	0.14164	0.14919	0.18084	0.16732	0.0	0.17808	0.17784	0.27277	0.0

LINE NUMBER 4 PIXEL NUMBER 289 SCAN ANGLE=-30.495 DEGREES

	1	2	3	4	5	6	7	8	9	10
LTOT	16.02338	16.87965	15.86263	17.23267	15.12864	0.0	12.87080	13.54238	23.07599	0.0
LPATH	3.93348	3.34605	2.18203	1.41356	1.07736	1.11857	1.13083	1.02382	0.88665	0.77281
LBEAM	12.08990	13.53360	13.68060	15.81911	14.05128	0.0	11.73997	12.51855	22.18933	0.0
LSURF	15.84900	16.48373	15.95551	18.09247	16.03366	0.0	13.98760	14.97534	26.53360	0.0
LINTR	19.03525	18.93901	17.93188	20.35326	18.13184	0.0	14.81232	15.61211	27.43144	0.0
RHOS	0.17496	0.14107	0.14369	0.17927	0.16309	0.0	0.15622	0.17845	0.34213	0.0

LINE NUMBER 4 PIXEL NUMBER 297 SCAN ANGLE=-32.589 DEGREES

	1	2	3	4	5	6	7	8	9	10
LTOT	15.15390	15.69281	14.51000	14.80733	11.55495	0.0	5.47379	3.88558	2.56400	0.0
LPATH	4.05665	3.45996	2.26206	1.46997	1.12524	1.17661	1.19556	1.08501	0.94085	0.82055
LBEAM	11.09725	12.23285	12.24794	13.33736	10.42970	0.0	4.27823	2.80056	1.62315	0.0
LSURF	14.63737	14.96627	14.33456	15.30063	11.93685	0.0	5.11760	3.36383	1.94882	0.0
LINTR	17.58003	17.19551	16.11014	17.21257	13.49893	0.0	5.41934	3.50686	2.01476	0.0
RHOS	0.16158	0.12809	0.12909	0.15161	0.12142	0.0	0.05716	0.04008	0.02513	0.0

LINE NUMBER 4 PIXEL NUMBER 305 SCAN ANGLE=-34.684 DEGREES

	1	2	3	4	5	6	7	8	9	10
LTOT	15.02969	15.29719	14.14110	14.29674	11.07845	0.0	5.02997	3.48559	1.92300	0.0
LPATH	4.18454	3.57821	2.34493	1.52809	1.17421	1.23539	1.26064	1.14627	0.99492	0.86803
LBEAM	10.84515	11.71898	11.79617	12.76865	9.90424	0.0	3.76933	2.33932	0.92808	0.0
LSURF	14.40268	14.40894	13.85940	14.69781	11.37319	0.0	4.52879	2.82752	1.11932	0.0
LINTR	17.29817	16.55516	15.57614	16.53442	12.86150	0.0	4.79581	2.94254	1.15719	0.0
RHOS	0.15899	0.12332	0.12481	0.14564	0.11568	0.0	0.05058	0.03363	0.01443	0.0

LINE NUMBER 4 PIXEL NUMBER 313 SCAN ANGLE=-36.778 DEGREES

	1	2	3	4	5	6	7	8	9	10
LTOT	15.65075	15.95655	14.26407	14.29674	11.19758	0.0	5.39982	3.71415	3.20500	0.0
LPATH	4.31689	3.70049	2.43025	1.58750	1.22377	1.29402	1.32494	1.20646	1.04783	0.91437
LBEAM	11.33387	12.25607	11.83381	12.70923	9.97380	0.0	4.07488	2.50769	2.15716	0.0
LSURF	15.16594	15.15251	13.96348	14.68458	11.49536	0.0	4.91991	3.04085	2.61470	0.0
LINTR	18.21486	17.40950	15.69311	16.51930	12.99966	0.0	5.20999	3.17015	2.70317	0.0
RHOS	0.16742	0.12968	0.12575	0.14550	0.11693	0.0	0.05095	0.03624	0.03371	0.0

LINE NUMBER 4 PIXEL NUMBER 321 SCAN ANGLE=-38.872 DEGREES

	1	2	3	4	5	6	7	8	9	10
LTOT	15.52654	15.82468	14.51000	14.16909	10.95933	0.0	5.10394	3.54273	1.92300	0.0
LPATH	4.45335	3.82642	2.51766	1.64783	1.27345	1.35170	1.38744	1.26461	1.09875	0.95883
LBEAM	11.07319	11.99826	11.99234	12.52125	9.68588	0.0	3.71650	2.27812	0.82425	0.0
LSURF	14.94189	14.92465	14.21812	14.52747	11.20924	0.0	4.51163	2.77785	1.00462	0.0
LINTR	17.94577	17.14769	15.97929	16.34279	12.67609	0.0	4.77763	2.89597	1.03861	0.0
RHOS	0.16494	0.12773	0.12804	0.14395	0.11402	0.0	0.05039	0.03310	0.01295	0.0

LINE NUMBER 4 PIXEL NUMBER 329 SCAN ANGLE=-40.966 DEGREES

	1	2	3	4	5	6	7	8	9	10
LTOT	16.02338	16.74779	14.87890	15.19028	11.31670	0.0	5.39982	3.82843	1.92300	0.0
LPATH	4.59359	3.95568	2.60679	1.70875	1.32286	1.40776	1.44730	1.31996	1.14706	1.00095
LBEAM	11.42979	12.79211	12.27211	13.48153	9.99388	0.0	3.95252	2.50847	0.77594	0.0
LSURF	15.56729	16.02036	14.62695	15.71399	11.61822	0.0	4.82717	3.07763	0.95156	0.0
LINTR	18.69690	18.40660	16.43875	17.67757	13.13860	0.0	5.11173	3.20849	0.98376	0.0
RHOS	0.17185	0.13711	0.13172	0.15570	0.11818	0.0	0.05391	0.03667	0.01227	0.0

LINE NUMBER 4 PIXEL NUMBER 337 SCAN ANGLE=-43.061 DEGREES

	1	2	3	4	5	6	7	8	9	10
LTOT	15.89918	16.74779	14.75593	14.55203	10.84021	0.0	5.02997	3.54273	2.56400	0.0
LPATH	4.73735	4.08804	2.69743	1.77000	1.37177	1.46166	1.50389	1.37196	1.19235	1.04042
LBEAM	11.16183	12.65975	12.05851	12.78203	9.46849	0.0	3.52608	2.17077	1.37165	0.0
LSURF	15.36040	15.97450	14.45708	14.97528	11.06312	0.0	4.33528	2.68160	1.69365	0.0
LINTR	18.44843	18.35393	16.24785	16.84656	12.51086	0.0	4.59085	2.79562	1.75096	0.0
RHOS	0.16956	0.13672	0.13019	0.14838	0.11253	0.0	0.04842	0.03195	0.02184	0.0

SIMULATION DATE IS: SEPTEMBER 24, 1976

LATITUDE= 41DEG 47MIN 0.0 SEC LONGITUDE= 82DEG 45MIN 0.0 SEC
TIME IS 14: 6: 0.0 TIME ZONE 5
SOLAR ZENITH ANGLE= 48 DEGREES 39 MINUTES 17.172 SECONDS
SOLAR AZIMUTH ANGLE= 323 DEGREES 23 MINUTES 51.738 SECONDS
PARTICULATE REFRACTIVE INDEX=1.50-0.01I

FIGURE A-3

Results of Using the Command File With Original OCS-2 Calibration Factors

INPUT OPTICAL THICKNESSES

	1	2	3	4	5	6
WAVELENGTH	0.4000000	0.5000000	0.6100000	0.7487000	0.8730000	1.0400000
OPTICAL THICKNESS (MEASURED)	0.4000000	0.2000000	0.1900000	0.1800000	0.1800000	0.2100000

AZIMUTH ANGLE FROM SUN TO SCAN PLANE=295 DEGREES, 0 MINUTES, 0.0 SECONDS
MAXIMUM SCAN ANGLE=0.7836000 RADIANS. ANGULAR RESOLUTION OF SCANNER IS 0.0045684 RADIANS.

CHANNEL	1	2	3	4	5	6	7	8	9	10
WAVELENGTH	0.42000	0.46600	0.50800	0.54900	0.59200	0.63700	0.67400	0.71400	0.75600	0.79400
INTERPOLATED OPTICAL THICKNESS	0.31271	0.23619	0.19497	0.18410	0.18781	0.19106	0.18884	0.18405	0.17934	0.17731
BACKGROUND ALBEDO	0.02000	0.02000	0.02000	0.02000	0.02000	0.02000	0.02000	0.02000	0.02000	0.02000
SINGLE SCATTERING ALBEDO	1.00000	0.98185	0.93054	0.83695	0.76230	0.84666	0.93333	0.96746	0.98024	0.98181
SCATTERING PARAMETER (FSCAT)	1.00000	1.00000	1.00000	1.00000	1.00000	1.00000	1.00000	1.00000	1.00000	1.00000

LINE NUMBER 4 PIXEL NUMBER 1 SCAN ANGLE= 44.897 DEGREES

	1	2	3	4	5	6	7	8	9	10
LTOT	21.11635	22.41853	20.90413	21.70035	20.25096	0.0	16.76656	12.95195	108.97118	0.0
LPATH	2.67908	2.24081	1.46501	0.94981	0 72285	0.74029	0.74419	0.67832	0.59518	0.52614
LBEAM	18.43726	20.17772	19.43912	20.75053	19.52811	0.0	16.02237	12.27363	108.37599	0.0
LSURF	25.62830	25.64763	23 43898	24.43234	22 92877	0.0	19 82739	15.26208	134.70673	0.0
LINTR	30.78056	29.46788	26.34232	27.48535	25.92926	0.0	20.99643	15.91188	139.26497	0.0
RHOS	0.28291	0.21950	0.21108	0.28209	0.23322	0.0	0.22145	0.18187	1.73694	0.0

LINE NUMBER 4 PIXEL NUMBER 9 SCAN ANGLE= 42.803 DEGREES

	1	2	3	4	5	6	7	8	9	10
LTOT	10 84801	11.60489	10.82096	11.40333	9.29162	0.0	5.98336	4.36811	1.70935	0.0
LPATH	2.68044	2,16785	1.41363	0.91371	0.69245	0.70461	0.70441	0.63967	0.55951	0.49340
LBEAM	8.24756	9.43704	9 40733	10.48962	8 59917	0.0	5.27896	3.72843	1 14984	0 0
LSURF	11.33478	11.89641	11.27001	12.28139	10.04086	0.0	6.48476	4.60175	1 41851	0 0
LINTR	13.61351	13.66840	12.66600	13.81604	11.35482	0.0	6.86710	4.79742	1 46651	0.0
RHOS	0.12512	0.10161	0.10149	0.12169	0.10213	0.0	0.07243	0.05484	0.01829	0.0

LINE NUMBER 4 PIXEL NUMBER 17 SCAN ANGLE= 40.709 DEGREES

	1	2	3	4	5	6	7	8	9	10
LTOT	10.93082	11.42906	10.98492	11.40333	9.52987	0.0	6.37787	4.46969	1.70935	0.0
LPATH	2.53424	2.10642	1.37023	0.88310	0 66655	0.67400	0.67013	0.60630	0.52866	0.46505
LBEAM	8.39658	9.32264	9.61468	10.52022	8.86132	0.0	5.70774	3.86339	1.18069	0.0
LSURF	11.42237	11.66513	11.45180	12.25501	10.29792	0.0	6.96531	4.73620	1 44678	0.0
LINTR	13.71670	13.40267	12.87031	13.78637	11.64552	0.0	7.37600	4.93759	1.49574	0.0
RHOS	0.12609	0.09983	0.10313	0.12143	0.10475	0.0	0.07779	0.05644	0 01866	0 0

LINE NUMBER 4 PIXEL NUMBER 25 SCAN ANGLE= 38.614 DEGREES

	1	2	3	4	5	6	7	8	9	10
LTOT	10.59958	11.25323	10.73899	11.40333	9.29162	0.0	6.18062	4.26652	2 56403	0.0
LPATH	2.47928	2.05536	1.33399	0.85738	0.64464	0.64788	0.64070	0.57756	0.50203	0.44053
LBEAM	8.12030	9.19787	9.40500	10.54594	8.64698	0.0	5.53991	3.68896	2 06200	0.0
LSURF	10.94550	11.43224	11.14373	12.22911	10.00167	0.0	6.72044	4.49495	2 51143	0.0
LTNTR	13.14597	13.13509	12.52408	13.75724	11.31050	0.0	7.11669	4.68608	2 59641	0.0
RHOS	0.12083	0.09784	0.10035	0.12117	0.10173	0.0	0.07506	0.05356	0.03238	0.0

LINE NUMBER 4 PIXEL NUMBER 33 SCAN ANGLE= 36.520 DEGREES

	1	2	3	4	5	6	7	8	9	10
LTOT	10.51677	11.07740	10.49306	10.97783	9.13279	0.0	6.04912	4.26652	0.85868	0.0
LPATH	2.43454	2.01368	1.30417	0.83605	0.62628	0.62573	0.61556	0.55290	0 47911	0.41939
LBEAM	8.08223	9.06371	9.18089	10.14178	8 50651	0.0	5.43355	3.71363	0 37557	0.0
LSURF	10.80437	11.19777	10.83657	11.71226	9.79957	0.0	6.55621	4.50028	0 45494	0.0
CINTR	12.97646	12.86570	12.17887	13.17580	11.08195	0.0	6.94277	4.69164	0 47033	0.0
RHOS	0.11927	0.09583	0.09759	0.11605	0.09968	0.0	0.07322	0.05363	0 00587	0.0

LINE NUMBER 4 PIXEL NUMBER 41 SCAN ANGLE= 34.426 DEGREES

	1	2	3	4	5	6	7	8	9	10
LTOT	10.43396	11.16531	10.49306	11.06293	8.97396	0.0	6.04912	4.21573	1.28201	0.0
LPATH	2.39913	1.98052	1.28016	0.81867	0.61111	0.60713	0.59422	0.53184	0.45946	0.40121
LBEAM	8.03483	9.18479	9.21289	10.24426	8.36285	0.0	5.45489	3.68389	0.82256	0.0
LSURF	10.66113	11.28583	10.81890	11.78689	9.59908	0.0	6.55024	4.44224	0.99148	0.0
LINTR	12.80442	12.96687	12.15901	13.25976	10.85523	0.0	6.93645	4.63113	1.02503	0.0
RHOS	0.11769	0.09659	0.09743	0.11679	0.09764	0.0	0.07316	0.05293	0.01278	0.0

LINE NUMBER 4 PIXEL NUMBER 49 SCAN ANGLE= 32.332 DEGREES

	1	2	3	4	5	6	7	8	9	10
LTOT	10.18553	10.90156	10.32910	10.89273	8.81515	0.0	5.91761	4.16494	2.13669	0.0
LPATH	2.37227	1.95514	1.26145	0.80486	0.59880	0.59170	0.57628	0.51399	0.44271	0.38567
LBEAM	7.81326	8.94643	9.06765	10.08787	8.21633	0.0	5.34133	3.65095	1.69398	0.0
LSURF	10.29760	10.93918	10.60769	11.56827	9.40001	0.0	6.38601	4.38295	2.03280	0.0
LINTR	12.36781	12.56859	11.92165	13.01382	10.63010	0.0	6.76253	4.56932	2.10159	0.0
RHOS	0.11367	0.09362	0.09553	0.11463	0.09561	0.0	0.07132	0.05223	0.02621	0.0

LINE NUMBER 4 PIXEL NUMBER 57 SCAN ANGLE= 30.237 DEGREES

	1	2	3	4	5	6	7	8	9	10
LTOT	9.93711	10.72573	10.00119	10.55233	8.73571	0.0	5.58086	3.91098	2.13669	0.0
LPATH	2.35726	1.93686	1.24754	0.79429	0.58908	0.57913	0.56137	0.49901	0.42856	0.37247
LBEAM	7.58384	8.78887	8.75365	9.75804	8.14663	0.0	5.02748	3.41197	1.70813	0.0
LSURF	9.93479	10.69916	10.20513	11.15643	9.29275	0.0	5.98724	4.07965	2.04159	0.0
LINTR	11.93207	12.29282	11.46922	12.55051	10.50881	0.0	6.34025	4.25312	2.11067	0.0
RHOS	0.10967	0.09157	0.09190	0.11055	0.09452	0.0	0.06687	0.04861	0.02632	0.0

LINE NUMBER 4 PIXEL NUMBER 65 SCAN ANGLE= 28.143 DEGREES

	1	2	3	4	5	6	7	8	9	10
LTOT	9.85430	10.63782	9.67329	10.12683	8.25922	0.0	5.32585	3.70781	1.28201	0.0
LPATH	2.34149	1.92511	1.23804	0.78668	0.58171	0.56912	0.54919	0.48660	0.41672	0.36137
LBEAM	7.51280	8.71271	8.43525	9.34016	7.67750	0.0	4.77666	3.22122	0.86529	0.0
LSURF	9.78815	10.56435	9.80348	10.64979	8.73435	0.0	5.66848	3.83768	1.03049	0.0
LINTR	11.75595	12.13793	11.01782	11.98057	9.87734	0.0	6.00270	4.00006	1.06536	0.0
RHOS	0.10805	0.09041	0.08828	0.10553	0.08884	0.0	0.06331	0.04573	0.01329	0.0

LINE NUMBER 4 PIXEL NUMBER 73 SCAN ANGLE= 26.049 DEGREES

	1	2	3	4	5	6	7	8	9	10
LTOT	9.68868	10.19824	9.42736	9.87154	8.17980	0.0	4.99710	3.60623	1.28201	0.0
LPATH	2.33643	1.91938	1.23258	0.78177	0.57649	0.56145	0.53946	0.47650	0.40698	0.35215
LBEAM	7.35224	8.27886	8.19478	9.08977	7.60331	0.0	4.45763	3.12973	0.87504	0.0
LSURF	9.53212	10.00252	9.49751	10.33912	8.62930	0.0	5.27313	3.71660	1.03873	0.0
LINTR	11.44845	11.49241	10.67395	11.63108	9.75854	0.0	5.58404	3.87464	1.07388	0.0
RHOS	0.10522	0.08561	0.08553	0.10245	0.08777	0.0	0.05889	0.04429	0.01379	0.0

LINE NUMBER 4 PIXEL NUMBER 81 SCAN ANGLE= 23.955 DEGREES

	1	2	3	4	5	6	7	8	9	10
LTOT	9.60587	9.93449	9.26340	9.53114	7.62389	0.0	4.79984	3.45385	1.28201	0.0
LPATH	2.33759	1.91922	1.23084	0.77934	0.57323	0.55589	0.53197	0.46849	0.39912	0.34463
LBEAM	7.26828	8.01527	8.03256	8.75180	7.05066	0.0	4.26787	2.98536	0.88290	0.0
LSURF	9.38199	9.65314	9.28632	9.93305	7.98497	0.0	5.03833	3.53487	1.04502	0.0
LINTR	11.26813	11.09099	10.43660	11.17426	9.02990	0.0	5.33116	3.68518	1.08039	0.0
RHOS	0.10357	0.08262	0.08163	0.09842	0.08122	0.0	0.05623	0.04212	0.01347	0.0

LINE NUMBER 4 PIXEL NUMBER 89 SCAN ANGLE= 21.860 DEGREES

	1	2	3	4	5	6	7	8	9	10
LTOT	9.44025	9.93449	9.09945	9.44804	7.46506	0.0	4.60259	3.50464	1.28201	0.0
LPATH	2.34456	1.92425	1.23257	0.77922	0.57178	0.55229	0.52653	0.46241	0.39299	0.33867
LBEAM	7.09569	8.01024	7.86688	8.66882	6.89328	0.0	4.07606	3.04223	0.88903	0.0
LSURF	9.12344	9.61964	9.07456	9.81753	7.79186	0.0	4.79592	3.59290	1.04957	0.0
LINTR	10.95761	11.05250	10.19863	11.04431	8.81151	0.0	5.07869	3.74567	1.08504	0.0
RHOS	0.10071	0.08233	0.08172	0.09728	0.07926	0.0	0.05356	0.04281	0.01353	0.0

LINE NUMBER 4 PIXEL NUMBER 97 SCAN ANGLE= 19.766 DEGREES

	1	2	3	4	5	6	7	8	9	10
LTOT	9.19182	9.67074	8.68956	9.02054	7.30623	0.0	4.60259	3.35227	1.28201	0.0
LPATH	2.35699	1.93415	1.23755	0.78127	0.57205	0.55056	0.52305	0.45819	0.38852	0.33421
LBEAM	6.83483	7.73659	7.45201	8.23927	6.73418	0.0	4.07953	2.89408	0.89349	0.0
LSURF	8.75761	9.26756	8.57910	9.31717	7.59915	0.0	4.78925	3.41009	1.05242	0.0
LINTR	10.51822	10.64797	9.84178	10.48143	8.59359	0.0	5.07162	3.55509	1.08804	0.0
RHOS	0.09667	0.07932	0.07726	0.09232	0.07730	0.0	0.05349	0.04064	0.01357	0.0

LINE NUMBER 4 PIXEL NUMBER 105 SCAN ANGLE= 17.672 DEGREES

	1	2	3	4	5	6	7	8	9	10
LTOT	9.35744	9.89491	8.60759	9.19074	7.06798	0.0	4.47108	3.35227	1.28201	0.0
LPATH	2.37460	1.94868	1.24564	0.78548	0.57398	0.55066	0.52152	0.45580	0.38570	0.33123
LBEAM	6.98284	7.94623	7.36195	8.40534	6.49400	0.0	3.94956	2.89647	0.89631	0.0
LSURF	8.92000	9.01946	8.46073	9.49059	7.31723	0.0	4.62751	3.40602	1.05362	0.0
LINTR	10.71126	10.36292	9.50475	10.67642	8.27478	0.0	4.90036	3.55085	1.08927	0.0
RHOS	0.09847	0.07719	0.07619	0.09404	0.07443	0.0	0.05168	0.04059	0.01359	0.0

LINE NUMBER 4 PIXEL NUMBER 113 SCAN ANGLE= 15.578 DEGREES

	1	2	3	4	5	6	7	8	9	10
LTOT	9.10901	9.23116	8.36165	8.68014	6.90915	0.0	4.33958	3.25068	1.28201	0.0
LPATH	2.39711	1.96760	1.25668	0.79151	0.57751	0.55253	0.52190	0.45521	0.38450	0.32970
LBEAM	6.71190	7.26356	7.10497	7.88863	6.33164	0.0	3.81768	2.79548	0.89751	0.0
LSURF	8.55114	8.66481	8.15308	8.89543	7.12506	0.0	4.46531	3.28149	1.05318	0.0
LINTR	10.27024	9.95545	9.10299	10.00699	8.05745	0.0	4.72859	3.42107	1.08882	0.0
RHOS	0.09440	0.07416	0.07342	0.08814	0.07247	0.0	0.04987	0.03910	0.01358	0.0

LINE NUMBER 4 PIXEL NUMBER 121 SCAN ANGLE= 13.484 DEGREES

	1	2	3	4	5	6	7	8	9	10
LTOT	9.19182	9.58283	8.36165	8.68014	6.67091	0.0	4.27383	3.14910	0.85468	0.0
LPATH	2.42429	1.99070	1.27055	0.79954	0.58257	0.55614	0.52416	0.45639	0.38490	0.32961
LBEAM	6.76753	7.59212	7.09110	7.88061	6.08833	0.0	3.74967	2.69271	0.46978	0.0
LSURF	8.60234	9.04171	8.12662	8.87633	6.84368	0.0	4.37929	3.15607	0.55043	0.0
LINTR	10.33174	10.38848	9.13324	9.90549	7.73920	0.0	4.63750	3.29027	0.56905	0.0
RHOS	0.09496	0.07738	0.07318	0.08795	0.06961	0.0	0.04891	0.03761	0.00710	0.0

LINE NUMBER 4 PIXEL NUMBER 129 SCAN ANGLE= 11.389 DEGREES

	1	2	3	4	5	6	7	8	9	10
LTOT	9.19182	9.23116	8.03375	8.68014	6.67091	0.0	4.01083	2.99673	0.85468	0.0
LPATH	2.45593	2.01781	1.28713	0.80939	0.58913	0.56146	0.52827	0.45933	0.38688	0.33094
LBEAM	6.73589	7.21335	6.74662	7.87075	6.08178	0.0	3.48256	2.53739	0.46780	0.0
LSURF	8.54564	8.57857	7.72337	8.85676	6.82985	0.0	4.06226	2.97024	0.54741	0.0
LINTR	10.28365	9.85536	8.68004	9.96548	7.72362	0.0	4.30178	3.09654	0.56593	0.0
RHOS	0.09433	0.07342	0.06955	0.08776	0.06947	0.0	0.04537	0.03539	0.00706	0.0

LINE NUMBER 4 PIXEL NUMBER 137 SCAN ANGLE= 9.295 DEGREES

	1	2	3	4	5	6	7	8	9	10
LTOT	9.10901	9.05533	8.36165	8.68014	6.75032	0.0	4.07658	3.14910	1.28201	0.0
LPATH	2.49181	2.04872	1.30629	0.82099	0.59710	0.56839	0.53415	0.46397	0.39038	0.33364
LBEAM	6.61721	7.00662	7.05536	7.85915	6.15322	0.0	3.54243	2.68513	0.89163	0.0
LSURF	8.38180	8.32311	8.06956	8.83677	6.90475	0.0	4.12787	3.13990	1.04229	0.0
LINTR	10.06606	9.56285	9.06911	9.94049	7.80832	0.0	4.37125	3.27341	1.07756	0.0
RHOS	0.09253	0.07123	0.07267	0.08756	0.07023	0.0	0.04610	0.03742	0.01344	0.0

LINE NUMBER 4 PIXEL NUMBER 145 SCAN ANGLE= 7.201 DEGREES

	1	2	3	4	5	6	7	8	9	10
LTOT	9.35744	9.75866	8.68956	9.10564	6.98857	0.0	4.33958	3.25068	1.70935	0.0
LPATH	2.53170	2.08323	1.32789	0.83425	0.60641	0.57686	0.54170	0.47020	0.39533	0.33764
LBEAM	6.82574	7.67543	7.36167	8.27139	6.38216	0.0	3.79788	2.78049	1.31403	0.0
LSURF	8.63514	9.10930	8.41392	9.29453	7.15729	0.0	4.42196	3.24871	1.53478	0.0
LINTR	10.37114	10.48614	9.45614	10.45596	8.09390	0.0	4.68268	3.38685	1.58671	0.0
RHOS	0.09532	0.07796	0.07577	0.09210	0.07280	0.0	0.04939	0.03871	0.01979	0.0

LINE NUMBER 4 PIXEL NUMBER 153 SCAN ANGLE= 5.107 DEGREES

	1	2	3	4	5	6	7	8	9	10
LTOT	9.10901	9.40699	8.60759	9.19074	6.98857	0.0	4.27383	3.25068	0.85468	0.0
LPATH	2.57543	2.12117	1.35181	0.84907	0.61706	0.58678	0.55085	0.47795	0.40166	0.34290
LBEAM	6.53359	7.28582	7.25578	8.34167	6.37157	0.0	3.72298	2.77273	0.45302	0.0
LSURF	8.25791	8.64108	8.28853	9.36921	7.14220	0.0	4.33216	3.23767	0.52880	0.0
LINTR	9.91806	9.92818	9.31522	10.53996	8.07684	0.0	4.58758	3.37534	0.54674	0.0
RHOS	0.09116	0.07395	0.07464	0.09214	0.07265	0.0	0.04838	0.03858	0.00682	0.0

LINE NUMBER 4 PIXEL NUMBER 161 SCAN ANGLE= 3.012 DEGREES

	1	2	3	4	5	6	7	8	9	10
LTOT	9.52306	9.58285	8.77154	9.19078	7.14740	0.0	4.53684	3.30148	0.42734	0.0
LPATH	2.62281	2.16239	1.37795	0.86539	0.62880	0.59809	0.56154	0.48718	0.40933	0.34937
LBEAM	6.90025	7.42043	7.39359	8.32535	6.51860	0.0	3.97530	2.81429	0.01801	0.0
LSURF	8.71605	8.79684	8.44305	9.34805	7.30485	0.0	4.62395	3.28488	0.02101	0.0
LINTR	10.46831	10.10714	9.48887	10.51617	8.26077	0.0	4.89658	3.42456	0.02172	0.0
RHOS	0.09622	0.07529	0.07603	0.09263	0.07430	0.0	0.05164	0.03914	0.00027	0.0

LINE NUMBER 4 PIXEL NUMBER 169 SCAN ANGLE= 0.918 DEGREES

	1	2	3	4	5	6	7	8	9	10
LTOT	9.35744	9.67074	8.85352	9.53114	7.30623	0.0	4.40533	3.30148	0.85468	0.0
LPATH	2.67371	2.20678	1.40422	0.88316	0.64177	0.61073	0.57371	0.49785	0.41851	0.35703
LBEAM	6.68373	7.46396	7.44729	8.64798	6.66446	0.0	3.83162	2.80363	0.43636	0.0
LSURF	8.44008	8.84656	8.50296	9.70891	7.46724	0.0	4.45599	3.27179	0.50906	0.0
LINTR	10.13686	10.16427	9.55620	10.92211	8.44441	0.0	4.71872	3.41092	0.52628	0.0
RHOS	0.09317	0.07571	0.07657	0.09620	0.07595	0.0	0.04977	0.03899	0.00656	0.0

LINE NUMBER 4 PIXEL NUMBER 177 SCAN ANGLE= -1.176 DEGREES

	1	2	3	4	5	6	7	8	9	10
LTOT	9.52306	9.93449	9.01747	9.53114	7.30623	0.0	4.60259	3.35227	0.85468	0.0
LPATH	2.72810	2.25433	1.43669	0.90244	0.65600	0.62487	0.58756	0.51015	0.42879	0.36607
LBEAM	6.79496	7.68016	7.58078	8.62878	6.65023	0.0	4.01503	2.84212	0.42588	0.0
LSURF	8.58070	9.10293	8.65547	9.68735	7.45137	0.0	4.66934	3.31676	0.49684	0.0
LINTR	10.30575	10.05883	9.72760	10.89787	8.42646	0.0	4.94464	3.45779	0.51365	0.0
RHOS	0.09472	0.07791	0.07795	0.09599	0.07579	0.0	0.05215	0.03952	0.00641	0.0

LINE NUMBER 4 PIXEL NUMBER 185 SCAN ANGLE= -3.270 DEGREES

	1	2	3	4	5	6	7	8	9	10
LTOT	9.35744	9.67074	8.93549	9.53114	7.54448	0.0	4.66834	3.50464	1.28201	0.0
LPATH	2.78617	2.30528	1.46956	0.92346	0.67175	0.64094	0.60364	0.52464	0.44129	0.37694
LBEAM	6.57127	7.36546	7.46593	8.60768	6.87272	0.0	4.06470	2.98000	0.84072	0.0
LSURF	8.30097	8.73204	8.52594	9.66534	7.70190	0.0	4.72811	3.47843	0.98100	0.0
LINTR	9.96978	10.03269	9.58203	10.87311	8.70978	0.0	5.00688	3.62634	1.01420	0.0
RHOS	0.09163	0.07473	0.07678	0.09577	0.07834	0.0	0.05281	0.04145	0.01265	0.0

LINE NUMBER 4 PIXEL NUMBER 193 SCAN ANGLE= -5.365 DEGREES

	1	2	3	4	5	6	7	8	9	10
LTOT	9.44025	9.67074	8.93549	9.44604	7.46506	0.0	4.53684	3.40306	2.13669	0.0
LPATH	2.84813	2.35989	1.50513	0.94648	0.68933	0.65941	0.62256	0.54191	0.45636	0.39016
LBEAM	6.59212	7.31085	7.43037	8.49956	6.77573	0.0	3.91428	2.86115	1.68033	0.0
LSURF	8.33270	8.67138	8.48844	9.54700	7.59560	0.0	4.55504	3.34112	1.96156	0.0
LINTR	10.00789	9.96299	9.53998	10.73997	8.58957	0.0	4.82361	3.48319	2.02793	0.0
RHOS	0.09198	0.07421	0.07644	0.09460	0.07726	0.0	0.05087	0.03981	0.02529	0.0

LINE NUMBER 4 PIXEL NUMBER 201 SCAN ANGLE= -7.459 DEGREES

	1	2	3	4	5	6	7	8	9	10
LTOT	9.35744	9.84657	9.18143	9.61624	7.78272	0.0	4.79984	3.50464	2.13669	0.0
LPATH	2.91412	2.41835	1.54357	0.97168	0.70894	0.68061	0.64472	0.56238	0.47437	0.40606
LBEAM	6.44332	7.42822	7.63786	8.64456	7.07378	0.0	4.15512	2.94227	1.66232	0.0
LSURF	8.15246	8.81678	8.73026	9.71451	7.93344	0.0	4.83834	3.43805	1.94176	0.0
LINTR	9.79142	10.13005	9.81166	10.92842	8.97162	0.0	5.12361	3.58424	2.00746	0.0
RHOS	0.08999	0.07546	0.07862	0.09626	0.08070	0.0	0.05404	0.04097	0.02504	0.0

LINE NUMBER 4 PIXEL NUMBER 209 SCAN ANGLE= -9.553 DEGREES

	1	2	3	4	5	6	7	8	9	10
LTOT	9.85430	10.28615	9.75526	11.06293	8.97396	0.0	6.64088	5.99345	4.27338	0.0
LPATH	2.98403	2.48054	1.58477	0.99896	0.73047	0.70435	0.66990	0.58583	0.49515	0.42448
LBEAM	6.87026	7.80561	8.17049	10.06397	8.24349	0.0	5.97097	5.40762	3.77823	0.0
LSURF	8.70388	9.27343	9.34592	11.31684	9.25112	0.0	6.95856	6.32421	4.41713	0.0
LINTR	10.85369	10.65472	10.50358	12.73047	10.46173	0.0	7.36884	6.59312	4.56860	0.0
RHOS	0.09608	0.07937	0.08416	0.11213	0.09410	0.0	0.07772	0.07536	0.05696	0.0

LINE NUMBER 4 PIXEL NUMBER 217 SCAN ANGLE=-11.647 DEGREES

	1	2	3	4	5	6	7	8	9	10
LTOT	10.59958	11.95655	11.80469	13.44571	12.30941	0.0	14.92553	12.08046	14.95683	0.0
LPATH	3.05774	2.54631	1.62860	1.02818	0.75375	0.73041	0.69783	0.61201	0.51843	0.44520
LBEAM	7.54183	9.41025	10.17609	12.41753	11.55566	0.0	14.22771	11.47647	14.43879	0.0
LSURF	9.57021	11.19303	11.65080	13.97465	12.97841	0.0	16.59837	13.43618	16.89403	0.0
LINTR	11.49419	12.86025	13.09396	15.72089	14.67678	0.0	17.57703	14.00750	17.46982	0.0
RHOS	0.10568	0.09579	0.10492	0.13847	0.13201	0.0	0.18538	0.16011	0.21789	0.0

LINE NUMBER 4 PIXEL NUMBER 225 SCAN ANGLE=-13.741 DEGREES

	1	2	3	4	5	6	7	8	9	10
LTOT	10.18553	11.07740	11.06690	12.08412	11.27701	0.0	14.85978	12.03769	12.82014	0.0
LPATH	3.13544	2.61567	1.67524	1.05963	0.77898	0.75905	0.72885	0.64125	0.54453	0.46846
LBEAM	7.05010	8.46152	9.39165	11.02459	10.49802	0.0	14.13093	11.39645	12.27561	0.0
LSURF	8.96386	10.07902	10.76472	12.41916	11.80189	0.0	16.50648	13.35989	14.38550	0.0
LINTR	10.76593	11.68031	12.09812	13.97104	13.34636	0.0	17.47972	13.92797	14.87228	0.0
RHOS	0.09895	0.08626	0.09694	0.12306	0.12004	0.0	0.18436	0.15920	0.18549	0.0

LINE NUMBER 4 PIXEL NUMBER 233 SCAN ANGLE=-15.836 DEGREES

	1	2	3	4	5	6	7	8	9	10
LTOT	11.17924	12.22030	11.88667	12.16922	10.80052	0.0	12.75574	11.58056	8.97410	0.0
LPATH	3.21745	2.68963	1.72508	1.09335	0.80652	0.79084	0.76364	0.67417	0.57801	0.49478
LBEAM	7.94179	9.53067	10.16159	11.07588	9.99399	0.0	11.99211	10.90639	8.40009	0.0
LSURF	10.14664	11.37182	11.66263	12.49136	11.24802	0.0	14.02924	12.80512	9.85903	0.0
LINTR	12.18650	13.06567	13.10726	14.05225	12.71995	0.0	14.85641	13.34961	10.19264	0.0
RHOS	0.11201	0.09732	0.10503	0.12377	0.11441	0.0	0.15669	0.15259	0.12712	0.0

LINE NUMBER 4 PIXEL NUMBER 241 SCAN ANGLE=-17.930 DEGREES

	1	2	3	4	5	6	7	8	9	10
LTOT	11.75891	13.89070	14.26400	15.82850	14.37422	0.0	15.32004	12.08848	13.67482	0.0
LPATH	3.30415	2.76802	1.77850	1.12996	0.83672	0.82628	0.80280	0.71138	0.60737	0.52458
LBEAM	8.45475	11.12269	12.48549	14.69854	13.53750	0.0	14.51724	11.37710	13.06745	0.0
LSURF	10.80406	13.29756	14.35187	16.59924	15.25626	0.0	17.01306	13.38172	15.36444	0.0
LINTR	12.97609	15.27825	16.12959	18.67345	17.25270	0.0	18.01616	13.95073	15.88435	0.0
RHOS	0.11927	0.11381	0.12928	0.16448	0.15518	0.0	0.19002	0.15946	0.19811	0.0

LINE NUMBER 4 PIXEL NUMBER 249 SCAN ANGLE=-20.024 DEGREES

	1	2	3	4	5	6	7	8	9	10
LTOT	10.35115	11.42906	10.82096	12.08417	10.56227	0.0	13.61051	12.03769	12.39280	0.0
LPATH	3.39586	2.85137	1.83581	1.16962	0.86983	0.86576	0.84678	0.75326	0.64494	0.55815
LBEAM	6.95529	8.57769	8.98515	10.91450	9.69244	0.0	12.76373	11.28443	11.74786	0.0
LSURF	8.91556	10.27812	10.34650	12.34486	10.93955	0.0	14.98815	13.30000	13.84122	0.0
LINTR	10.70792	11.80907	11.62610	13.88745	12.37111	0.0	15.87186	13.86554	14.30958	0.0
RHOS	0.09842	0.08796	0.09317	0.12232	0.11127	0.0	0.16740	0.15848	0.17847	0.0

LINE NUMBER 4 PIXEL NUMBER 257 SCAN ANGLE=-22.118 DEGREES

	1	2	3	4	5	6	7	8	9	10
LTOT	10.43396	10.98948	10.49306	10.89273	9.76811	0.0	12.62424	11.68215	9.40144	0.0
LPATH	3.49274	2.93986	1.89714	1.21244	0.90592	0.90931	0.89557	0.79980	0.68669	0.59541
LBEAM	6.94122	8.04961	8.59592	9.68029	8.86219	0.0	11.72867	10.88235	8.71474	0.0
LSURF	8.92092	9.67014	9.91812	10.96805	10.01966	0.0	13.80412	12.85603	10.29154	0.0
LINTR	10.72397	11.11052	11.14666	12.33860	11.33184	0.0	14.61802	13.40269	10.63079	0.0
RHOS	0.09857	0.08276	0.08932	0.10868	0.10192	0.0	0.15418	0.15319	0.13270	0.0

LINE NUMBER 4 PIXEL NUMBER 265 SCAN ANGLE=-24.213 DEGREES

	1	2	3	4	5	6	7	8	9	10
LTOT	10.43396	11.34174	10.98492	11.65863	10.72110	0.0	13.54476	11.93611	11.53813	0.0
LPATH	3.59489	3.03364	1.96253	1.25841	0.94098	0.95682	0.94901	0.85081	0.73241	0.63613
LBEAM	6.83907	8.30754	9.02238	10.40021	9.77612	0.0	12.59574	11.08530	10.80571	0.0
LSURF	8.83250	10.00889	10.43369	11.80697	11.07437	0.0	14.86275	13.13024	12.79434	0.0
LINTR	10.60817	11.49972	11.72609	13.28934	12.52358	0.0	15.73907	13.68856	13.22728	0.0
RHOS	0.09750	0.08566	0.09396	0.11699	0.11264	0.0	0.16600	0.15646	0.16497	0.0

LINE NUMBER 4 PIXEL NUMBER 273 SCAN ANGLE=-26.307 DEGREES

	1	2	3	4	5	6	7	8	9	10
LTOT	10.68239	11.78072	11.14807	12.33942	10.95935	0.0	12.49274	12.03769	16.23883	0.0
LPATH	3.70242	3.13262	2.03195	1.30743	0.98680	1.00795	1.00660	0.90574	0.78153	0.67980
LBEAM	6.97997	8.64810	9.11692	11.03199	9.97255	0.0	11.48614	11.13195	15.45730	0.0
LSURF	9.05467	10.45302	10.56971	12.55187	11.32141	0.0	13.59252	13.22439	18.35483	0.0
LINTR	10.87501	12.01001	11.87896	14.12033	12.80295	0.0	14.39395	13.78671	18.97696	0.0
RHOS	0.09995	0.08946	0.09518	0.12437	0.11516	0.0	0.15181	0.15758	0.23668	0.0

LINE NUMBER 4 PIXEL NUMBER 281 SCAN ANGLE=-28.401 DEGREES

	1	2	3	4	5	6	7	8	9	10
LTOT	10.43396	11.25323	10.90294	11.57353	10.32402	0.0	12.88725	11.98690	12.39280	0.0
LPATH	3.81532	3.23684	2.10521	1.35925	1.03106	1.06209	1.06751	0.96373	0.83324	0.72562
LBEAM	6.61864	8.01639	8.79773	10.21427	9.29296	0.0	11.81973	11.02317	11.55956	0.0
LSURF	8.62871	9.72460	10.22849	11.45017	10.57549	0.0	14.03233	13.13830	13.77232	0.0
LINTR	10.36341	11.17309	11.89547	13.10595	11.95941	0.0	14.85969	13.69696	14.23835	0.0
RHOS	0.09525	0.08323	0.09211	0.11544	0.10757	0.0	0.15672	0.15656	0.17758	0.0

LINE NUMBER 4 PIXEL NUMBER 289 SCAN ANGLE=-30.495 DEGREES

	1	2	3	4	5	6	7	8	9	10
LTOT	10.68239	11.25323	10.57503	11.48843	10.08578	0.0	11.44072	12.03769	15.38417	0.0
LPATH	3.93348	3.34605	2.18203	1.41346	1.07736	1.11857	1.13083	1.02382	0.88665	0.77281
LBEAM	6.74091	7.90718	8.39301	10.07487	9.00841	0.0	10.30989	11.01387	14.49751	0.0
LSURF	8.84734	9.63085	9.78866	11.52273	10.27934	0.0	12.28372	13.17536	17.33586	0.0
LINTR	10.62599	11.06535	11.00116	12.96259	11.62451	0.0	13.00794	13.73559	17.92247	0.0
RHOS	0.09767	0.08242	0.08815	0.11417	0.10456	0.0	0.13719	0.15700	0.22353	0.0

LINE NUMBER 4 PIXEL NUMBER 297 SCAN ANGLE=-32.589 DEGREES

	1	2	3	4	5	6	7	8	9	10
LTOT	10.10272	10.46196	9.67329	9.87154	7.70331	0.0	4.86559	3.45385	1.70935	0.0
LPATH	4.05665	3.45996	2.26206	1.46997	1.12524	1.17661	1.19556	1.08501	0.94085	0.82055
LBEAM	6.04607	7.00703	7.41122	8.40157	6.57807	0.0	3.67003	2.36884	0.76850	0.0
LSURF	7.97482	8.56662	8.67384	9.63828	7.52863	0.0	4.39008	2.84527	0.92269	0.0
LINTR	9.57806	9.84263	9.74825	10.84267	8.51384	0.0	4.64892	2.96826	0.95392	0.0
RHOS	0.08803	0.07332	0.07811	0.09550	0.07658	0.0	0.04903	0.03390	0.01190	0.0

LINE NUMBER 4 PIXEL NUMBER 305 SCAN ANGLE=-34.684 DEGREES

	1	2	3	4	5	6	7	8	9	10
LTOT	10.01991	10.19824	9.42736	9.53114	7.38565	0.0	4.47108	3.09831	1.28201	0.0
LPATH	4.18454	3.57821	2.34493	1.52869	1.17421	1.23539	1.26064	1.14627	0.99492	0.86803
LBEAM	5.83537	6.62002	7.08242	8.00365	6.21143	0.0	3.21044	1.95204	0.28709	0.0
LSURF	7.74955	8.13957	8.32119	9.21220	7.13268	0.0	3.85729	2.35524	0.34625	0.0
LINTR	9.30750	9.35198	9.35192	10.36334	8.06608	0.0	4.08472	2.45539	0.35797	0.0
RHOS	0.08555	0.06966	0.07494	0.09128	0.07255	0.0	0.04308	0.02807	0.00446	0.0

LINE NUMBER 4 PIXEL NUMBER 313 SCAN ANGLE=-36.778 DEGREES

	1	2	3	4	5	6	7	8	9	10
LTOT	10.43396	10.61782	9.50933	9.53114	7.46506	0.0	4.79984	3.30148	2.13669	0.0
LPATH	4.31689	3.70049	2.43025	1.58750	1.22377	1.29402	1.32894	1.20646	1.04783	0.91437
LBEAM	6.11707	6.93733	7.07908	7.94364	6.24129	0.0	3.47490	2.09502	1.08886	0.0
LSURF	8.18931	8.57681	8.35306	9.17816	7.19343	0.0	4.19551	2.54044	1.31980	0.0
LINTR	9.83087	9.85034	9.38774	10.32504	8.13477	0.0	4.44288	2.68846	1.36446	0.0
RHOS	0.09036	0.07340	0.07522	0.09094	0.07317	0.0	0.04686	0.03027	0.01702	0.0

LINE NUMBER 4 PIXEL NUMBER 321 SCAN ANGLE=-38.872 DEGREES

	1	2	3	4	5	6	7	8	9	10
LTOT	10.35115	10.54990	9.67329	9.44604	7.30623	0.0	4.53684	3.14910	1.28201	0.0
LPATH	4.45335	3.82647	2.51766	1.64783	1.27345	1.35170	1.38744	1.26461	1.09875	0.95883
LBEAM	5.89780	6.72348	7.15563	7.79821	6.03278	0.0	3.14940	1.88449	0.18327	0.0
LSURF	7.95838	8.36338	8.48371	9.04767	6.98159	0.0	3.82319	2.29787	0.22337	0.0
LINTR	9.55828	9.60908	9.53457	10.17825	7.89521	0.0	4.04861	2.39558	0.23093	0.0
RHOS	0.08785	0.07158	0.07640	0.08965	0.07101	0.0	0.04270	0.02738	0.00288	0.0

LINE NUMBER 4 PIXEL NUMBER 329 SCAN ANGLE=-40.966 DEGREES

	1	2	3	4	5	6	7	8	9	10
LTOT	10.68239	11.16531	9.91922	10.12683	7.54448	0.0	4.79984	3.40306	1.28201	0.0
LPATH	4.59359	3.95568	2.60679	1.70875	1.32286	1.40776	1.44730	1.31996	1.14706	1.00095
LBEAM	6.08880	7.20963	7.31243	8.41809	6.22162	0.0	3.35254	2.08310	0.13495	0.0
LSURF	8.29290	9.02908	8.71558	9.81207	7.23287	0.0	4.09438	2.55574	0.16550	0.0
LINTR	9.96009	10.37397	9.79516	11.03816	8.17937	0.0	4.33578	2.66441	0.17110	0.0
RHOS	0.09154	0.07727	0.07849	0.09722	0.07357	0.0	0.04573	0.03045	0.00213	0.0

LINE NUMBER 4 PIXEL NUMBER 337 SCAN ANGLE=-43.061 DEGREES

	1	2	3	4	5	6	7	8	9	10
LTOT	10.59958	11.16531	9.83724	9.70134	7.22682	0.0	4.47108	3.14910	1.70935	0.0
LPATH	4.73735	4.08804	2.69743	1.77006	1.37172	1.46166	1.50389	1.37196	1.19235	1.04042
LBEAM	5.86223	7.07727	7.13982	7.93134	5.85510	0.0	2.96720	1.77714	0.51701	0.0
LSURF	8.06733	8.93034	8.56001	9.29226	6.84118	0.0	3.64810	2.19534	0.63837	0.0
LINTR	9.68917	10.26053	9.82032	10.45141	7.73643	0.0	3.86320	2.28868	0.65997	0.0
RHOS	0.08905	0.07643	0.07709	0.09207	0.06959	0.0	0.04074	0.02616	0.00823	0.0

REFERENCES

1. R M Goody, Atmospheric Radiation, Oxford, (1964), pg. 294

2. B. Edlén, Metrologia, 2, (1966), pg. 12

3 E Vigroux, Contributions a l'etude experimentale de l'absorption de l'ozone, Ann. Phys. (Paris), 8, (1966), pg 709.

4. G. Mie, Ann Physik, 25, (1908), pg 377.

5 H. C van de Hulst, Light Scattering by Small Particles, Wiley, New York, (1957).

6 M. Kerker, The Scattering of Light and Other Electromagnetic Radiation, Academic Press, New York, (1969)

7 R E. Turner, Radiative Transfer in Real Atmospheres, Final Report, ERIM 190100-24-T, (1974).

8. U.S. Standard Atmosphere, 1976, National Oceanic and Atmospheric Administration, National Aeronautics and Space Administration, United States Air Force, (1976)

9. R A McClatchey, R W. Fenn, J E A Selby, J S Garing, and F E. Volz, Optical Properties of the Atmosphere, AFCRL-72-0497, Environmental Research Papers, No 411, (1972).

10. A J Krueger, R. A. Minzner, A Mid-Latitude Ozone Model for the 1976 U.S. Standard Atmosphere, J of Geophys. Res , 81, No. 24, (1976), pg. 4477.

11 A. Vassy, Atmospheric Ozone, Advances in Geophysics, Vol. 11, (1965), pg 115

12. A. E S. Green, The Middle Ultraviolet; Its Science and Technology, Wiley, New York, (1966).

13. S. L Valley, Handbook of Geophysics and Space Environments, Air Force Cambridge Research Laboratories, Office of Aerospace Research, United States Air Force, (1965)

14 D Deirmendjian, Electromagnetic Scattering on Spherical Polydispersions, Elsevier, New York, (1969)

REFERENCES (Continued)

15. R. Penndorf, The Vertical Distribution of Mie Particles in the Troposphere, AFCRC Technical Report 54-5, Air Force Cambridge Research Center, (1954).

16. L. Elterman, Vertical-Attenuation Model with Eight Surface Meteorological Ranges 2 to 13 Kilometers, AFCRL-70-0200, Environmental Research Papers, No. 318, Air Force Cambridge Research Laboratories, (1970).

17. W. E. K. Middleton, Vision Through the Atmosphere, Univ of Toronto Press (1952).

18. L. Elterman, U.V., Visible, and IR Attenuation for Altitudes to 50 km., 1968, AFCRL-68-0153, Environmental Research Papers, No. 285, Air Force Cambridge Research Laboratories, (1968).

19. S Chandrasekhar, Radiative Transfer, Dover Publications (1960).

20. R. E. Turner, Remote Sensing in Hazy Atmospheres, Proceedings of ACSM/ASP Meeting in Washington, D.C., March, 1972.

21. R. E. Turner, Atmospheric Effects on Remote Sensing, Remote Sensing of Earth Resources, Vol. II, F. Shahrokhi (Ed.), Univ. of Tennessee, 1974

22. N. G. Jerlov, Marine Optics, Elsevier Scientific Publishing Co., New York, (1976), pg. 75.

23. W. V. Burt, Albedo Over Wind-Roughened Water, J. Meteorol., 11; (1954) pg. 283-290.

24. R. W. Preisendorfer, Exact Reflectance Under a Cardiodial Luminescence Distribution, Q. J. R. Meteorol. Soc. 83, (1957), pg. 540.

25. R. Siegel and J. R Howell, Thermal Radiation Heat Transfer, McGraw-Hill, Inc., New York, 1972

26. C. T. Wezernak, R. E. Turner, and D. R. Lyzenga, Spectral Reflectance and Radiance Characteristics of Water Pollutants, NASA Contractor Report, NASA CR-2665, Environmental Research Institute of Michigan (1976).

REFERENCES (Continued)

27 M. P. Thekaekara and A. J. Drummund, Standard Values for the Solar Constant and Its Spectral Components, Nature Phys. Sci , Vol. 229, Jan. 4, (1971).

28. R. Kumar, Radiation from Plants - Reflection and Emission: A Review, Purdue Research Foundation, Research Project No. 5543, AA&ES 72-2-2, (1972).

29. V. Leeman, D. Earing, R K Vincent, S. Ladd, NASA Earth Resources Spectral Information System, A Data Compilation, Infrared & Optics Laboratory, Willow Run Laboratories, Institute of Science and Technology, The University of Michigan, NASA CR 31650-24-T, 1972

30. C. T. Wezernak, R. E. Turner, and D. R. Lyzenga, Spectral Reflectance and Radiance Characteristics of Water Pollutants, NASA CR-2665, Environmental Research Institute of Michigan, Ann Arbor, Mich., (1976).

Technical and Final Report Distribution List

NASA Contract NAS3-20483

NAME	NO. OF COPIES
NASA Project Manager NASA Lewis Research Center Attention: Mr. Bruce Shuman Contract Section D, Mail Stop 500-213 21000 Brookpark Road Cleveland, Ohio 44135	4
NASA Scientific and Technical Information Facility P.O. Box 8957 Baltimore Washington International Airport Maryland 21240	10
NASA Lewis Research Center Attention: Library (Mail Stop 60-3) 21000 Brookpark Road Cleveland, Ohio 44135	2
NASA Research Center Attention: Thom Coney, (Mail Stop 54-2) 21000 Brookpark Road Cleveland, Ohio 44135	50

DEC 1978
RECEIVED